

Twelve Channel Optical Fiber Connector Assembly: from commercial off the shelf to space flight use

7/22/98

[Click here to start](#)

Table of Contents

Author: Melanie Ott

[Twelve Channel Optical Fiber Connector Assembly: from commercial off the shelf to space flight use](#)

Email: Melanie.Ott@gsfc.nasa.gov

Home Page:
<http://misspiggy.gsfc.nasa.gov/tva>

[Outline](#)

[FODB Objectives for Connector Assembly](#)

[Issues](#)

[MTP Twelve Channel Ribbon Cable Assembly](#)

[MTP Optical Fiber Ribbon Cable Assembly](#)

[Testing Parameters](#)

[Axis Definitions for Vibration Testing](#)

[Random Vibration Test One: Cable set 1, Channel 6.](#)

[Random Vibration Test One: Cable set 2,
Channel 12.](#)

[Random Vibration Test One: Cable set 3,
Channel 9](#)

[Summary of Random Vibration Test One](#)

[Thermal Cycling Test Results: Cable Set 2](#)

[Thermal Cycling Test Results: Cable Set 3](#)

[Random Vibration Test Two Results](#)

[Random Vibration Test Two Results](#)

[Summary of All Tests](#)

[Conclusions](#)

[Acknowledgements](#)

Twelve Channel Optical Fiber Connector Assembly: from commercial off the shelf to space flight use

Melanie N. Ott,

Component Technologies & Radiation Effects
Swales Aerospace/Goddard Space Flight Center
301-286-0127

Joy W. Bretthauer,

Flight Electronics,
Goddard Space Flight Center

SPIE Conference on Photonics for Space Environments VI
NASA Goddard Space Flight Center

7/22/98



Slide 1 of 19

Outline

- **FODB Objectives**
- **Issues**
- **Cable assembly for characterization**
- **Testing parameters**
 - **random vibration 1, thermal cycling, random vibration 2**
- **Testing results (3 sets of tests)**
- **Summary of test results**
- **Conclusions**

July 22, 1998

NASA Goddard Space Flight Center



Slide 2 of 19

FODB Objectives for Connector Assembly

- Commercial cable assembly
- Smaller, less weight, less expensive, state of the art.
- High data rate communications for science data transmissions.
- For use on future missions (re-useable technology).
- Partnerships with vendors.
- Testing for known failure mechanisms.
- Non operational during launch.
- Mission duration of 1 to 3 years.

July 22, 1998

NASA Goddard Space Flight Center



Slide 3 of 19

Issues

- **Outgassing of Materials** (analysis & ASTM E595 testing)
 - **Boot change: Kraton**, TML 15.53%, CVC/M 10.04%.
- **Vibration** (analysis and testing)
 - **Ferrule size change, ONI will use larger core fiber** (100/140 instead of 62.5/125 micron)
- **Radiation Effects** (analysis only)
 - **Commercial Fiber**
 - **EO-1 Radiation Environment:** 15 Krads, 4E-2 rads/sec, 12 ft length, -15°C, 1300 nm, power loss < .13 dB.
- **Thermal** (testing)
 - **Epoxy low Tg** (TBD if change necessary)
 - **Gore available cable data:** .01 dB @ -15°C, $\lambda = 850$ nm, 12 ft length

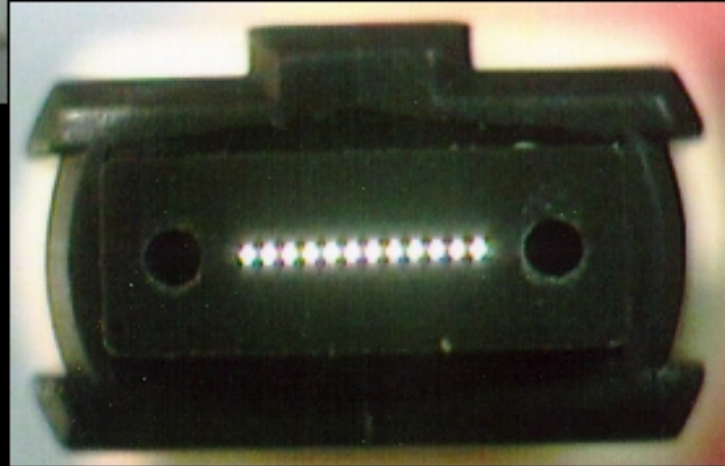
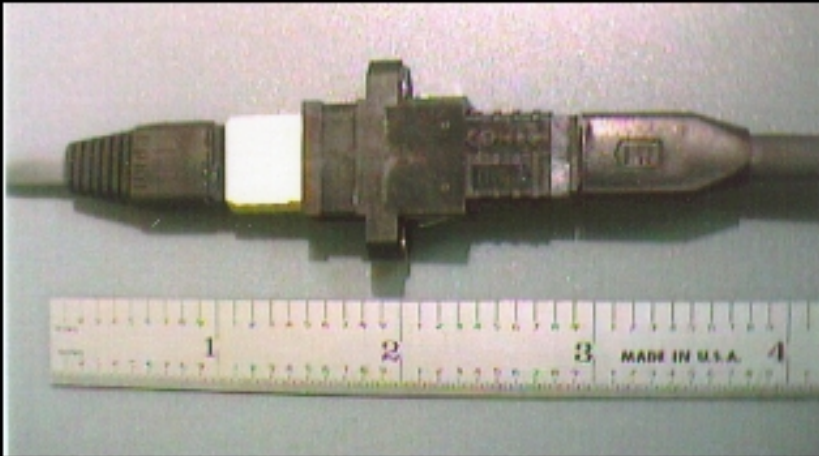
July 22, 1998

NASA Goddard Space Flight Center



Slide 4 of 19

MTP Twelve Channel Ribbon Cable Assembly



July 22, 1998

NASA Goddard Space Flight Center



Slide 5 of 19

MTP Optical Fiber Ribbon Cable Assembly

- 12 channel cable assembly: MTP connector (US Conec) and (W.L. Gore) 12 channel ribbon cable.
- 33 times lighter and 20 times less expensive than 38999 type connectors currently flying.
- Terminations by W.L. Gore with help of US Conec and GSFC.
- Rated for -20°C to +85°C, losses .35 dB/channel on average.
- Enhanced version: 100/140 micron optical fiber with new ferrule and boot, kynar jacket, lower loss < .2 dB/channel, 1300 nm wavelength.
- Characterized 62.5/125 micron twelve optical fiber ribbon cable assembly with kraton boot, kynar jacket for 1300 nm.

July 22, 1998

NASA Goddard Space Flight Center



Slide 6 of 19

Testing Parameters

- **Random vibration test one:** active monitoring of one channel and post optical measurements of all 12 channels. (14.1 grms, 1 minute/axis)
- **Thermal test:**
 - 30 cycles, -20 °C to +85 °C, 1 °C/min.
 - 42 cycles, -20 °C to +85 °C, 3 °C/min up, 2 °C/min down.
- **Random vibration test two:** active monitoring of one channel and post optical measurements of all 12 channels. (20 grms, 3 minutes/axis)

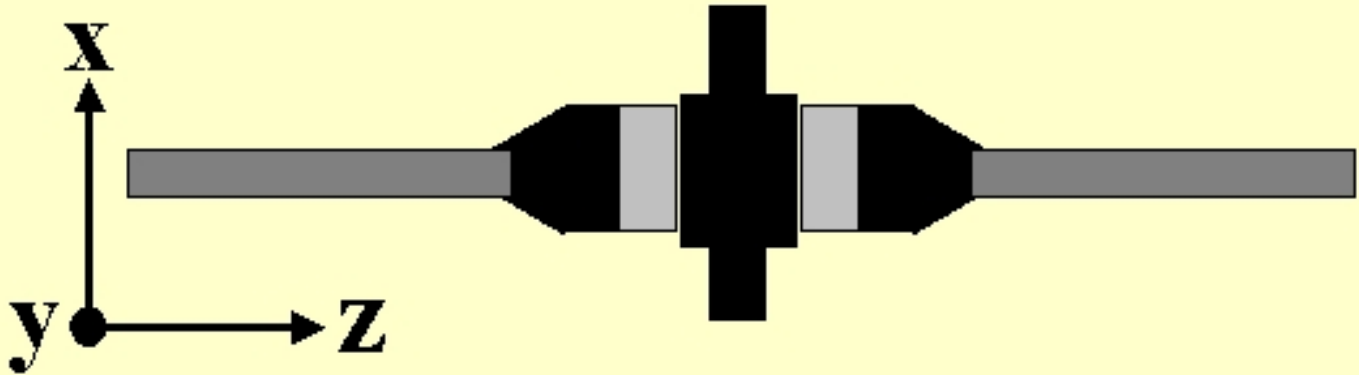
July 22, 1998

NASA Goddard Space Flight Center



Slide 7 of 19

Axis Definitions for Vibration Testing



MTP twelve channel ribbon connector assembly

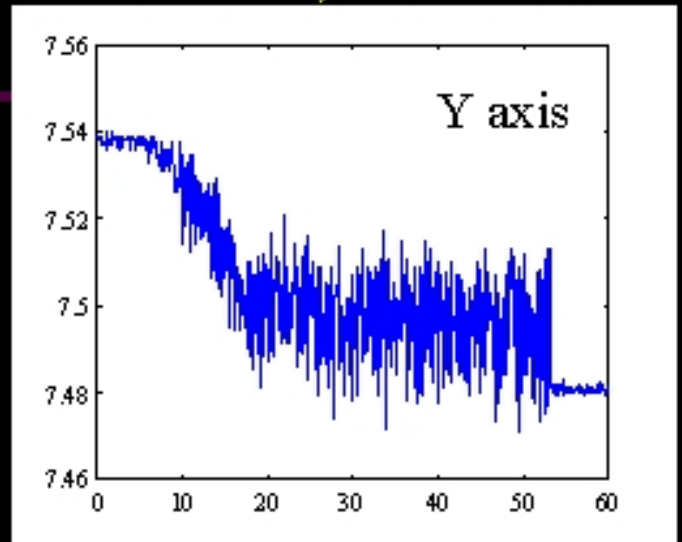
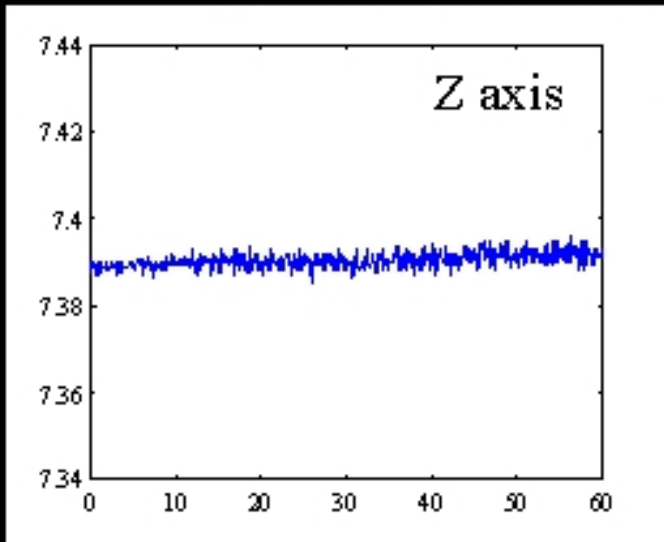
July 22, 1998

NASA Goddard Space Flight Center

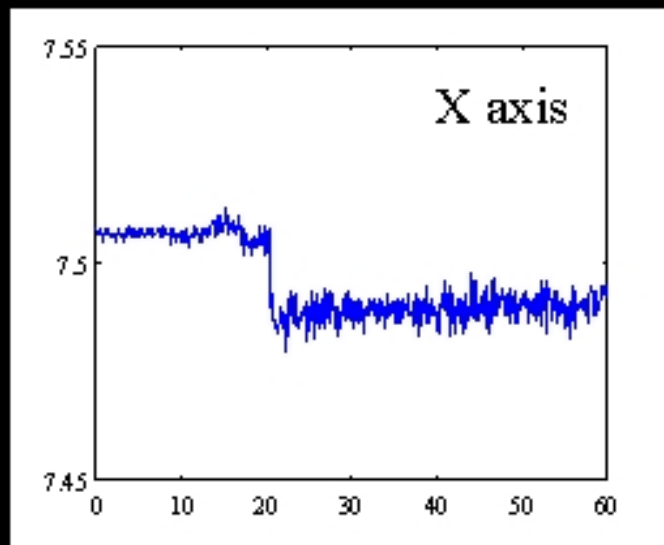


Slide 8 of 19

Random Vibration Test One: Cable set 1, Channel 6.



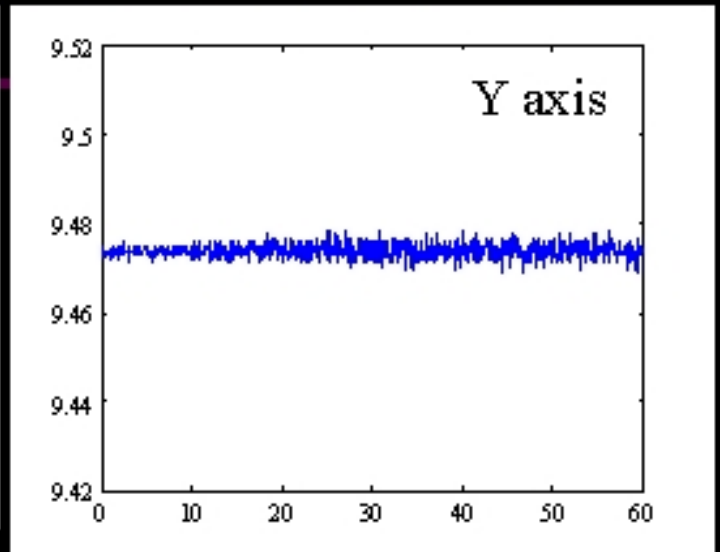
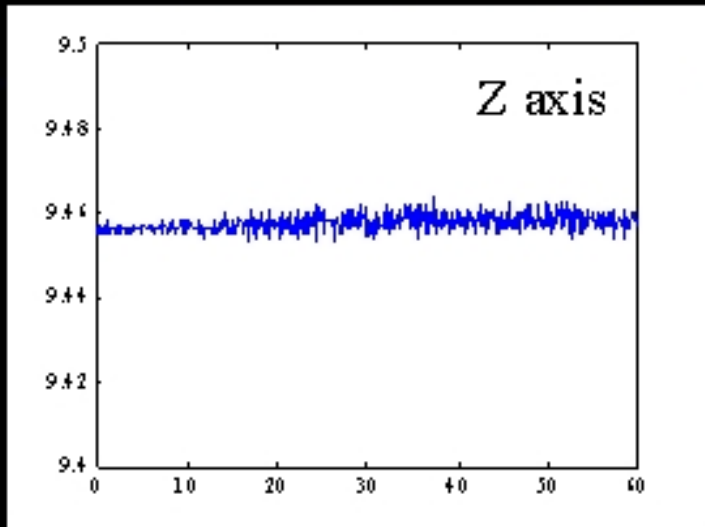
Full range scale
.10 microwatt
all graphs



July 22, 1998

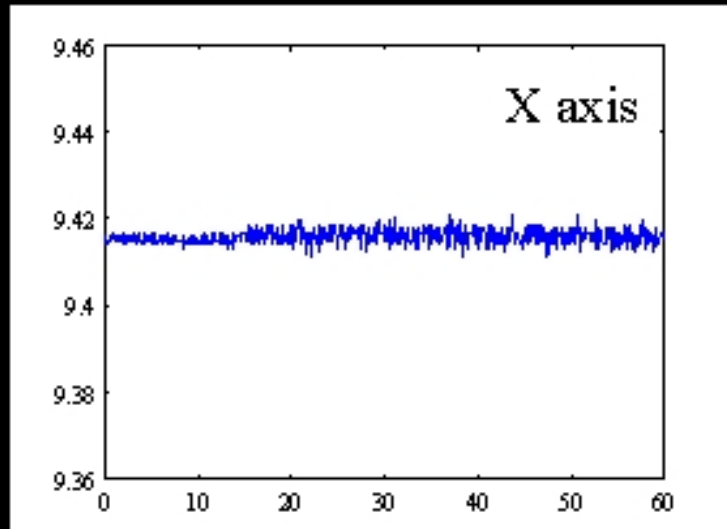


Random Vibration Test One: Cable set 2, Channel 12.

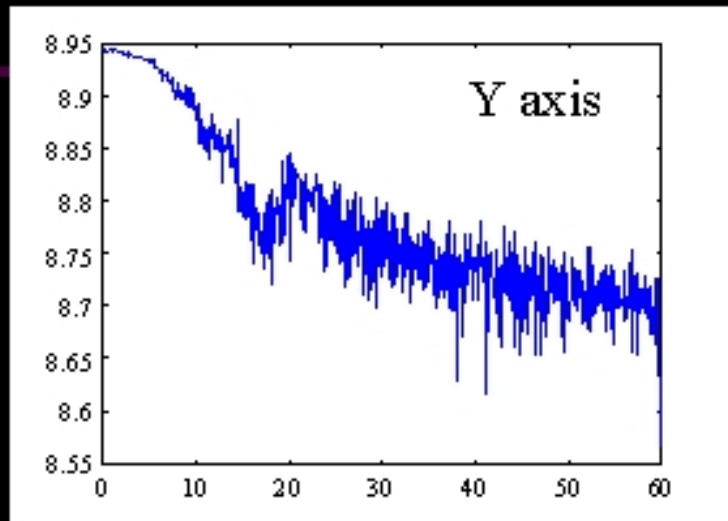
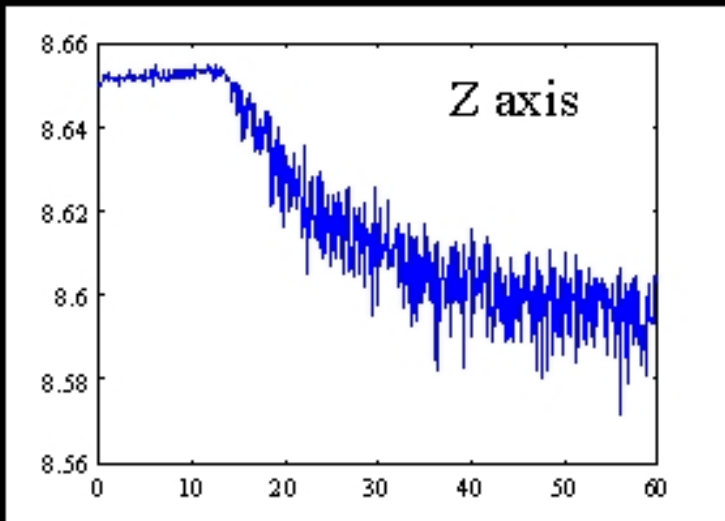


Full range scale
.10 microwatt
all graphs

July 22, 1998

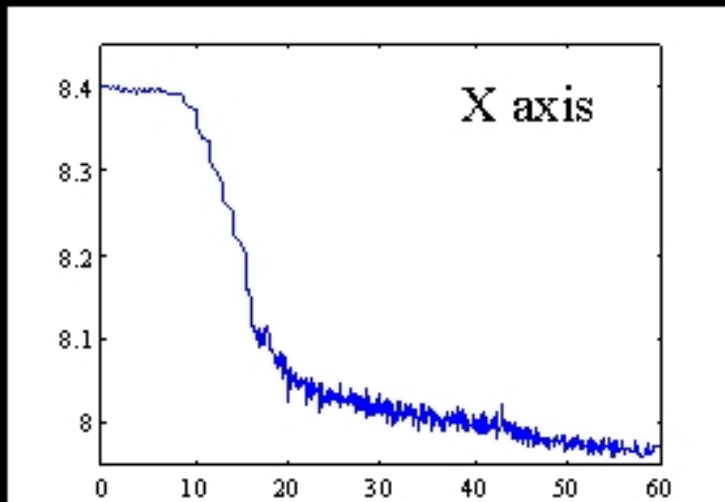


Random Vibration Test One: Cable set 3, Channel 9



Full range
scale for Z axis
test is .10
microwatts

July 22, 1998



Full range
scale on Y and
X axis tests
.4 microwatts,
and .5 microwatts
respectively.



Acknowledgements

John Keesee & team (*US Conec*);

Doug Hardy, Dr. David Jurbergs & team (*W.L. Gore*);

Dr. Michele Gates, Richard Katz, Dr. Henning Leidecker, Pat
Friedberg, Harry Shaw, John Kolasinski, Janet Barth

Janet Jew, (*NASA GSFC*);

Dr. Mark Fan, Clay Eveland, (*Swales Aerospace/GSFC*);

Igor Kleyner, (*J & T /GSFC*);

Dr. John LeNard, Susan Ritter, (*Litton/GSFC*);

Chuck Chulfant, *ONI*;

Bob Kiwak, John Slonaker (*Unisys/GSFC*);

Fred Orlando (*OAI*)

July 22, 1998

NASA Goddard Space Flight Center



Slide 19 of 19

Technology Validation Assurance (TVA)

Home

Current Projects

Past Topics in...

TVA Library

Validation Methods

TVA Group Members

Links

Site Index

Welcome to the NEW Technology Validation Assurance Web Site!

Recent Papers/Updates:

- [*Characterization of the Twelve Channel 100/140 Micron Optical Fiber, Ribbon Cable and MTP Array Connector Assembly for Space Flight Environments*](#), NEPP Web Publication, October 4, 2001
Authors: Melanie Ott, Shawn Macmurphy, Patricia Friedberg
- [*Radiation Testing of Commercial off the Shelf 62.5/125/250 Micron Optical Fiber for Space Flight Environments*](#), NEPP Web Publication, October 17, 2001
Authors: Melanie Ott, Shawn Macmurphy, Matthew Dodson
- [*Fiber Optic Epoxy Outgassing Study for Space Flight Applications*](#), NEPP Web Publication, October 4, 2001
Authors: Matthew Bettencourt, Melanie Ott
- [*Evaluation of Vertical Cavity Surface Emitting Lasers \(VCSEL\) mounted on CVD Diamond Substrates*](#), NEPP Web Publication, October 2001
Authors: Harry Shaw, Melanie Ott, Shawn Macmurphy, Jong Kadesch, Patricia Friedberg
- [*Tailoring Cores of Optical Fibers by a Sol-Gel Method*](#)
Authors: Harry Shaw, Michele Manuel, Melanie Ott
- **Current Projects** section has been updated and includes NEPP deliverables.
- [*Technology Validation of Optical Fiber Cables for Space Flight Environments*](#), SPIE Proceedings Vol. 4216, Optical Devices for Fiber Communication II, Conference November 8, 2000, Boston MA.
Authors: Melanie Ott, Patricia Friedberg
[Companion Viewgraph Presentation](#) <--*Now Available!*
- [*TID Radiation Induced Attenuation Testing at 1300 nm Using ISS Requirements on Three Optical Fibers Manufactured by Lucent SFT*](#), September 2000
Author: Melanie Ott

- [Evaluation of ESD Effects During Removal of Conformal Coatings Using Micro Abrasive Blasting](#) (September 2000)
Authors: Harry Shaw, Nitin Parekh, Carroll Clatterbuck, Felix Frades
- [ISS Fiber Optic Failure Investigation Root Cause Report](#) has been finished and released to the public! (August 2000)

Overview:

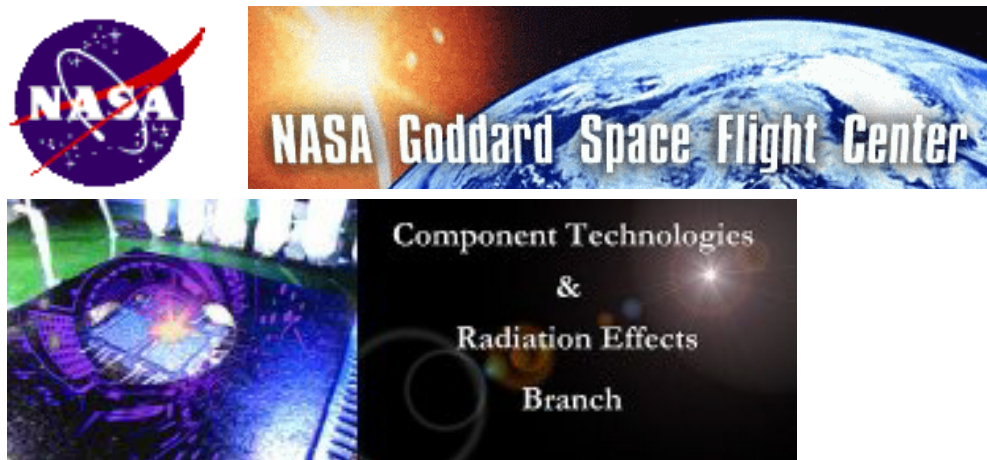
The purpose of Technology Validation Assurance (TVA) is to provide a short cycle, low cost approach to building in quality through design optimization, and quality and reliability analysis for critical electronic hardware. Concurrent engineering, theoretical analysis and empirical data are used to produce information about a technology's mechanical, thermal and electrical limitations and its most likely failure mechanisms.

Curator: [Jesse Frank](#)

NASA Official: [Darryl D. Lakins](#)

[NASA/GSFC Security and Privacy Statement](#)

This Page Last Modified: 2/28/2001



Random Vibration Test One: Cable set 2, Channel 12.

Full range scale

.10 microwatt

all graphs

Z axis

Y axis

X axis

[Previous slide](#)

[Next slide](#)

[Back to first slide](#)

[View graphic version](#)

Conclusions

- Twelve channel MTP connector/ribbon cable assembly with 62.5/125 micron fiber, characterized for EO-1 environment.
- During vibration test one (1 min/axis): transients $< .25$ dB, post test loss nearly zero.
- Thermal cycling: $-.026$ dB & $-.16$ dB (loss) @ -20 °C, post test average loss $< -.50$ dB.
- Post vibration test two (twice levels of test one for 3 minutes/axis) average loss $< -.10$ dB.
- Sources of uncertainty: source stability, fan out cables, rates of degradation.
- One fiber in 48 pistoned (cracked) as a result of testing.
- Enhanced connector assembly characterization data will be available late 1998.

July 22, 1998

NASA Goddard Space Flight Center



Slide 18 of 19

Acknowledgements

John Keesee & team (US Conec);

Doug Hardy, Dr. David Jurbergs & team (W.L. Gore);

Dr. Michele Gates, Richard Katz, Dr. Henning Leidecker, Pat Friedberg, Harry Shaw, John Kolasinski, Janet Barth

Janet Jew, (NASA GSFC);

Dr. Mark Fan, Clay Eveland, (Swales Aerospace/GSFC);

Igor Kleyner, (J & T /GSFC);

Dr. John LeNard, Susan Ritter, (Litton/GSFC);

Chuck Chulfant, ONI;

Bob Kiwak, John Slonaker (Unisys/GSFC);

Fred Orlando (OAI)

•

[Previous slide](#)

[Back to first slide](#)

[View graphic version](#)

Summary of Random Vibration Test One

Cable Set	Optical Channel	Axis Test	Maximum Value (microwatts)	Minimum Value (microwatts)	Range of Fluctuations (dB)
1	#6	Y	7.54	7.471	< 0.04
1	#6	X	7.513	7.48	< 0.04
1	#6	Z	7.396	7.385	< 0.01
2	#12	Y	9.478	9.469	< 0.01
2	#12	X	9.421	9.411	< 0.01
2	#12	Z	9.464	9.453	< 0.01
3	#9	Y	8.945	8.563	< 0.12
3	#9	X	8.401	7.958	< 0.24
3	#9	Z	8.655	8.572	< 0.04

Average Post Vibration Optical Measurements

Cable Set 2: .056 dB, and .11 dB stand.dev.

Cable Set 3: -.008 dB, and .43 dB stand. dev.

July 22, 1998

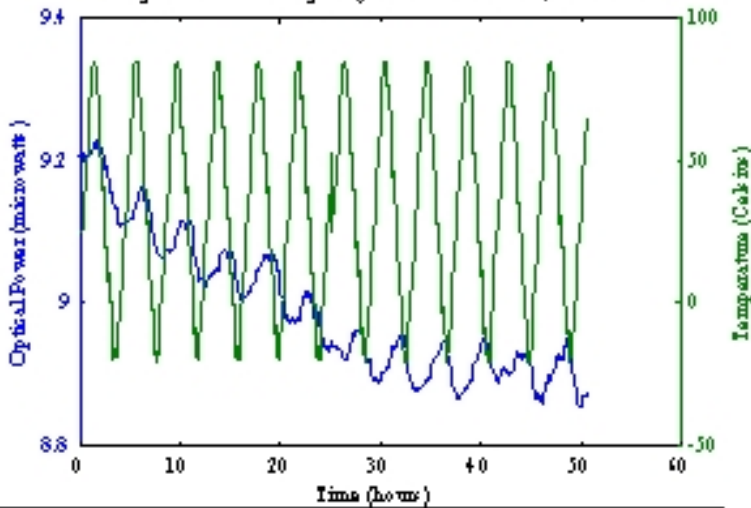
NASA Goddard Space Flight Center



Slide 12 of 19

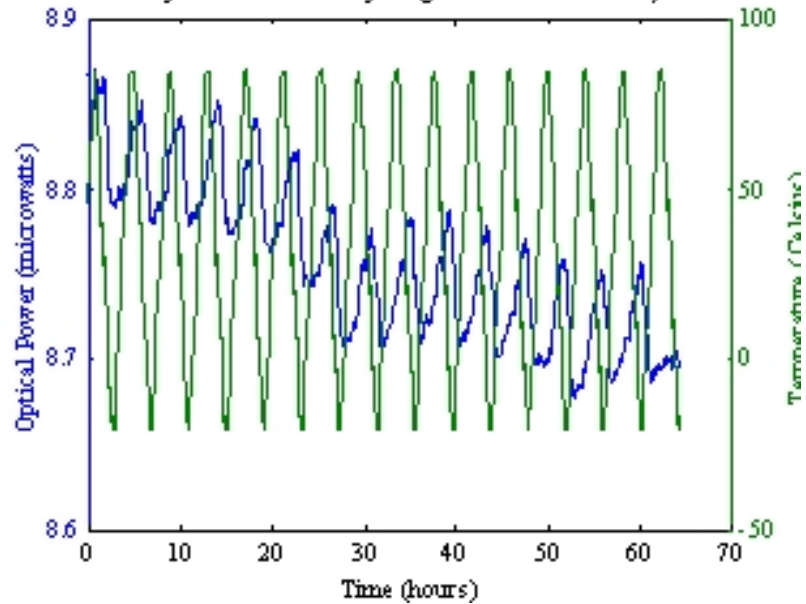
Thermal Cycling Test Results: Cable Set 2

First Twelve Cycles of Thermal Cycling Test for Cable Set 2, Channel 12



30 cycles
-20°C to +85°C, 1 °C/min

Last Fifteen Cycles of Thermal Cycling Test for Cable Set 2, Channel 12



Post thermal test optical power
average = -.46 dB,
stand. Dev. .52 dB

Loss -.025 dB at -20°C

July 22, 1998

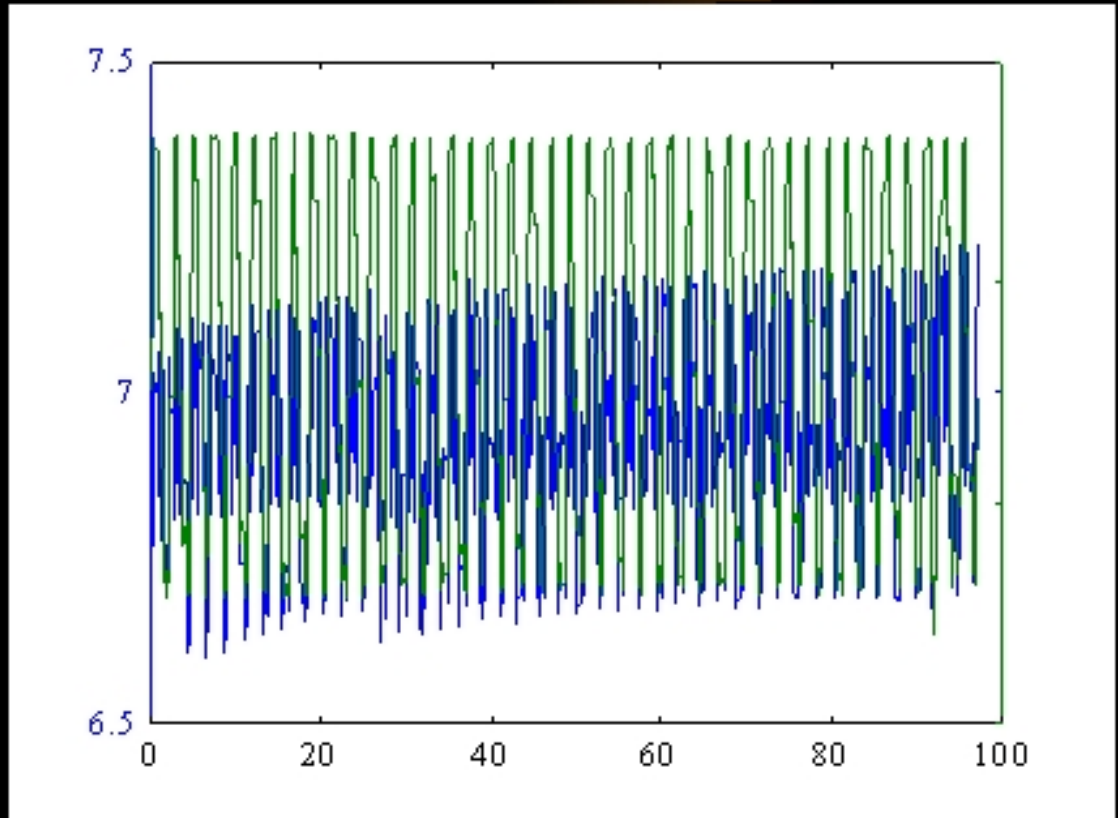


Thermal Cycling Test Results: Cable Set 3

42 cycles
-20°C to +85°C,
3 °C/min up
2 °C/min down

Post thermal
optical power
average = -.13 dB
Stand. Dev. .70 dB

Loss -.16 dB @
-20°C



July 22, 1998

NASA Goddard Space Flight Center



Slide 14 of 19

Random Vibration Test Two Results

Cable Set	Optical Channel	Axis Test	Maximum Value (microwatts)	Minimum Value (microwatts)	Range of Fluctuation (dB)
2	#12	Y	10.003	9.993	<0.01
2	#12	X	9.982	9.949	<0.01
2	#12	Z	10.021	10.013	<0.01
3	#9	Y	8.700	8.284	<0.23
3	#9	X	8.151	7.782	<0.20
3	#9	Z	8.687	8.537	<0.08

Cable Set 2 post vib test average optical power
all channels = -.08 dB, stand. Dev. .57 dB

Cable Set 3 post vib average optical power
all channels = -.09 dB, stand. Dev. .81 dB.

July 22, 1998

NASA Goddard Space Flight Center



Slide 15 of 19

Random Vibration Test Two Results

Cable Set	Optical Channel	Axis Test	Maximum Value (microwatts)	Minimum Value (microwatts)	Range of Fluctuation (dB)
2	# 12	Y	10.003	9.993	< 0.01
2	# 12	X	9.982	9.949	< 0.01
2	# 12	Z	10.021	10.013	< 0.01
3	# 9	Y	8.700	8.284	< 0.23
3	# 9	X	8.151	7.782	< 0.20
3	# 9	Z	8.687	8.537	< 0.08

Cable Set 2 post vib test average optical power
all channels = -.08 dB, stand. Dev. .57 dB

Cable Set 3 post vib average optical power
all channels = -.09 dB, stand. Dev. .81 dB.

July 22, 1998

NASA Goddard Space Flight Center

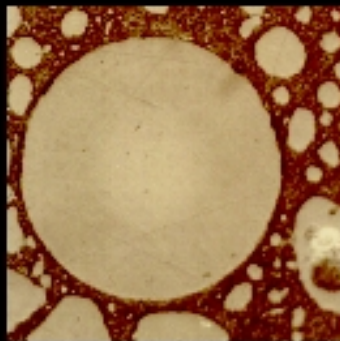


Slide 16 of 19

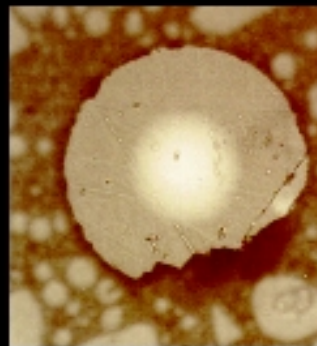
Summary of All Tests

Post Test Measurements	Cable Set 2 (dB)	Cable Set 3 (dB)
Vibration Average Loss	.056	-.008
Vibration Standard Dev.	.11	.43
Thermal Average Loss	-.46	-.13
Thermal Standard Dev.	.52	.70
Vibration 2 Average Loss	-.08	-.09
Vibration 2 Standard Dev.	.57	.81

Channel
#12 endface
pictures
cable set 2



Pre thermal testing



Post thermal testing

July 22, 1998

NASA Goddard Space Flight Center



Slide 17 of 19

Current Projects

Home

Current Projects

Past Topics in...

TVA Library

Validation Methods

TVA Group Members

Links

Site Index

These are SOME of our current projects, click the link to see details:

- [In-house manufacturing of microelectronics for Explorers, ESSP and 600 in-house instruments](#)
[Download PDF File of this presentation.](#)
- [Diamond Substrate Heat-Spreader for Space-Based X-Band Power MMICs](#)
- [Laser Light in Fiber Optic Communication](#)
- [Reworkable Underfill Characterization](#)
- [Photonic and Fiber Optic Documents](#) (TVA Library)

- [NEPP Deliverables](#)

More Coming Soon!

This page last updated: December 15, 2000

Past Topics in...

[Home](#)

[Current Projects](#)

[Past Topics in...](#)

[TVA Library](#)

[Validation Methods](#)

[TVA Group Members](#)

[Links](#)

[Site Index](#)

- [Photonics](#)
- [Advanced Electronic Packaging](#)
- [Fluid Embedded Electronics - The DDF Task](#)
- [Synthetic Diamond: Thermal and Interconnect Strategies](#)
- [COTS](#)
- [TVA Library](#) (past and present topics)

TVA Library

[Home](#)

[Current Projects](#)

[Past Topics in...](#)

[TVA Library](#)

[Validation Methods](#)

[TVA Group Members](#)

[Links](#)

[Site Index](#)

- [Photonic and Fiber Optic Documents](#)
- [Advanced Electronic Packaging Documents](#)
- [All Other TVA Documents](#)

- [NEPP Deliverables](#)
- [1998 Advanced Interconnect Program Deliverables](#)

Validation Methods

[Home](#)[Current Projects](#)[Past Topics in...](#)[TVA Library](#)[Validation Methods](#)[TVA Group Members](#)[Links](#)[Site Index](#)

- [Overview](#)

TVA elements being used currently for validating new and emerging Advanced Interconnect, Packaging and EEE Parts technologies are the following:

- [Process Analysis](#)
- [Construction and Materials Analysis](#)
- [Structural/Thermal Analysis of the Mechanical Design](#)
- [Test](#)
 - [Thermal](#)
 - [Mechanical](#)
 - [Electrical](#)
 - [Radiation and Other Environmental Effects](#)
- [Feedback/Reporting](#)

- [TVA Process Flow Used for Advanced Interconnect, Packaging and EEE Parts Technology Validation](#)

- [Background](#)

TVA Group Members

[Home](#)

[Current Projects](#)

[Past Topics in...](#)

[TVA Library](#)

[Validation Methods](#)

[TVA Group Members](#)

[Links](#)

[Site Index](#)

Click on the name of the person you want to know more about.

For questions or inquiries, feel free to contact someone by phone or email!

- [Dr. Mark Fan](#)
- [Dr. Henning Leidecker](#)
- [Melanie Ott](#)
- [Jeannette Plante](#)
- [Harry Shaw](#)
- [Bob Cummings](#)
- [Steve Waterbury](#)

Links

Home

Current Projects

Past Topics in...

TVA Library

Validation Methods

TVA Group Members

Links

Site Index

General Links






- [EPIMS-WEB](#) (space parts information database)
- [Radiation Effects Homepage](#)
- [EEE Links: NASA Parts, Packaging, Processes and Materials Newsletter.](#)
- [Cosmic Ray Effects on Micro Electronics Homepage](#)
- [Parts Inventory at Vendors](#)
- [Component Technologies & Radiation Effects Branch](#) (Code 562)

Photonics Links

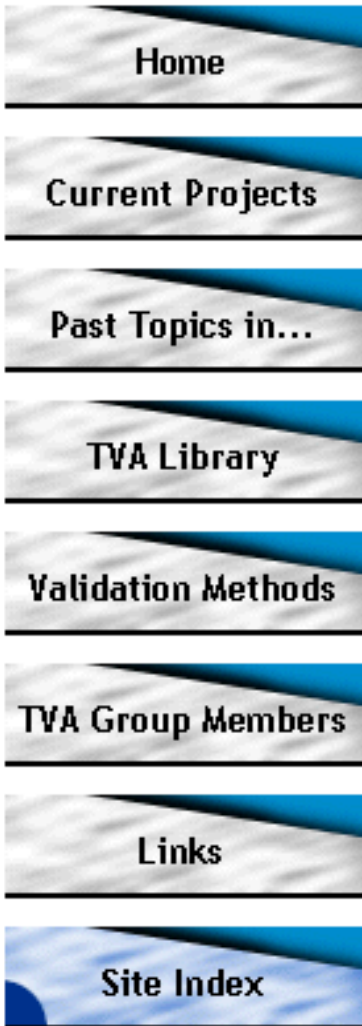
- [Photonics.com](#)
- [Lasers and Optronics Online](#)
- [SPIE Web: OE Reports](#)
- [IEEE Lasers & Electro-Optics Society](#)
- [Fiber Optic Product Review Online](#)
- [The Photonics Resource Center](#)
- [Laser Focus World](#)
- [ThorLabs, Inc.](#)
- [OpticsNet](#)
- [FOTEC](#)
- [Melles Griot Online](#)
- [Oriel Instruments](#)
- [Lumitek International, Inc.](#)
- [Broadband Guide](#)
- [Spectra-Physics: The Solid State Physics Company](#)
- [Halbo Optics On-Line Product Guide](#)
- [Pave Technology Co.](#)
- [Photonics Yellow Pages](#)
- [Fusite](#)
- [International Light](#)

 [Optical Networks Incorporated / University of Arkansas](#)

FEA Links

-  [Finite Element Resources](#)
-  [FEM Software](#)
-  [Engineering Animation, Inc.](#)
-  [MSC \(Patran, etc.\)](#)
-  [ABAQUS Product suite](#)

Site Index



Don't have time to browse? Here's a quick index...

● [Current Projects...](#)

- [Photonic and Fiber Optic Documents \(TVA Library\)](#)
- [Diamond Substrate Heat-Spreader for Space-Based X-Band Power MMICs](#)
- [Laser Light in Fiber Optic Communication](#)
- [Reworkable Underfill Characterization](#)
- [NEPP Deliverables](#)

● [Past topics in...](#)

- [Photonics](#)
- [Advanced Electronic Packaging](#)
- [Fluid Embedded Electronics - The DDF Task](#)
- [Synthetic Diamond: Thermal and Interconnect Strategies](#)
- also see [TVA Library](#) for past and present documents

● [TVA Library...](#)

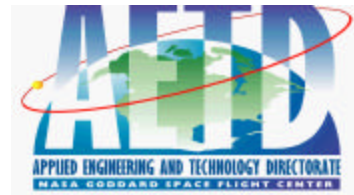
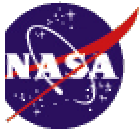
- [Photonic and Fiber Optic Documents](#)
- [Advanced Electronic Packaging Documents](#)
- [All Other TVA Documents](#)
- [NEPP Deliverables](#)
- [1998 Advanced Interconnect Program Deliverables](#)

● [Validation Methods...](#)

- [Overview](#)
- [Process Analysis](#)
- [Construction and Materials Analysis](#)
- [Structural/Thermal Analysis of the Mechanical Design](#)
- [Test](#)
- [Feedback/Reporting](#)

● [TVA Group Members...](#)

● [Links...](#)



Characterization of the Twelve Channel 100/140 Micron Optical Fiber, Ribbon Cable and MTP Array Connector Assembly for Space Flight Environments.

Melanie Ott, Sigma Research & Engineering
301-286-0127
melanie.ott@gsfc.nasa.gov

Shawn Macmurphy, Sigma Research & Engineering

Patricia Friedberg, NASA GSFC
Code 562
NASA Goddard Space Flight Center

Abstract

Presented here is the second set of testing conducted by the Technology Validation Laboratory for Photonics at NASA Goddard Space Flight Center on the 12 optical fiber ribbon cable with MTP array connector for space flight environments. In the first set of testing the commercial 62.5/125 cable assembly was characterized using space flight parameters (published in SPIE Vol. 3440).[1] The testing showed that the cable assembly would survive a typical space flight mission with the exception of a vacuum environment. Two enhancements were conducted to the existing technology to better suit the vacuum environment as well as the existing optoelectronics and increase the reliability of the assembly during vibration. The MTP assembly characterized here has a 100/140 optical commercial fiber and non outgassing connector and cable components. The characterization for this enhanced fiber optic cable assembly involved vibration, thermal and radiation testing. The data and results of this characterization study are presented which include optical in-situ testing.

Background

This is a follow up paper to the publication entitled "Twelve channel optical fiber connector assembly: from commercial off the shelf to space flight use". SPIE vol. 3440. In the first paper the commercial version of the MTP and ribbon cable assembly was investigated and suggestions were made to enhance its performance. This paper investigates the results of those enhancements through performance testing. The twelve fiber ribbon cable with MTP array connector was selected to support the cable harnessing for the Spaceborne Fiber Optic Data Bus (SFODB) on space flight missions selected to utilize this communications system. The ribbon cable itself was selected with a Kynar jacket and manufactured by W.L. Gore. The MTP connector with the two enhancements mentioned above was manufactured by USCONEC. The terminations were fabricated by USCONEC using space flight procedures as adjusted to the array connectors and with compliance to NASA-STD-8739.5.

Originally a materials analysis was conducted on the commercially available 62.5/125 micron ribbon cable and MTP array connector assembly to determine which materials would be suitable for a vacuum environment. The analysis led to the enhancements of the boot and ferrule boot components of the connector.

A second enhancement to increase the reliability of the connection link during vibration was made to the commercially available cable/connector assembly. The ferrule size was changed from the 125 micron hole size to the 140 micron hole size to accommodate the 100/140 micron optical fiber that was preferred by the optoelectronics provider for the SFODB system.

The types of testing chosen for this study was designed to bring out known failure mechanisms of the cable assembly system and this sequence of environmental testing was developed based on previous research.[2-4] This characterization study was conducted in three sections 1) vibration characterization, 2) thermal characterization and 3) radiation characterization, respectively. The sequence of testing was conducted in this order with visual inspections before and after each test and optical performance monitoring conducted in-situ for some channels based on available equipment.

Experimental Summary

Three mated pair connector/cable assemblies were tested of length 5.24 m and the sequence and summary of testing is in table 1.

Table 1: Cable Channels monitored during testing

Test	Cable Designation	Channel Optically Monitored	Channel Visual Inspection
Vibration	DUTA	1,3,5,6,8,10,12	All
	DUTB	1,3,5,6,8,10,12	All
	DUTC	1,3,5,6,8,10,12	All
Thermal	DUTA	1, 5, 8, 12	All
	DUTB	1, 5, 12	All
	DUTC	1,3,5,6,8,10,12	All
Radiation	DUTA	12	All
	DUTB	12	All

A visual and optical performance verification was performed prior to any environmental testing on all Device Under Test (DUT) cable sets and testing fan out cables. Three mated pairs of cables were tested during vibration and thermal and two of the three cables were testing during radiation characterization.

Vibration Characterization

The main purpose of the vibration testing was to verify that the MTP assemblies would in fact survive typical launch vehicle conditions. In addition however, an interrupt test was conducted to verify whether the connector assemblies could be in operation during a launch.

The MTP ribbon connector assemblies were tested in three dimensions x, y, and z. The same fixturing and axis conventions were used as were used during the research conducted in 1998 [1]. The HP81552SM 1310 nm laser source was used for in-situ testing, coupled into a 1 X 8 100/140 micron diameter optical fiber coupler. The coupler mated to the input fan out cable and then into lead cables that mated to the DUT mated

pair that was attached to the vibration shaker fixturing. Figure 1A shows the z axis mounting of the MTP assemblies on the vibration shaker and Figure 1B shows the entire set up for the vibration characterization.

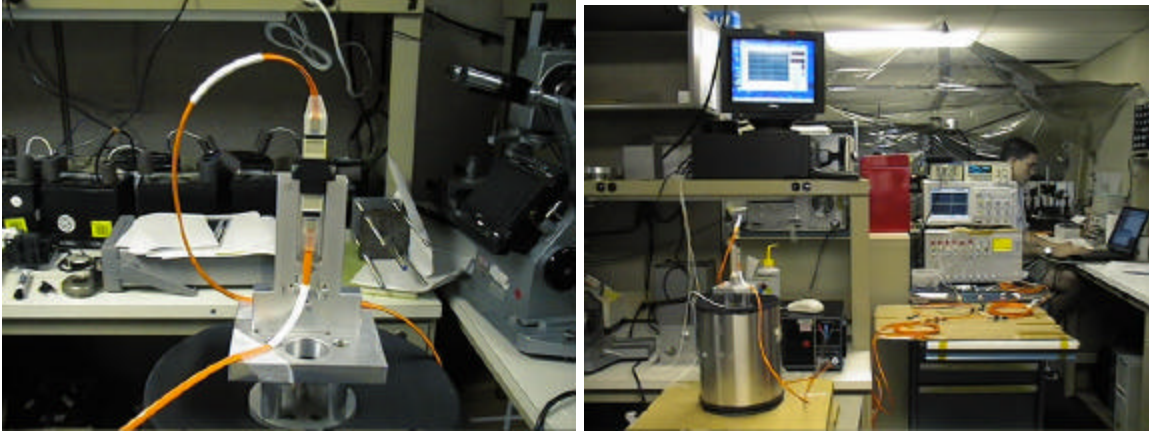


Figure 1, 1A: Z axis fixturing of the MTP connectors, 1B: Experimental setup for vibration characterization of MTP assemblies.

During axis test, channel six was monitored with an optical to electrical converter and oscilloscope in order to detect interrupts occurring larger than a 25 micro second sampling rate. The remaining channels were monitored via the HP8166 multichannel optical power multimeter.

The parameters used for this testing are summarized in Table 2.

Table 2: Vibration profile for MTP vibration testing

Frequency (Hz)	Protoflight Level
20	.052 g ² /Hz
20-50	+6 dB/octave
50-800	.32 g ² /Hz
800-2000	-6 dB/octave
2000	.052 g ² /Hz
Overall	20.0 grms

The duration for testing at each axis position was three minutes and the axis sequence of testing was x, y, z respectively. After each axis test was completed, all optical fiber end faces were visually inspected for damage. Optical data was collected during the testing and recorded via lap top computers to excel spreadsheet files using custom written Labview data acquisition programs.

Vibration Characterization Results

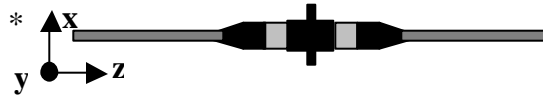
For each mated pair cable assembly under test, two types of optical in-situ testing was conducted. For each DUT, six channels were monitored actively with the HP8166 for transmission interruptions or “static” losses that occur slowly while testing. One channel, channel six, of each mated pair was monitored with an optical to electrical (O/E) converter and digital oscilloscope to measure intermittent transmission losses. A 25 microsec sampling rate was the shortest sampling rate we attained for the in-situ

“dynamic” monitoring of channel six. Again, the point was to monitor for events that signified a drop out of optical power transmission (or transient) through the mated pair. For each axis, this data was collected for each mated pair. The laser source was monitored during data acquisition from the HP8166 such that the variation of the laser power was subtracted from variations in transmission as a result of the vibration. Concluding each axis test, a visual inspection of the MTP endface was performed and as a result no damage was detected as compared to the initial state of each connector endface recorded prior to testing.

In Table 3 the data is summarized for each cable and axis test, in the order the tests were conducted. The data presented is for channel six of each cable set tested using a 25 microsec sampling rate.

Table 3: Vibration induced events (dynamic losses) for channel six of each cable Assembly, mated pair for each axis

DUT Test Set	Vibration Test Axis*	Loss events registering below noise level
A	X	Less than 1.2 dB
A	Y	Less than 0.1 dB
A	Z	Less than 0.1 dB
B	X	Less than 0.1 dB
B	Y	Less than 0.1 dB
B	Z	Less than 0.1 dB
C	X	Less than 0.1 dB
C	Y	Less than 0.1 dB
C	Z	Less than 0.2 dB



With the exception of DUT A during the x axis orientation vibration test, most of the event losses were around or less than 0.1 dB and the events lasted no more than the sample rate of 25 microsec. Figure 2 is an example of the data summarized in Table 3. In this example the mated pair set is DUT A and the test is along the y axis for detecting negative transients below the noise. The test duration was 3 minutes or 180 seconds and data just before and after the vibration test for a few seconds is recorded as well.

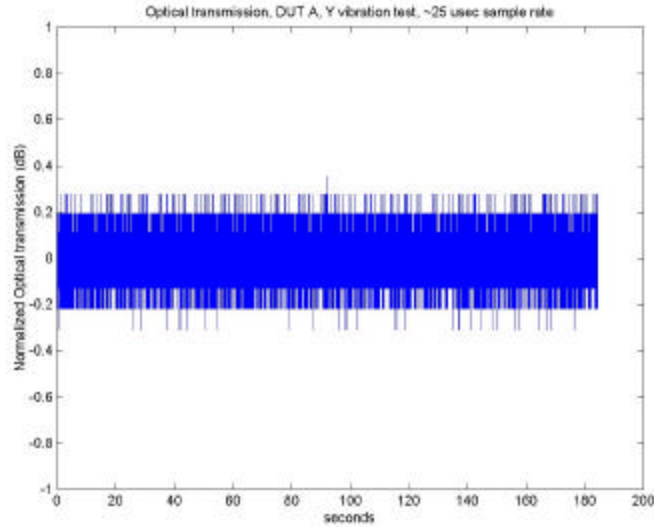


Figure 2: Optical transmission, normalized (dB) vs. time in seconds for the y axis vibration test of DUT A using a 25 micro second sampling rate.

In Table 4, the vibration data is summarized for the remaining channels that were monitored optically during testing for “static” losses. The data summarized in Table 4 represents the slow losses measured at approximately a 5 sec sample rate. These are referred to as the static losses because they are slow changes in transmission performance that occur as a result of vibration induced effects. The source noise, which was never greater than .03 dB max at any given time, was subtracted out of the final data summary.

Table 4: Summary of MTP vibration data (static losses) on channels 1,3,5,8,10, & 12.

Cable Assembly (DUT)	Axis Test	Transmission Loss Recorded
A	X	Less than .08 dB
A	Y	Less than .10 dB
A	Z	Less than .11 dB
B	X	Less than .13 dB
B	Y	Less than .35 dB
B	Z	Less than .03 dB
C	X	Less than .15 dB
C	Y	Less than .40 dB
C	Z	Less than .28 dB

Figures 3 through 11 display the data summarized above in Table 4 for each test. These graphs represent the “static” losses as a result of vibration testing during the three minute test. In some cases it can be noted that the performance during the static or slower monitoring of the transmission is similar to the channel six dynamic high speed tests summarized in Table 3 and in other cases some of the monitored channels show a shift in alignment of the MTP interconnection during the testing. Some cable data shows some channels shift into a gain transmission situation while other cables show decrease in optical transmission. This can be seen in Figure 6 during the y vibration testing of DUT B and could be due to a twisting along the z direction. In Figure 7 the z axis testing of DUT

B there seems to be a gain over the duration of the testing. This could indicate a movement along the x axis that could cause better alignment along this axis. Another cause for this would be if the connectors are not actually physically touching as they are supposed to do when inside the connector adapter, they could be moving uniformly in the z direction and forcing a better physical contact between the two interfaces of each connector end. In all cases the losses never exceeded 0.5 dB for any of the channels tested and none of the optical fiber interfaces were damaged as a result of the vibration launch conditions used in this experiment. This fact was verified through visual inspection.

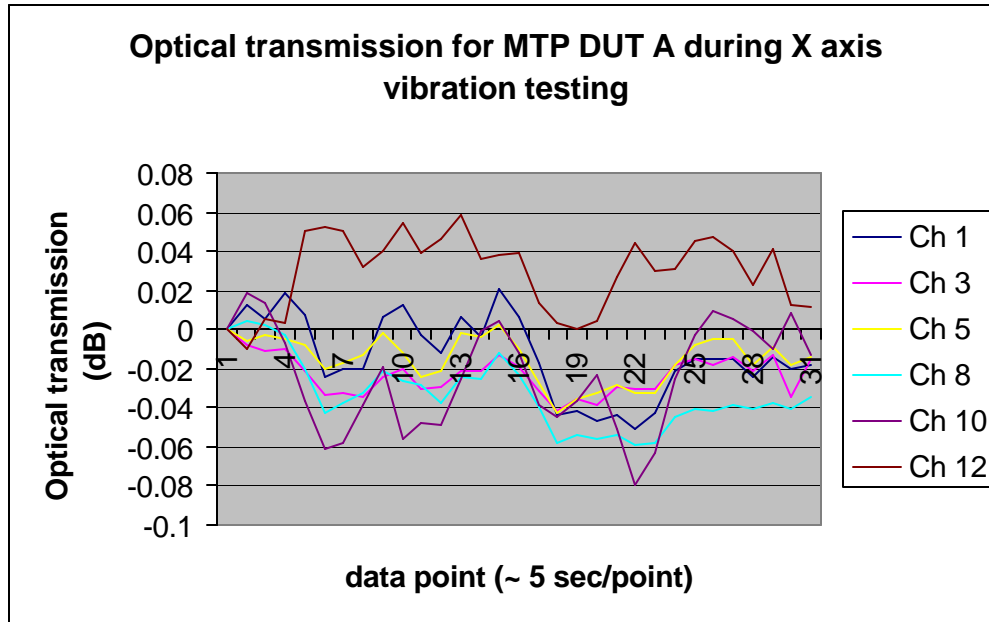


Figure 3: In-situ optical data of DUT A during X vibration testing for all channels monitored: 1,2,3,5,8,10 and 12.

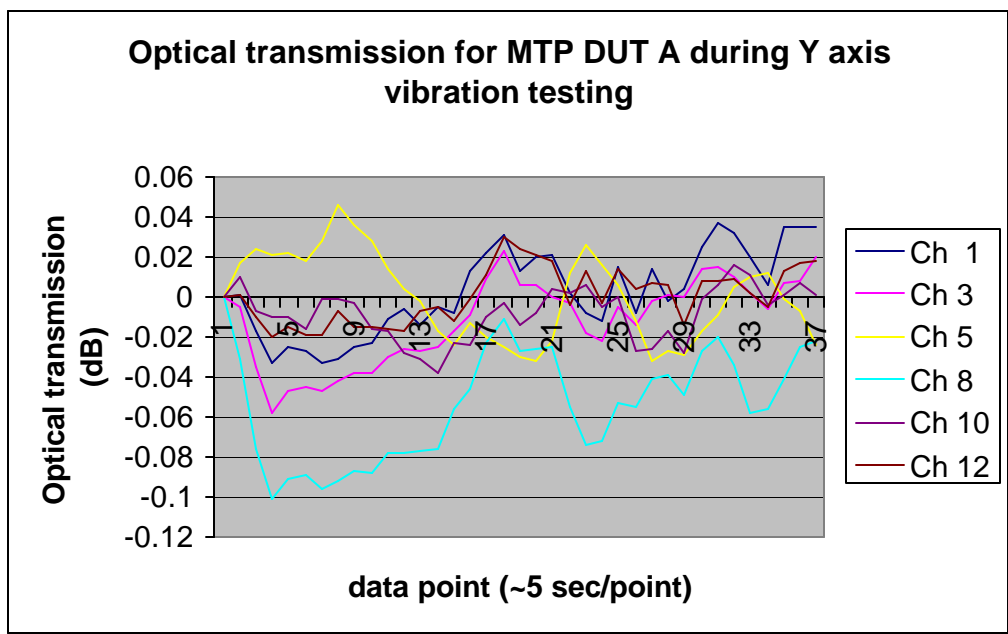


Figure 4: In-situ optical data of DUT A during Y vibration testing for all channels monitored 1,2,3,5,8,10 and 12.

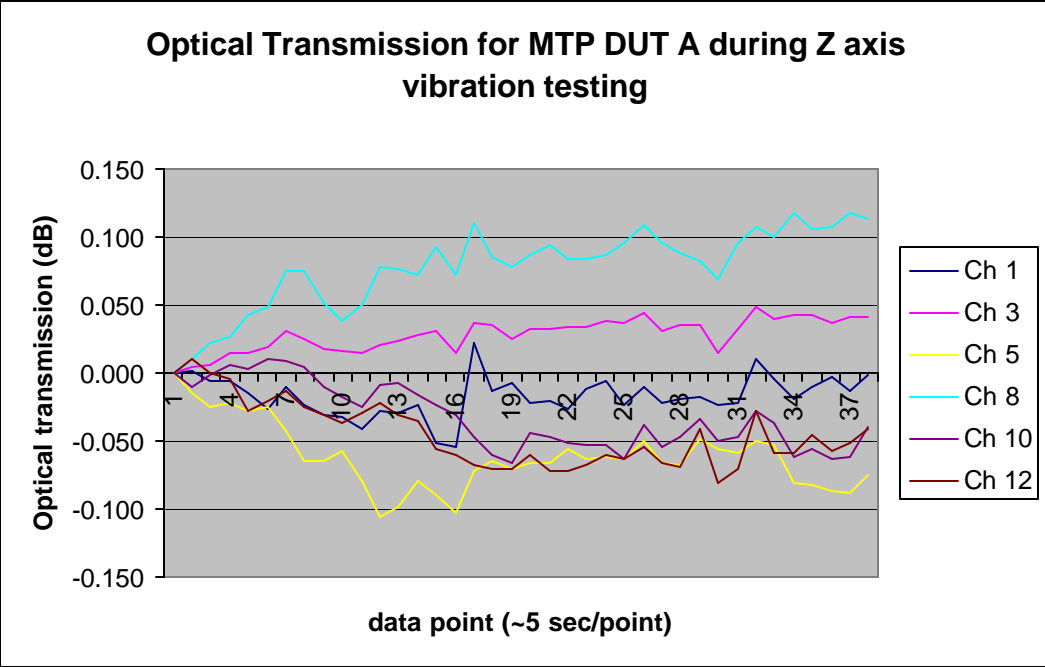


Figure 5: In-situ optical data of DUT A during Z vibration testing for all channels monitored 1,2,3,5,8,10 and 12.

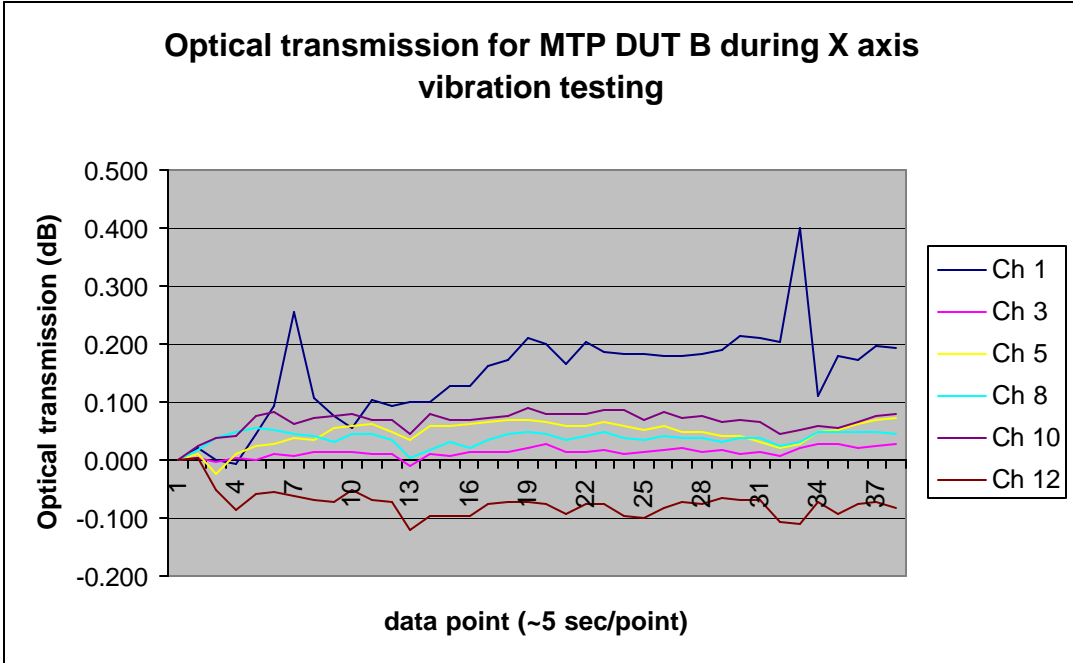


Figure 6: In-situ optical data of DUT B during X vibration testing for all channels monitored 1,2,3,5,8,10 and 12.

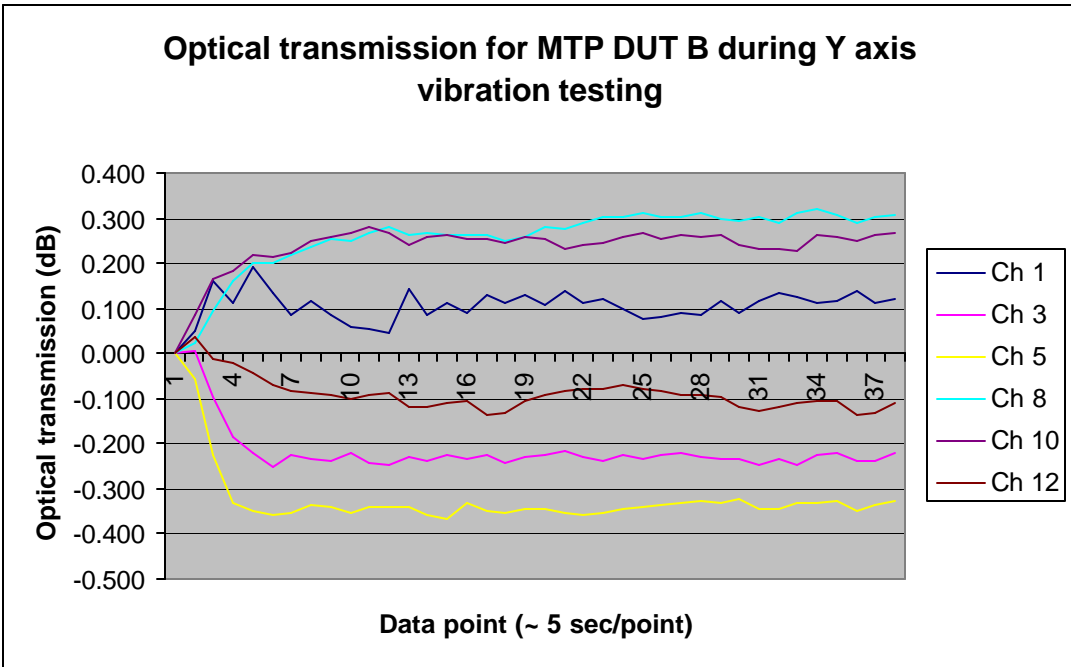


Figure 7: In-situ optical data of DUT B during Y vibration testing for all channels monitored 1,2,3,5,8,10 and 12.

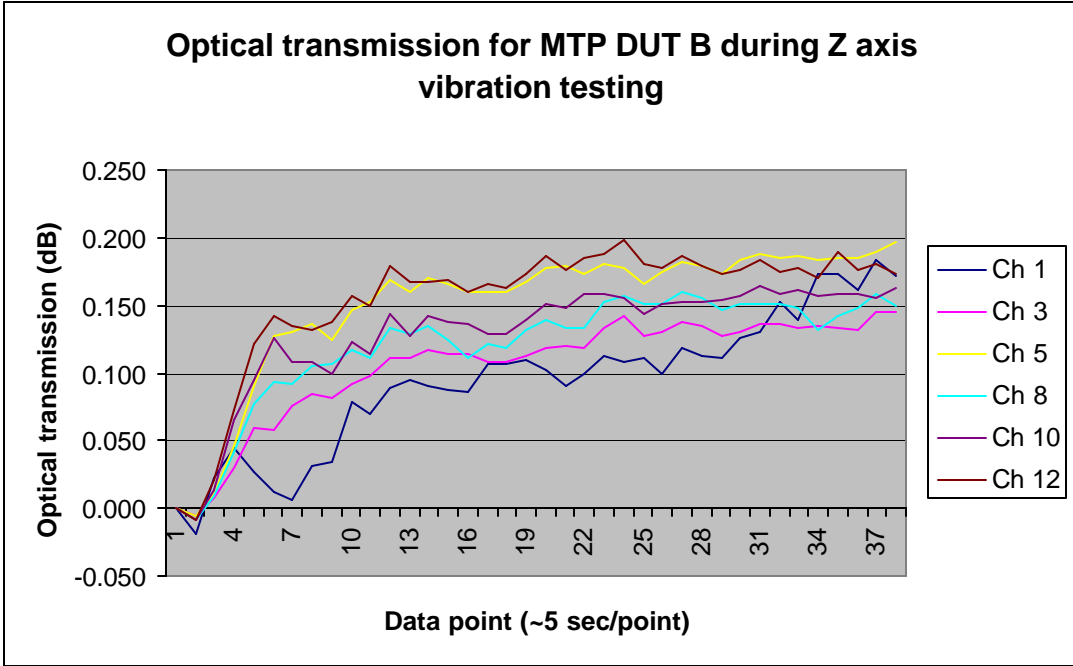


Figure 8: In-situ optical data of DUT B during Z vibration testing for all channels monitored 1,2,3,5,8,10 and 12.

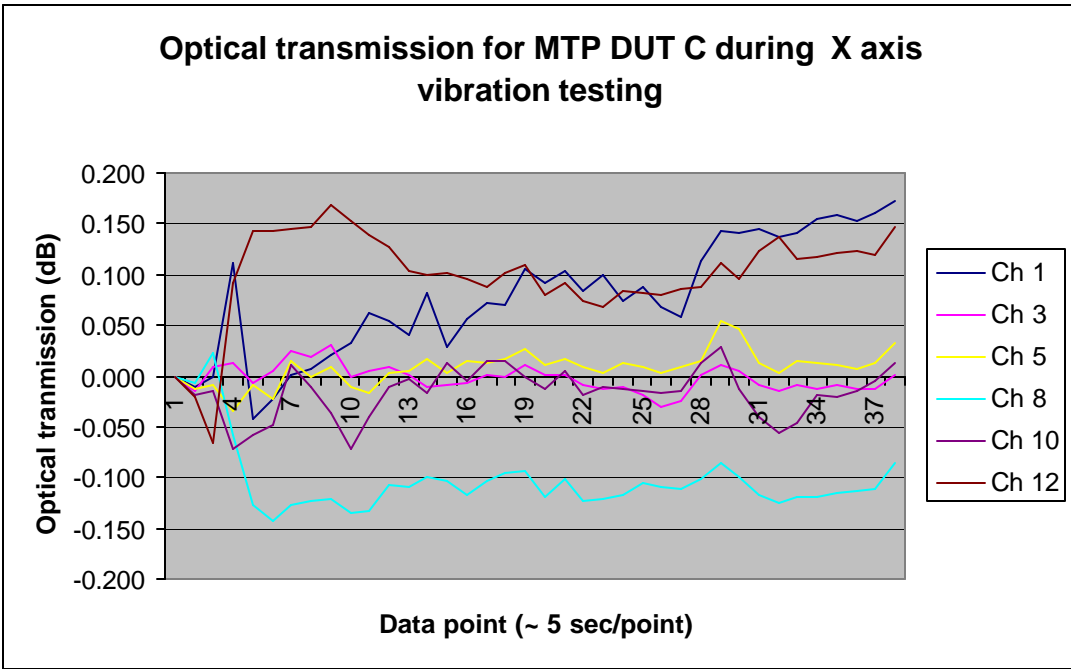


Figure 9: In-situ optical data of DUT C during X vibration testing for all channels monitored 1,2,3,5,8,10 and 12.

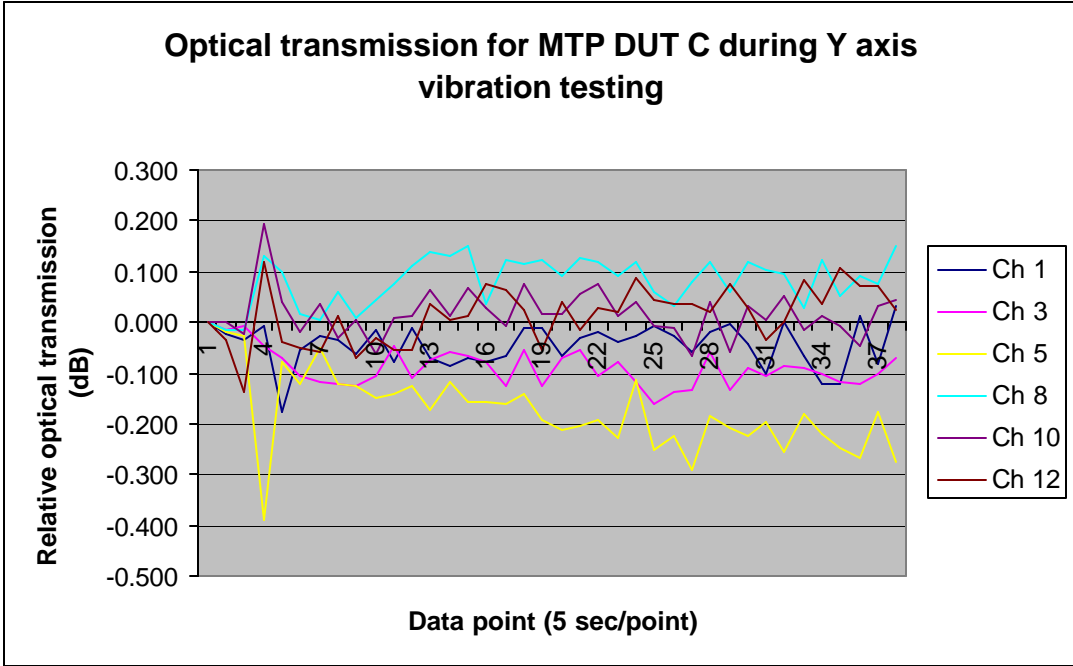


Figure 10: In-situ optical data of DUT C during Y vibration testing for all channels monitored 1,2,3,5,8,10 and 12.

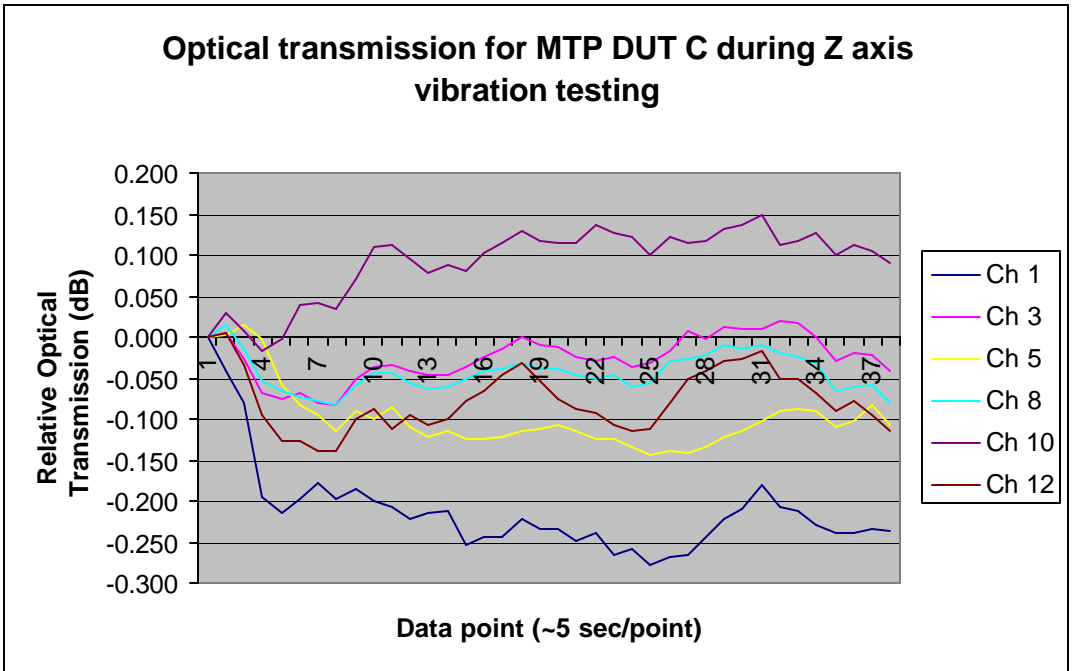


Figure 11: In-situ optical data of DUT C during Z vibration testing for all channels monitored 1,2,3,5,8,10 and 12.

Thermal Characterization

The MTP DUTs (mated pairs) were placed inside the thermal chamber with the other ends just outside the chamber and mated to the fan out cables that connect the MTP connector to individual channels on the HP8166. The bulk of the 5.24 m was inside the chamber. As in the experimental set up for the vibration test, the same laser source was used. The environmental parameters were 38 cycles for DUT A and B, and 18 cycles for DUT C, from -20°C to $+85^{\circ}\text{C}$, with a ramp rate of $1^{\circ}\text{C}/\text{min}$ and dwell times at the extremes of 25 minutes. The source light was coupled into eight optical fibers and then connected to the MTP fan out cables which in turn connected to the test set (DUT) mated pair that was inside the thermal chamber. DUT A and DUT B were tested using the same pair of fan out cables and were monitored for 38 thermal cycles. DUT C was monitored for a total of 18 thermal cycles.



Figure 12: Two views of the optical monitoring experimental set up that was used during thermal cycling testing.

Thermal Results:

The data and summary of results are presented in Table 5. The source power drift was subtracted from the data such that only changes as a result of thermal testing would be presented. In the summary in Table 5, the data is described in column three by the maximum amount of thermally induced power changes within a single optical cycle. In the last column the data is described but the total amount of thermally induced power changes during testing or the difference between the maximum measured optical transmission and the minimum measured optical transmission. The data is not normalized for the length of cable tested because there was a mated pair included in the oven during testing which introduces other types of variables in addition to thermal related expansion and contraction of the cable components themselves.

Table 5: Summary of thermal induced optical transmission changes for all cable channels tested for DUT A, B & C.

DUT Cable	Channel of DUT	Maximum Transmission Δ within a cycle	Maximum Δ over entire test duration.
A	1	1.6 dB	1.8 dB
A	5	0.8 dB	1.3 dB
A	8	0.1 dB	1.4 dB
A	12	1.2 dB	1.4 dB
B	1	0.9 dB	1.2 dB
B	5	1.2 dB	1.9 dB
B	12	0.8 dB	1.1 dB
C	1	1.4 dB	1.6 dB
C	3	1.3 dB	1.3 dB
C	5	1.0 dB	1.2 dB
C	6	0.9 dB	1.6 dB
C	8	0.7 dB	1.0 dB
C	10	1.3 dB	1.4 dB
C	12	1.5 dB	1.6 dB

An example of the data summarized in table 5 is shown in Figure 13. In Figure 13 the collected data for DUT A channel 8 is presented. The data can not be scaled by the length of the cables that were tested due to the mated pair of MTP connectors also under test. The most significant factor here was how much of a total change in transmittance was observed as a result of thermally induced effects.

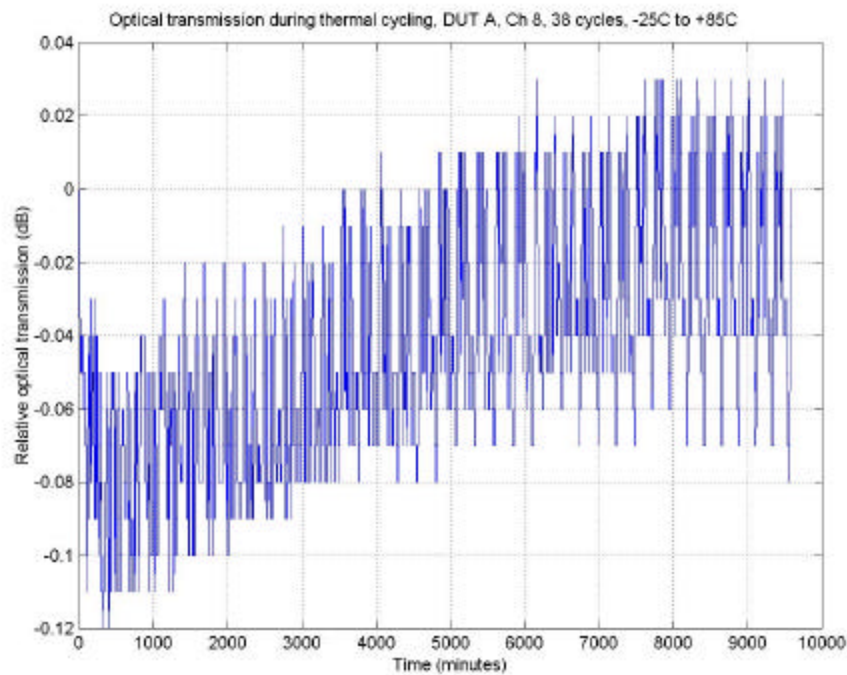


Figure 13: Thermally induced optical transmission changes for DUT A channel 8.

Again, the optical source power drift has been subtracted from the thermally induced optical transmittance changes. The average maximum transmittance change for DUT A using the channels tested was 1.48 dB, for DUT B using the three channels tested was 1.4 dB, and for DUT C for all seven channels tested was 1.39 dB. The performance of all three cables was similar in spite of the fact that DUT C was cycled 20 times less than DUT A and DUT B. A visual inspection of all mated pair end faces was conducted to verify the integrity of each channel of the optical fiber ends that were mated in the thermal chamber. All end faces passed visual inspection. No damage was noticed on all the recorded images. An example of the final visual inspection is presented in Figures 14 and 15. In Figure 14 the before and after testing visual inspection pictures are shown taken from the A side of the DUT A mated pair, for channel one. Figure 15 shows the before and after pictures for the B side of the DUT A mated pair for channel one.

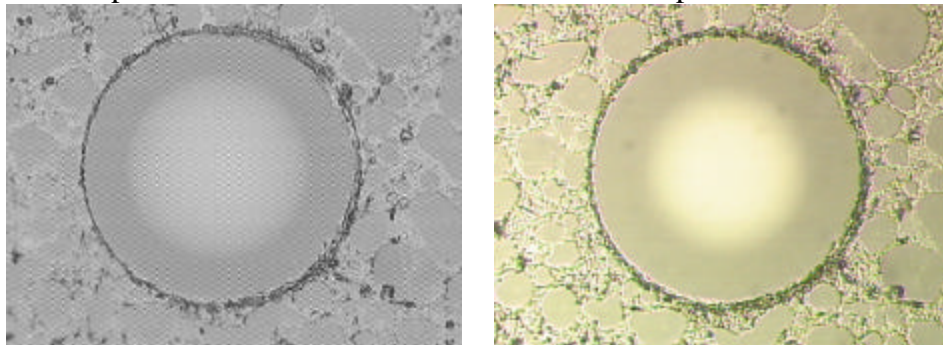


Figure 14: Cable set DUT A, connector side A on channel one before and after the vibration and thermal testing sequence.

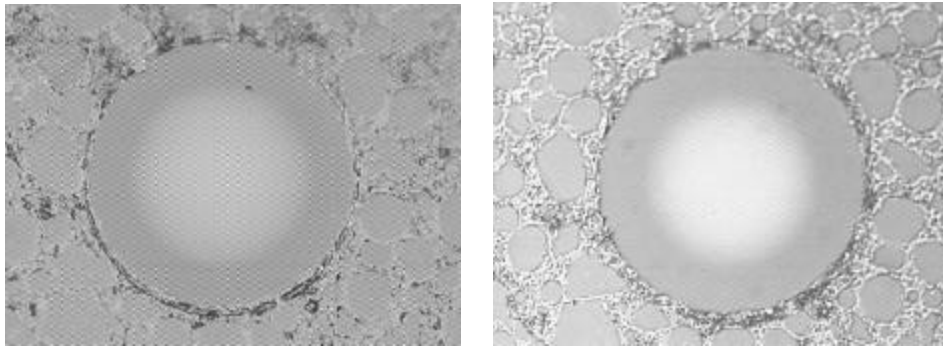


Figure 15: Cable set DUT A, connector side B on channel one before and after the vibration and thermal testing sequence.

All images collected, that total 72 images before (3 mated pairs= 6 endfaces*12 channels) and 72 images after, showed no damage as a result of the vibration and thermal sequence of testing. The complete collection of visual images is presented in Appendix A for cable set DUT A, Appendix B for cable set DUT B, and Appendix C for cable set DUT C.

Radiation Characterization:

Two of the cable assemblies were tested in a gamma radiation environment at room temperature 25 °C. DUT A and DUT B were tested for radiation effects at two different dose rates. The purpose of using DUT A and DUT B was to use the cables that had experienced the most thermal cycling or aging. Both DUT A and DUT B had been thermal cycled 38 times. The fiber inside of the cables was a 100/140/250 acrylate coated fiber that was not rated as “rad hard” and because of this is a commercial off the shelf product.

Table 6: Radiation Testing Parameters for DUT A and DUT B

Cable Set DUT	Radiation Dose Rate	Total Dose	Length*
A	4 rads/min	~ 62 Krads	5.24 m
B	27 rads/min	~ 403 Krads	5.24 m

* Length includes mated pair MTP interconnection

The dose rate and total dose for each test are summarized in Table 6. The cables were placed inside of lead box to eliminate external lower energy reflections and the dose rate inside of the box was measured and used for analysis (Table 6). Lead cables were used to connect the equipment outside of the Co60 chamber to the DUT cables. The input power to the DUT cables was attenuated such that the measured optical power at the output of the lead cable measured 0.88 microwatts CW. Measurements were made every minute and the test was started prior to opening the radiation gamma source shutter such that reference measurement could be made. The source was monitored throughout testing and source power drift was subtracted from the collected data such that it would not be included in the final analysis. A similar experimental set up was used as was used in the vibration and the thermal testing, however, an LED (RIFOCS 752L dual LED source) at 1300 nm was used as the source and an attenuator (JDS HA9 optical attenuator) was used between the output of the coupler (the input of the coupler was connected to the LED source) and the lead-in cable. The purpose was to limit the incoming optical signal to the DUT. The output lead-out cable connected the other end of the DUT to the detector equipment positioned outside of the radiation chamber. Again the HP8166 was used to detect the optical transmission signal. In both tests, channel twelve was tested. The objective of this testing was not to provide data that would necessarily would lead to an absolute model for the cable but that would provide an insight in to possible performance at room temperature. However, the data was used to provide a model that could be used to predict lower dose attenuation if all the assumptions made were correct.

Radiation characterization results

The testing for DUT A at 4 rads/minute was conducted for approximately 10 days and 18 hours. The test was continued after the radiation exposure was ceased, to gather additional recovery data. In Figure 16, the entire collected data set for DUT A during and just after radiation testing is plotted vs. time. At approximately 15489 minutes (~62 Krads) the gamma source shutter was closed, ending the radiation exposure (gamma source off). The data presented has the LED source variations subtracted from the data.

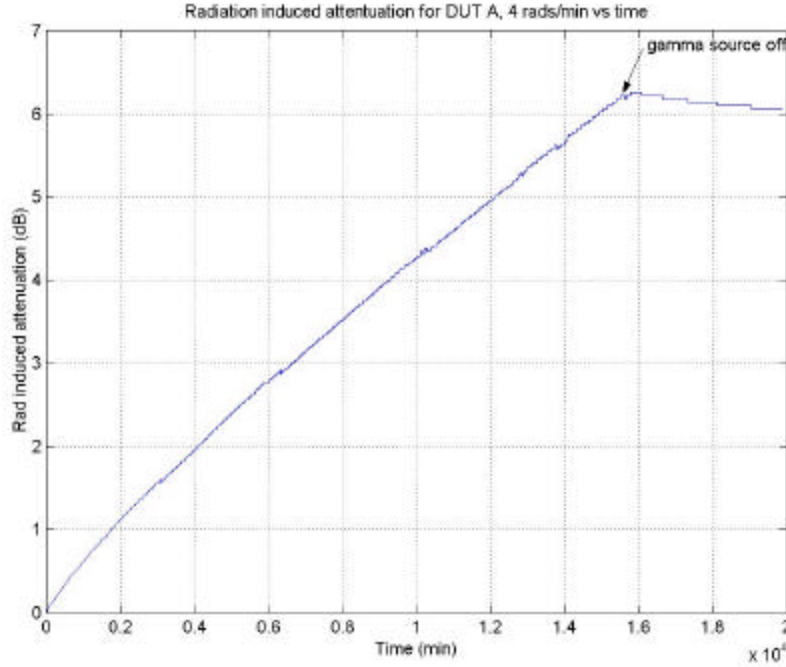


Figure 16: Radiation induced attenuation with recovery data for DUT A tested at 4 rads/min to a total of ~ 62 Krads,

The radiation induced attenuation for DUT A ends at 6.18 dB (15489 minutes) and over the next 3 days recovers to only 6 dB induced attenuation. The equation that describes the radiation induced attenuation during the exposure is

$$A(D)=8.9*10^{-4}D^{.8007}, \quad (1)$$

where $A(D)$ is the radiation induced attenuation and D is the total dose. The form of this equation is chosen to fit the model developed by Friebele et al [5] and used in previous reports to model the radiation induced attenuation of germanium doped fiber [3]. Figure 17 shows the data along with the curve fit for the exposure data, equation 1. The red plot is the graph of equation 1 and the blue plot is the actual radiation data during exposure of DUT A.

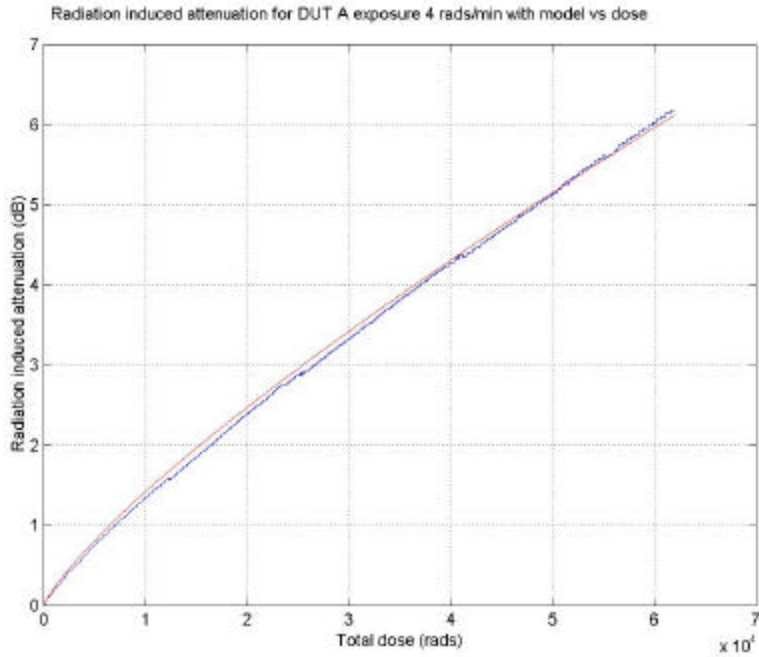


Figure 17: Radiation induced attenuation for DUT A during radiation exposure of 4 rads/min (blue) and the results of graphing equation 1 (red).

The data for the radiation exposure of DUT B possessing the same configuration and fiber from the same lot as DUT A is presented in Figure 18.

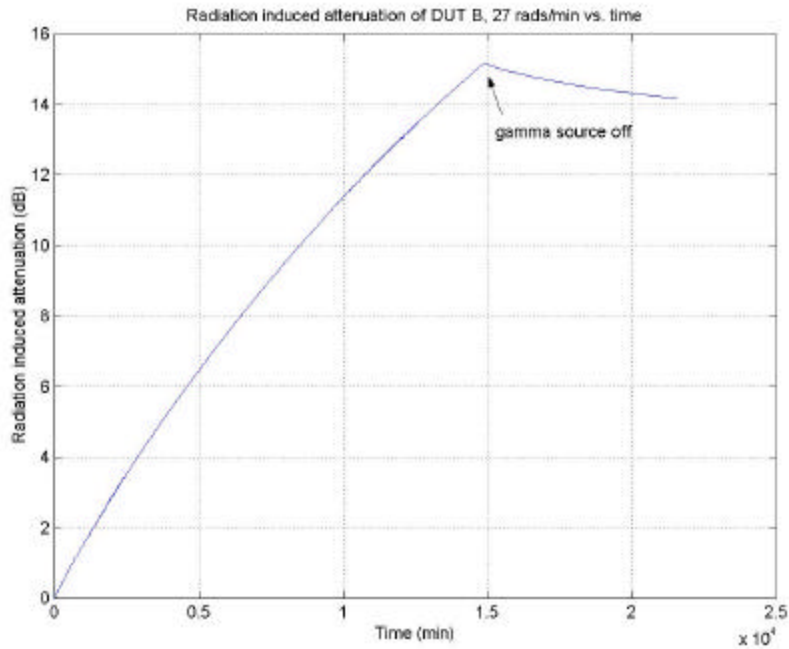


Figure 18: Radiation induced attenuation of DUT B with recovery data, exposed at 27 rads/min vs. time, to a total dose of 403 Krads.

For the 27 rads/min dose rate exposure of this cable the highest attenuation at 403 Krads was measured as 15.18 dB. The cable recovery data shows that after another 4.6 days, the attenuation drops to 14.16 dB. Based on the Friebele model and using equation 1 as a basis for the model at 27 rads/min, the equation for attenuation as a result of radiation exposure is

$$A(D) = 5.0 \cdot 10^{-4} D^{.8007} \quad (2)$$

Where again, $A(D)$ is radiation induced attenuation dependent on total dose in rads and D is total dose in rads. The model and actual data for the 27 rads/min test is presented in Figure 19.

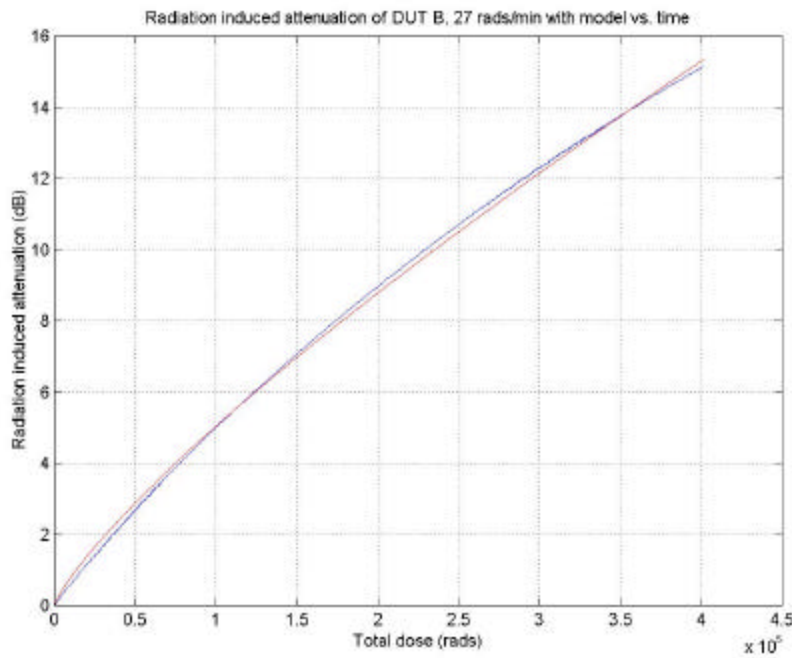


Figure 19: Radiation induced attenuation for DUT B at 27 rads/min during gamma exposure (blue) and the curve fit plot of equation 2 (red).

Based upon the model equations no general model can be derived without making new assumptions about the constant C_0 . The Friebele model takes the form:

$$A(D) = C_0 \phi^{1-f} D^f \quad (3)$$

Where ϕ is the dose rate, D is the total dose, f is less than 1, and C_0 is the constant [5]. Two sets of data are necessary to determine which f and C_0 are appropriate to use the equation for extrapolation to other dose rates. The equation is used to describe the radiation induced attenuation on typical germanium doped optical fiber. It has not been specified for cable, which is what was tested here. The value for f was determined by analysis of the two data sets and under the assumption that f is the same for both data sets, than the only variable left undetermined is C_0 . Using equation 1 where the dose rate was 4 rads/min $C_0 = 6.75 \cdot 10^{-4}$, and using equation 2 where the dose rate was 27 rads/min, $C_0 = 2.59 \cdot 10^{-4}$. The constants would need to be the same in order to write a general extrapolation expression for other dose rates. Perhaps the difference in constants

is related to the cabling used on top of the fiber or other factors when setting up the arrangement of the cable in the chamber. The cable was not spooled tightly the way fiber is usually tested and because only one channel was tested on each cable of the twelve optical fibers available, the way the cable was lying near the source could have created variations in the normal response. However, those would be normal variations that would occur in an actual space application where cable is not spooled when installed on the spacecraft.

If we assume that the cabling configuration was the largest contributing factor and did affect the constant such that it became dependent on the dose rate, than a relationship using both data sets and a linear assumption (since there are only two data sets) can be used to make a model for C_0 at other dose rates.

Solving for $C_0(\phi)$ using both data sets the expression for the constant is

$$C_0 = -1.8 \cdot 10^{-5} \phi + 7.47 \cdot 10^{-4} \quad (4)$$

Where ϕ is the dose rate and C_0 becomes the new constant in equation 3. This equation is graphed in Figure 20. Using this plot and from equation 4, as the dose rate becomes very small or less than 1 rad/min which is typical of space flight background radiation, C_0 becomes $7.47 \cdot 10^{-4}$ therefore making the dependence on dose rate for the constant a non issue.

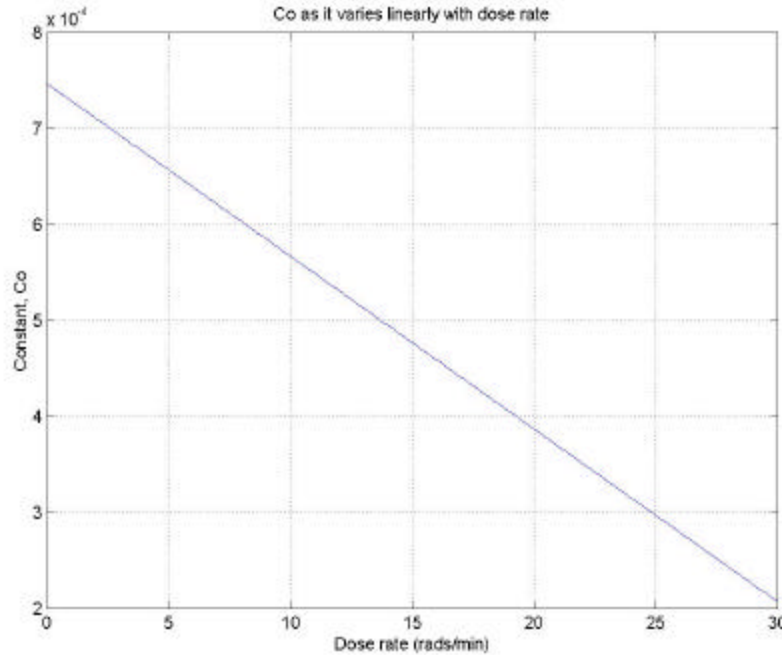


Figure 20: The constant C_0 as it varies linearly with dose rate based on equation 4.

Using the assumption that most space flight environments that will use the commercial twelve fiber ribbon cable will have back ground radiation at levels less than 1 rad/min, the expression for radiation induced attenuation can be described as:

$$A(D) = 7.47 \cdot 10^{-4} \phi^{.1993} D^{.8007} \quad (5)$$

Again, this model is only valid at very low dose rates using all the assumptions described previously.

Table 7: Radiation induced attenuation summary of actual and extrapolated data

Cable Set	Dose Rate	Total Dose	Attenuation
DUT A	4 rads/min	62 Krads	6.18 dB
DUT B	27 rads/min	403 Krads	15.18 dB
Extrapolated	.1 rads/min	100 Krads	4.75 dB
Extrapolated	.1 rads/min	10 Krads	.75 dB

Table 7 summarizes the final radiation induced attenuation for DUT A and DUT B and also gives the results of extrapolation to a 0.1 rads/min dose rate for radiation induced attenuation. These attenuation values are based on the entire 5.24 m of cable in the chamber and are not represented as attenuation/m as is usually the case. In this case the purpose was to qualify a mated cable pair such that would be used between two instruments in a space flight application. Figure 21 is the entire extrapolated data set for 0.1 rads/min up to 100Krads.

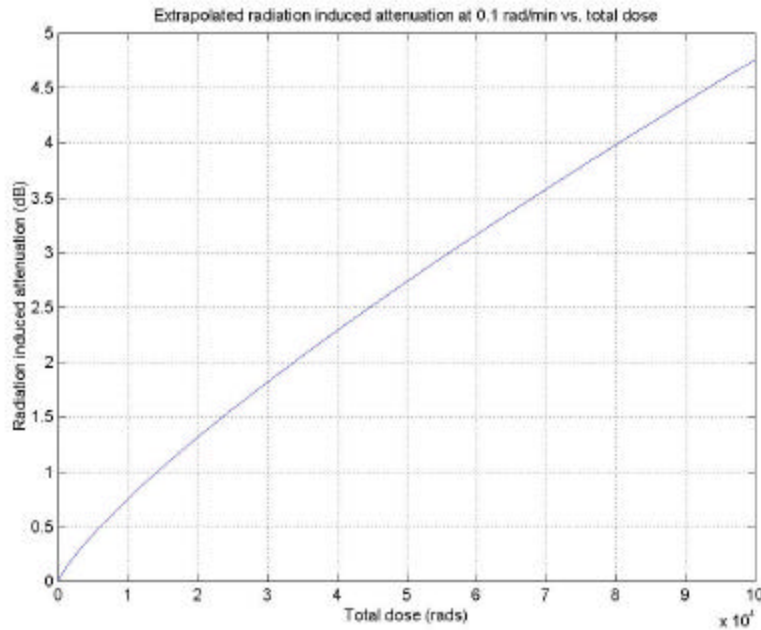


Figure 21: Extrapolated values for radiation induced attenuation using 0.1 rads/min for a total dose of 100 Krads.

Conclusions:

The twelve channel optical fiber (with 100/140/250 optical fiber) ribbon cable (W.L. Gore) assembly with USConec MTP array connector was characterized for a space flight environment using the environmental specifications for Goddard Mission GLAST. Three cable sets were tested which consisted of a mated pair of MTP connectors. The length of the mated pair was 5.24 m.

During vibration testing one channel (channel six) was optically monitored for “dynamic” transients at a 25 microsec sampling rate. Three tests were conducted per cable, one in each axis (x,y,&z) direction. There were nine tests conducted total (3 tests per cable, 3 cables). From the collected data of the nine tests conducted, six data sets showed loss transients less than 0.1 dB, one showed loss transients less than 0.2 dB, and the other showed loss transients less than 1.2 dB.

During the “static” testing (monitoring for slow changes in optical performance) of the cables, six channels on each cable assembly were optically monitored for losses as a result of vibration. The largest static losses registered were from DUT C during Y axis vibration testing at 0.4 dB.

Thermal cycling or accelerated aging tests were conducted on all three cable test sets. DUT A and DUT B were tested using 38 cycles, and 18 cycles were used for DUT C. Four channels of DUT A were optically monitored for shifts in the transmission, three channels of DUT B were monitored and seven channels of DUT C were monitored. The collected data shows that the largest overall transmission change for all the channels tested was registered from DUT B at 1.9 dB. The largest change within a cycle (thermally induced optical cycle) was recorded from DUT A channel 1. The average measured losses were 1.48 dB for DUT A, 1.4 dB for DUT B, and 1.38 dB for DUT C.

Two of the cable test sets were exposed to gamma radiation. DUT A was tested at 4 rads/min to a total dose of 62 krads and was monitored optically throughout the testing. The largest recorded radiation induced attenuation was 6.18 dB for the entire 5.24 m length just before the radiation shutter was closed. DUT B was tested at 27 rads/min to a total dose of 403 rads/min and the final radiation induced attenuation measured before ceasing exposure was 15.18 dB. Using the extrapolation method for a dose rate of 0.1 rad/min the estimated radiation induced attenuation at 10Kkrads total dose would be .75 dB for the entire 5.24 m and 4.75 dB at 100 Krads.

After all testing was completed, visual inspection data was recorded and compared to visual inspection images taken prior to testing. No damage was detected. The complete visual inspection collection of images is presented in Appendix A, B and C corresponding to the letter designation of each cable test set.

It is evident that the cable assemblies did pass characterization with minimal losses and no damaged optical endfaces. The cable/connector assemblies have proven the ability to withstand the space flight environments used for this characterization.

References:

1. Melanie N. Ott, Joy W. Bretthauer, “Twelve channel optical fiber connector assembly: from commercial off the shelf to space flight use,” Photonics For Space Environments VI, Proceedings of SPIE Vol. 3440, 1998.
2. Melanie N. Ott, Jeannette Plante, Jack Shaw, M. Ann Garrison-Darrin, “Fiber Optic Cable Assemblies for Space Flight Applications: *Issues and Remedies*,” Paper 975592 SAE/AIAA 1997 World Aviation Congress, October 13-16, Anaheim, CA.
3. Melanie N. Ott, “Fiber Optic Cable Assemblies for Space Flight II: Thermal and Radiation Effects,” Photonics For Space Environments VI, Proceedings of SPIE Vol. 3440, 1998.
4. Melanie N. Ott, Patricia Friedberg, “Technology validation of optical fiber cables for space flight environments,” Optical Devices for Fiber Communication II, Proceedings of SPIE Vol. 4216, 2001.
5. E. J. Friebele, M.E. Gingerich, D. L. Griscom, “Extrapolating Radiation-Induced Loss Measurements in Optical Fibers from the Laboratory to Real World Environments”, 4th Biennial Department of Defense Fiber Optics and Photonics Conference, March 22-24, 1994.

Appedix A

MTP optical fiber end face visual inspection images before and after environmental testing (vibration and thermal).

Before

After

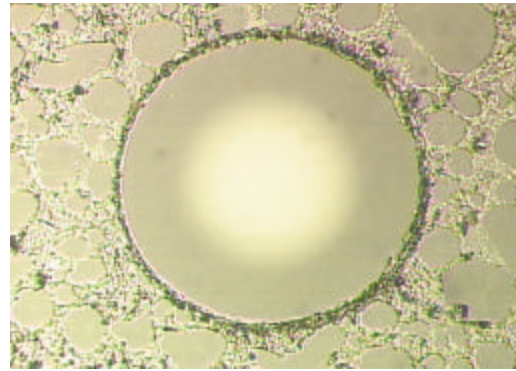
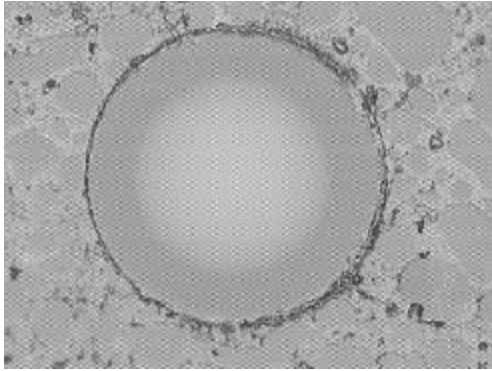


Figure A1: Cable set DUT A, Side A, Channel 1 before and after the vibration and thermal testing sequence.

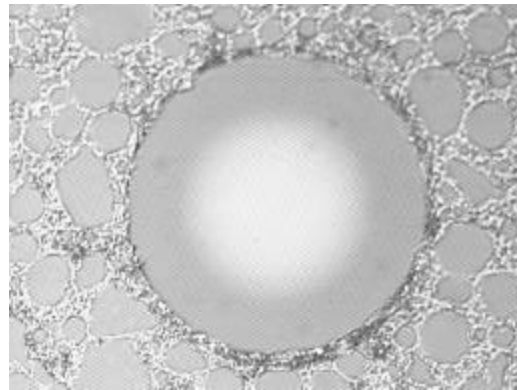
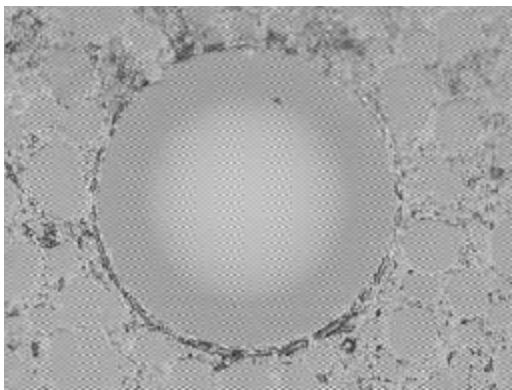


Figure A2: Cable set DUT A, Side B, Channel 1 before and after the vibration and thermal testing sequence.

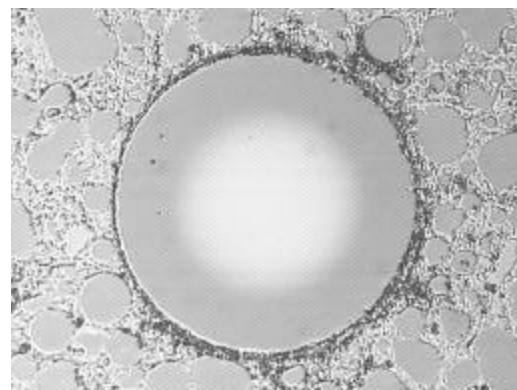
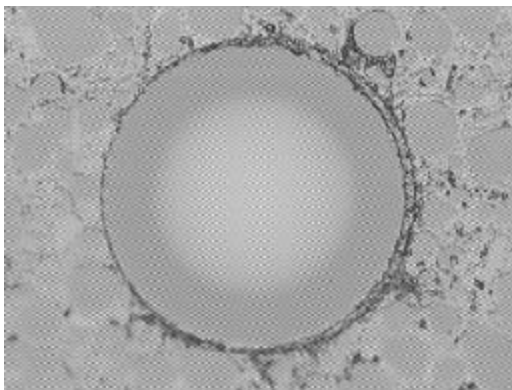


Figure A3: Cable set DUT A, Side A, Channel 2 before and after the vibration and thermal testing sequence.

Before

After

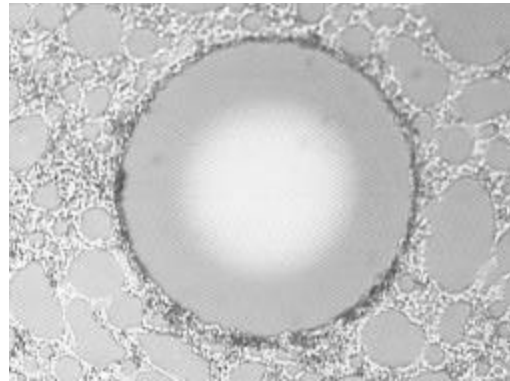
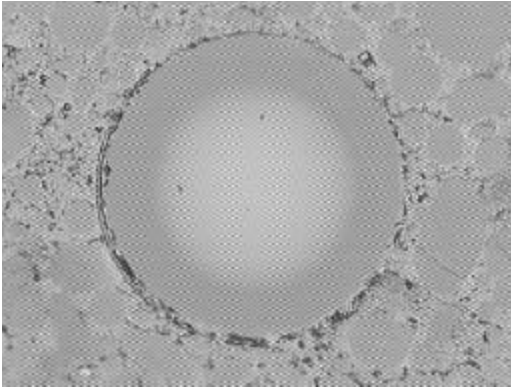


Figure A4: Cable set DUT A, Side B, Channel 2 before and after the vibration and thermal testing sequence.

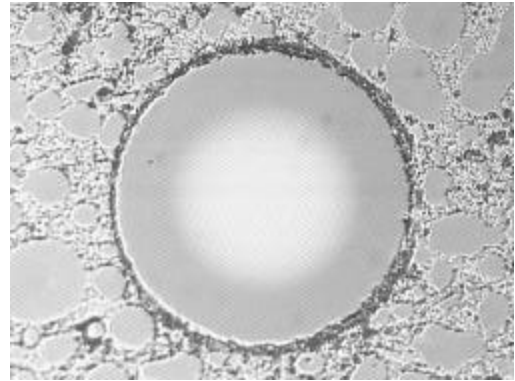
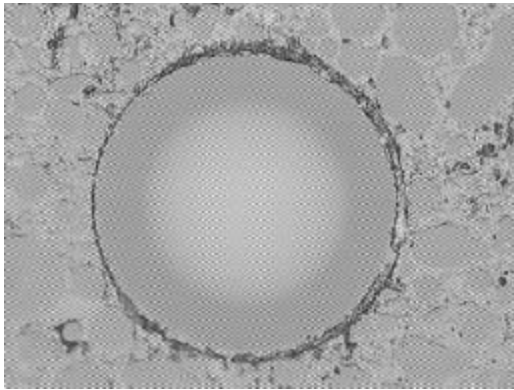


Figure A5: Cable set DUT A, Side A, Channel 3 before and after the vibration and thermal testing sequence.

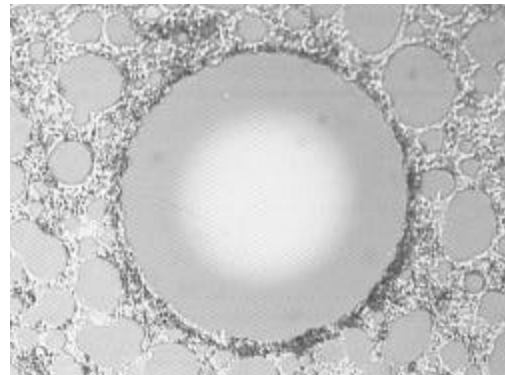
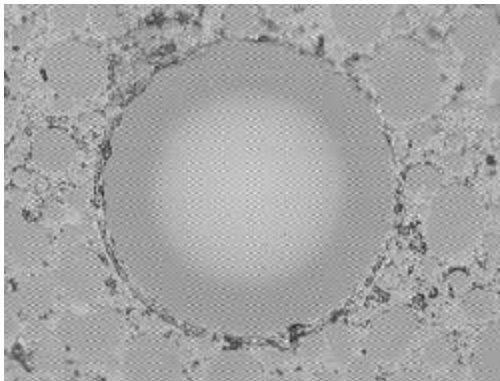


Figure A6: Cable set DUT A, Side B, Channel 3 before and after the vibration and thermal testing sequence.

Before

After

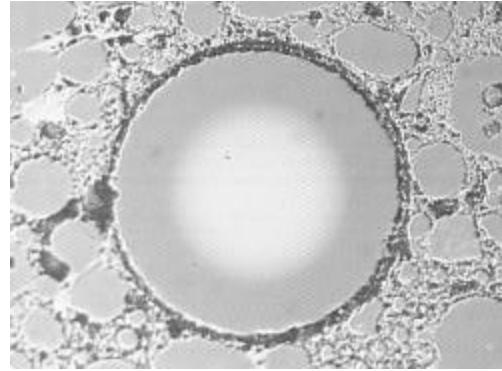
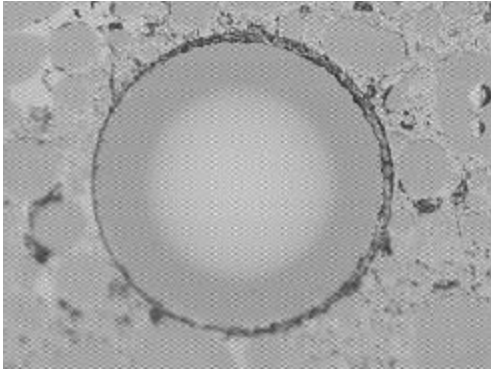


Figure A7: Cable set DUT A, Side A, Channel 4 before and after the vibration and thermal testing sequence.

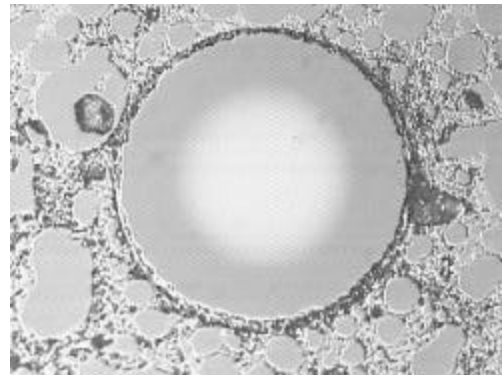
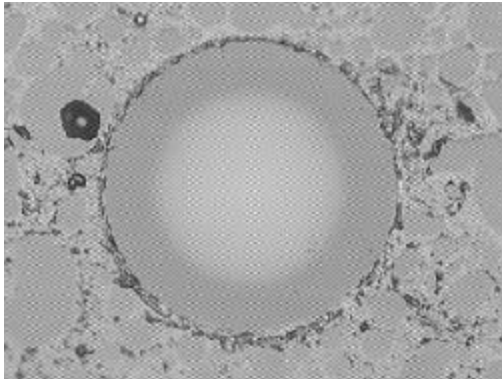


Figure A8: Cable set DUT A, Side B, Channel 4 before and after the vibration and thermal testing sequence.

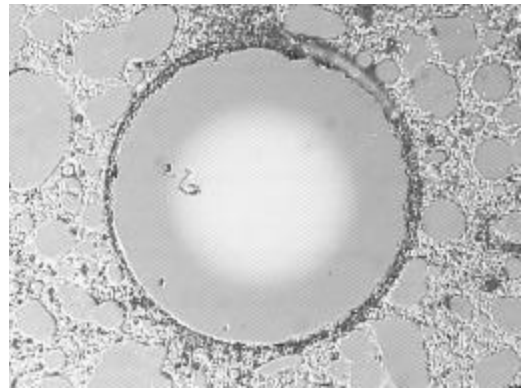
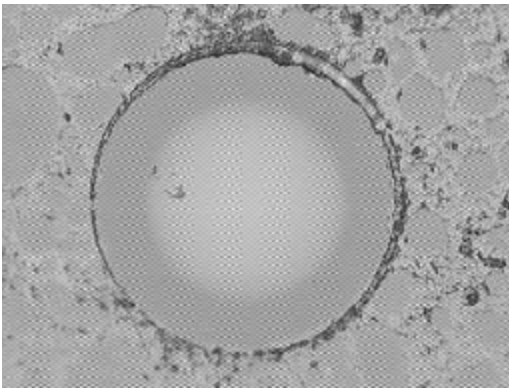


Figure A9: Cable set DUT A, Side A, Channel 5 before and after the vibration and thermal testing sequence.

Before

After

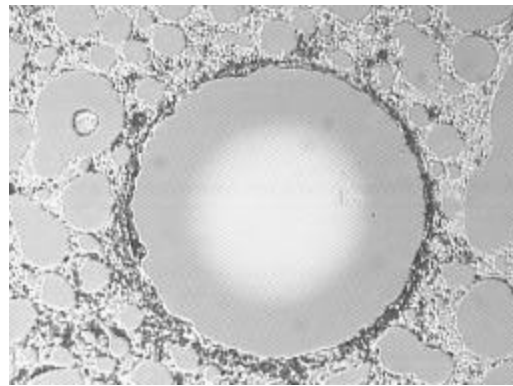
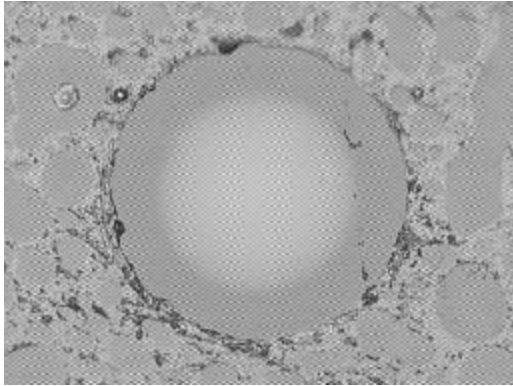


Figure A10: Cable set DUT A, Side B, Channel 5 before and after the vibration and thermal testing sequence.

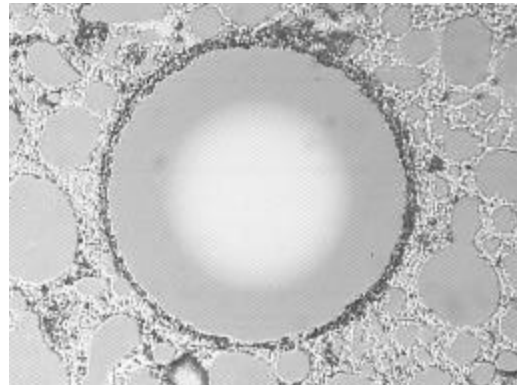
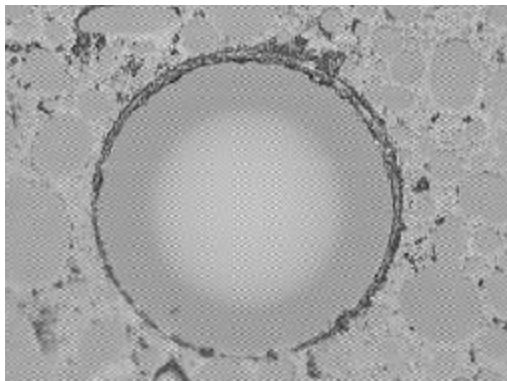


Figure A11: Cable set DUT A, Side A, Channel 6 before and after the vibration and thermal testing sequence.

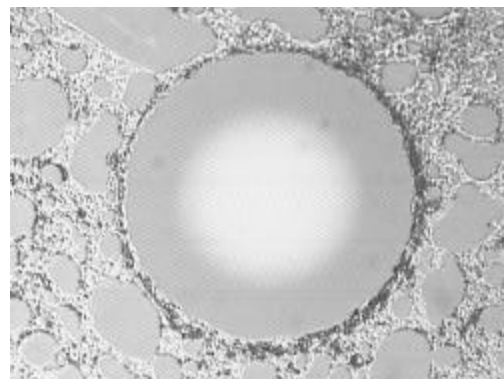
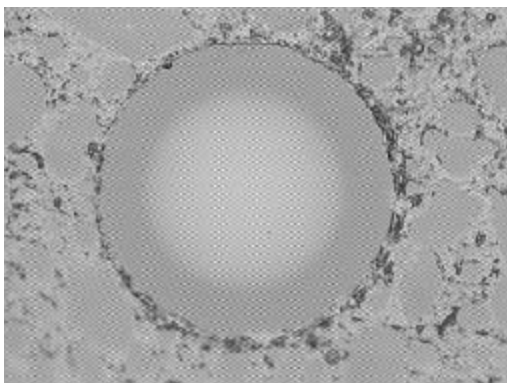


Figure A12: Cable set DUT A, Side B, Channel 6 before and after the vibration and thermal testing sequence.

Before

After

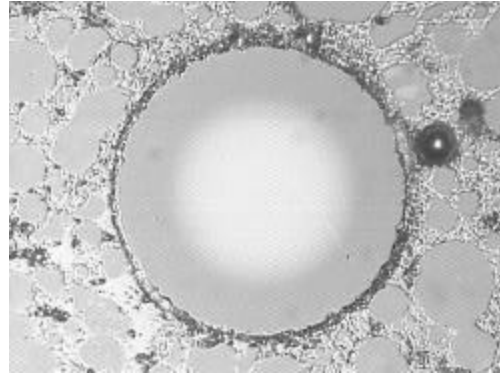
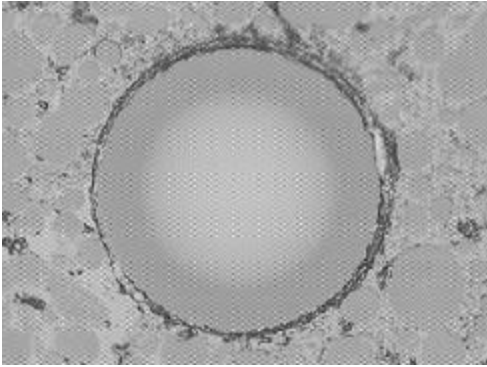


Figure A13: Cable set DUT A, Side A, Channel 7 before and after the vibration and thermal testing sequence.

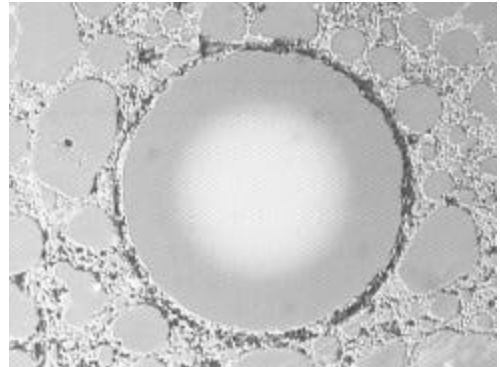
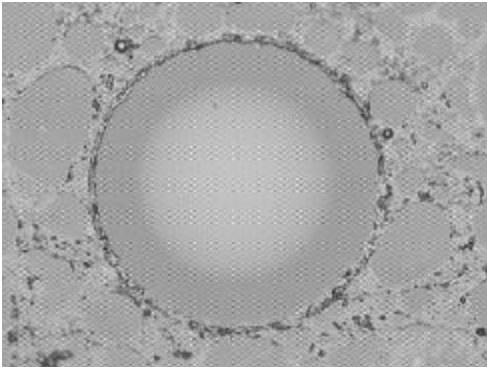


Figure A14: Cable set DUT A, Side B, Channel 7 before and after the vibration and thermal testing sequence.

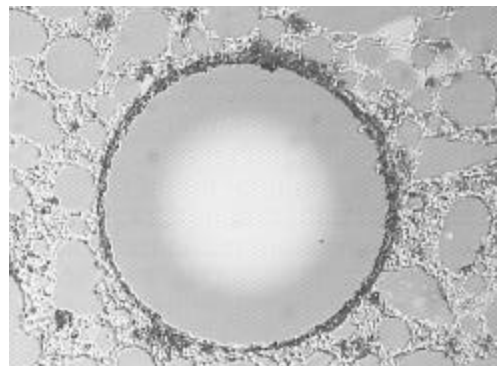
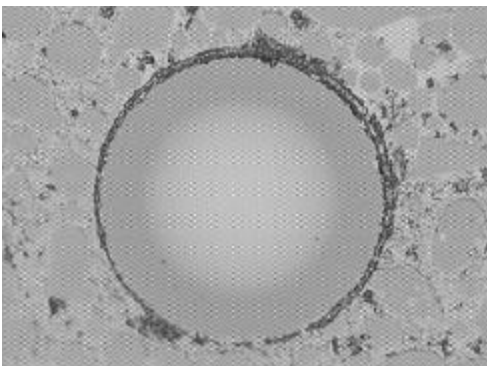


Figure A15: Cable set DUT A, Side A, Channel 8 before and after the vibration and thermal testing sequence.

Before

After

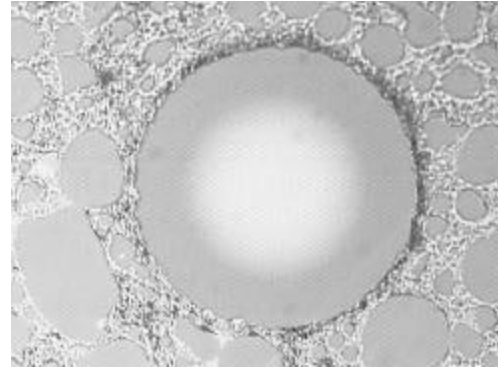
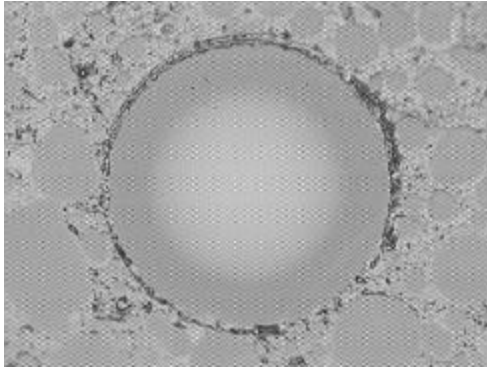


Figure A16: Cable set DUT A, Side B, Channel 8 before and after the vibration and thermal testing sequence.

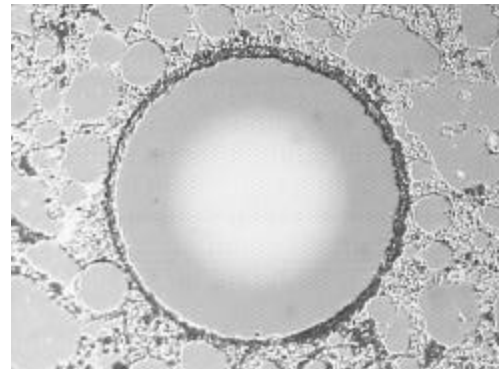
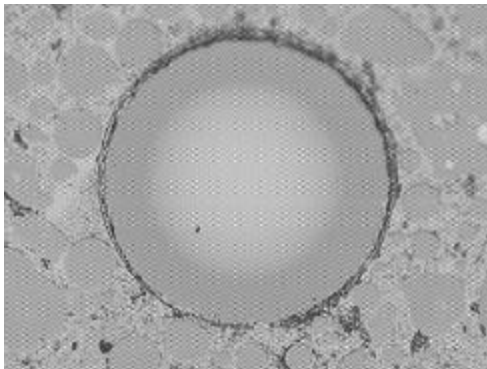


Figure A17: Cable set DUT A, Side A, Channel 9 before and after the vibration and thermal testing sequence.

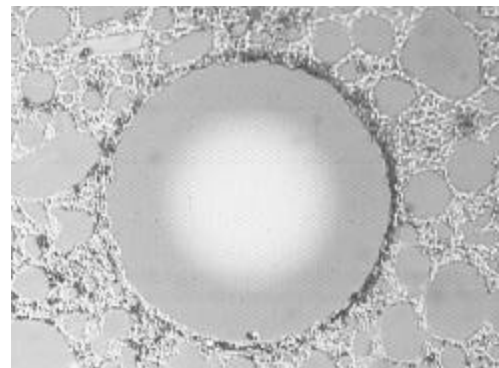
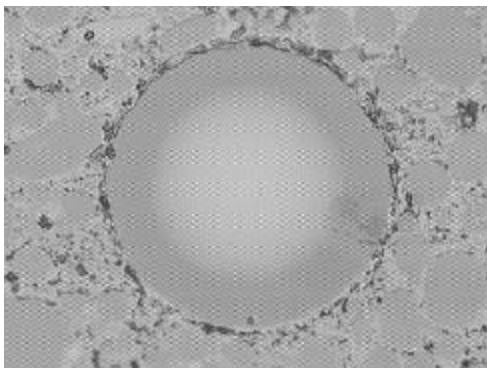


Figure A18: Cable set DUT A, Side B, Channel 9 before and after the vibration and thermal testing sequence.

Before

After

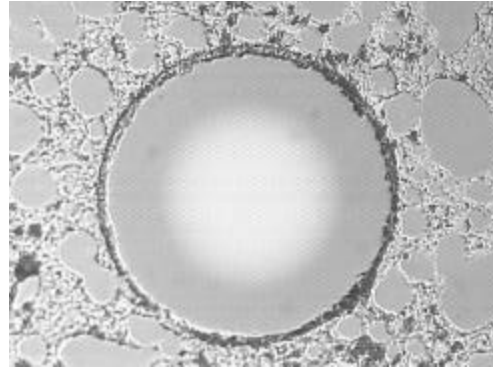
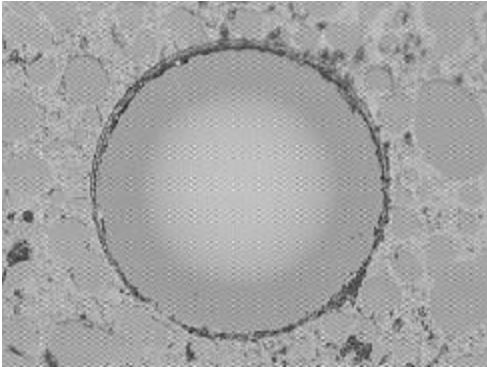


Figure A19: Cable set DUT A, Side A, Channel 10 before and after the vibration and thermal testing sequence.

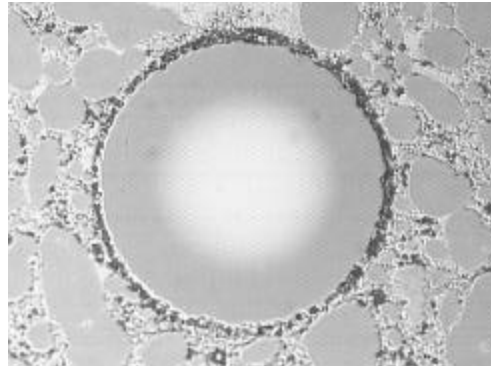
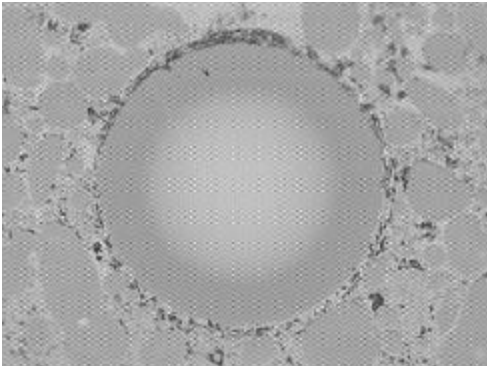


Figure A20: Cable set DUT A, Side B, Channel 10 before and after the vibration and thermal testing sequence.

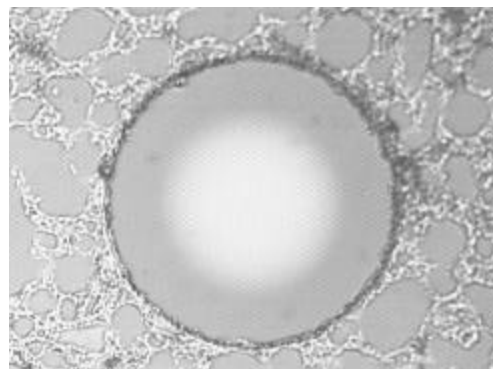
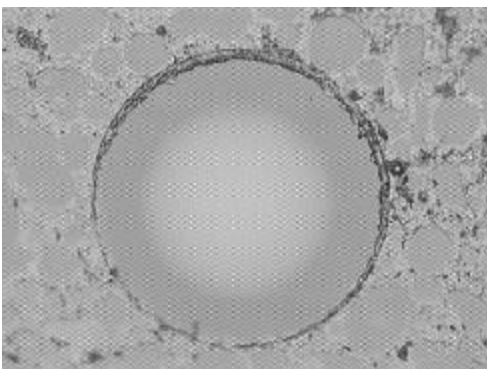


Figure A21: Cable set DUT A, Side A, Channel 11 before and after the vibration and thermal testing sequence.

Before

After

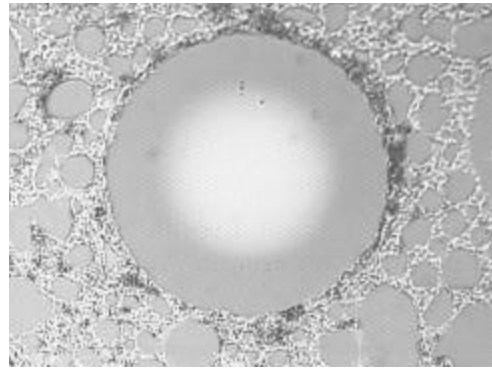
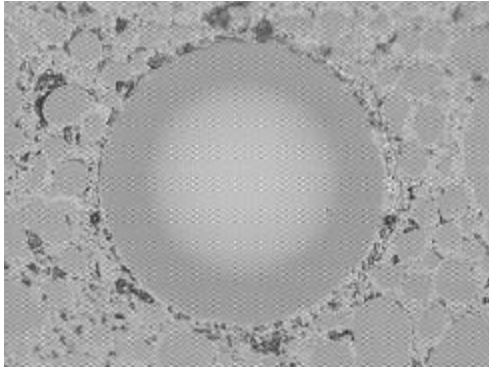


Figure A22: Cable set DUT A, Side B, Channel 11 before and after the vibration and thermal testing sequence.

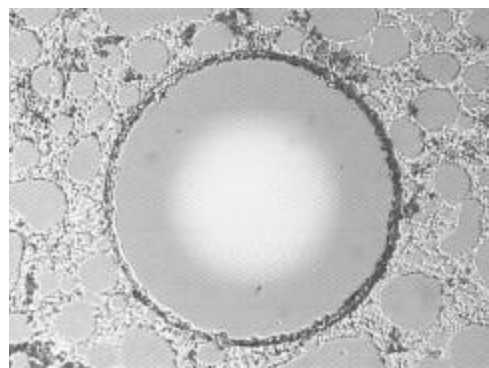
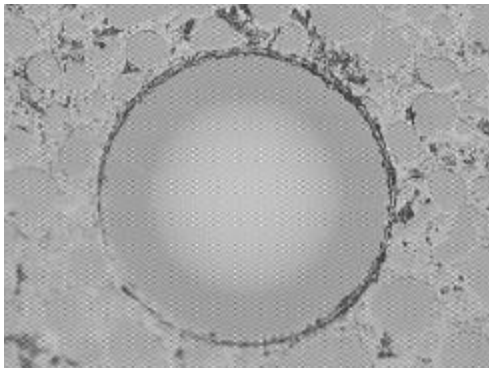


Figure A23: Cable set DUT A, Side A, Channel 12 before and after the vibration and thermal testing sequence.

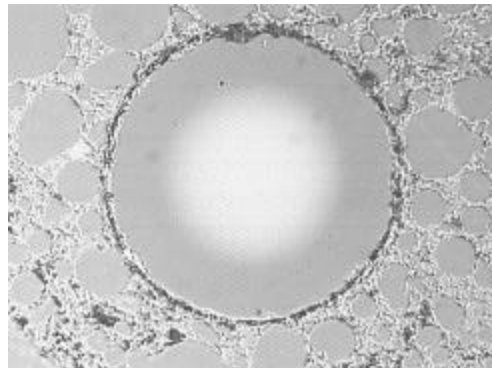
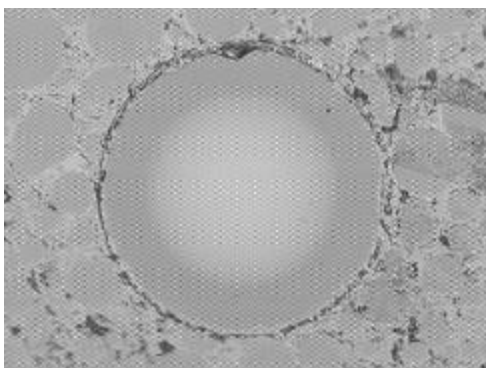


Figure A24: Cable set DUT A, Side B, Channel 12 before and after the vibration and thermal testing sequence.

Appedix B
MTP optical fiber end face visual inspection images before and after
environmental testing (vibration and thermal).

Before

After

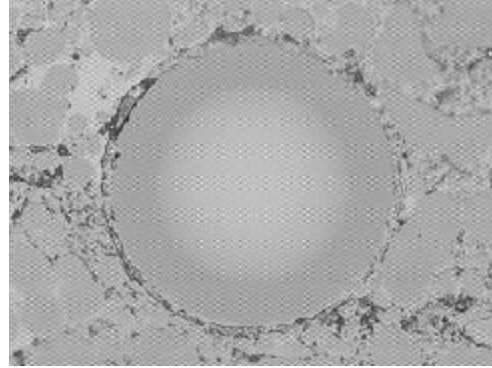
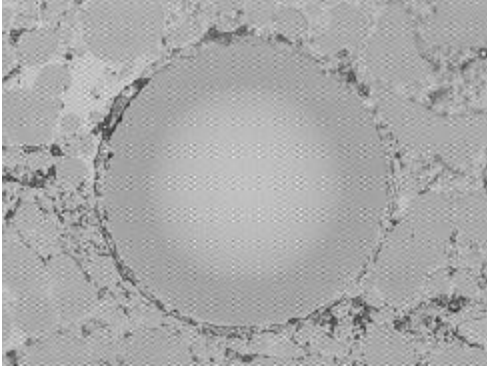


Figure B1: Cable set DUT B, Side A, Channel 1 before and after the vibration and thermal testing sequence.

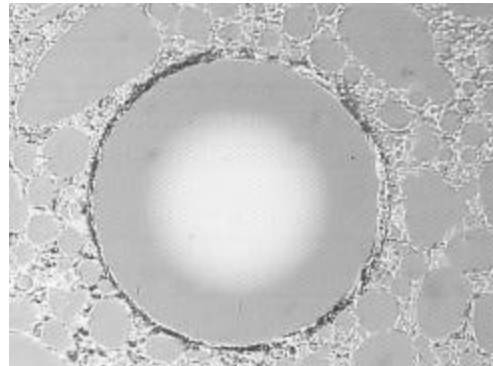
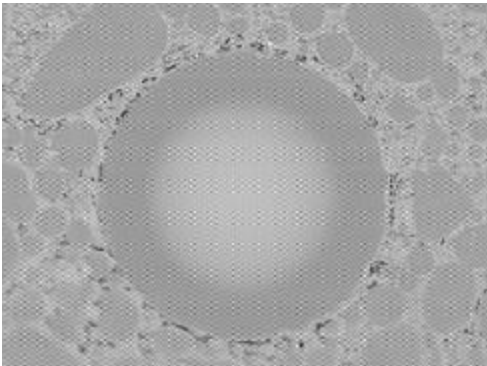


Figure B2: Cable set DUT B, Side B, Channel 1 before and after the vibration and thermal testing sequence.

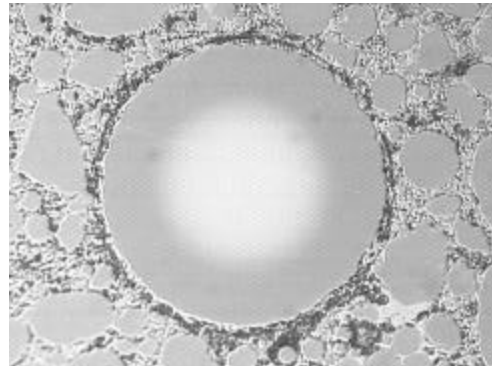
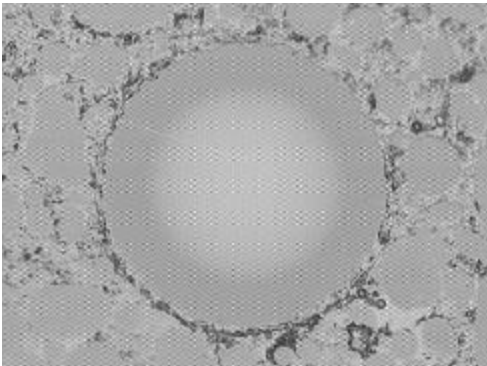


Figure B3: Cable set DUT B, Side A, Channel 2 before and after the vibration and thermal testing sequence.

Before

After

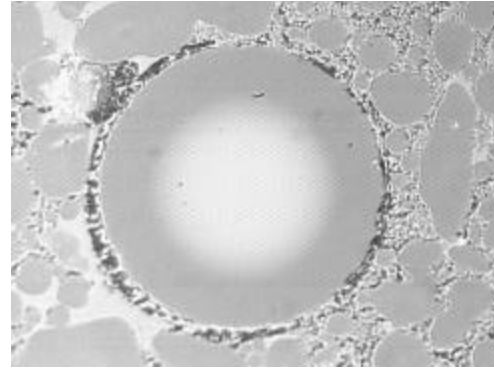
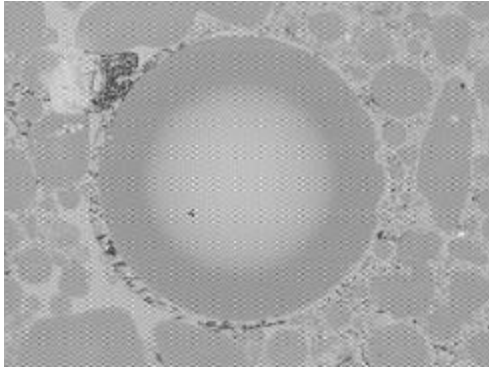


Figure B4: Cable set DUT B, Side B, Channel 2 before and after the vibration and thermal testing sequence.

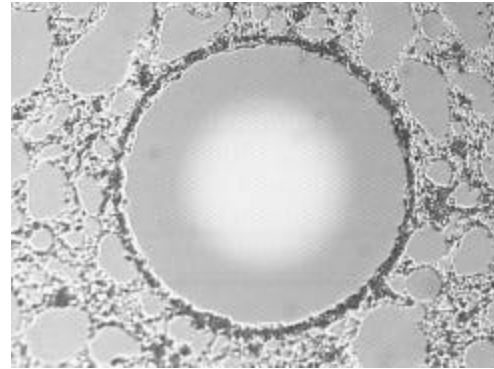
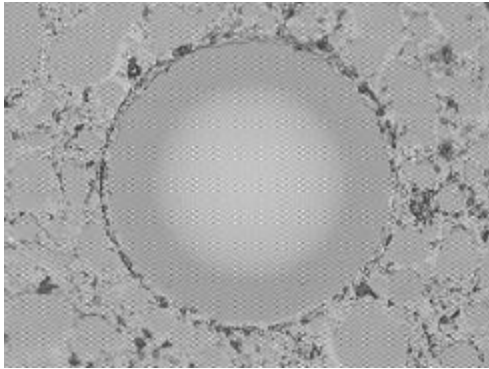


Figure B5: Cable set DUT B, Side A, Channel 3 before and after the vibration and thermal testing sequence.

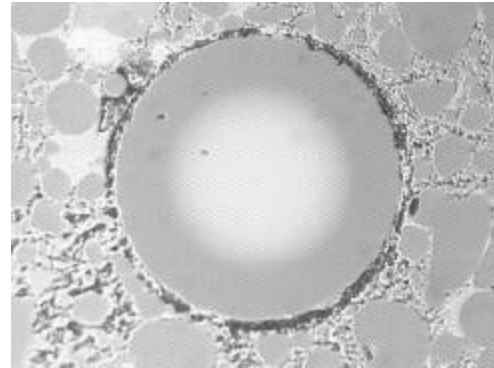
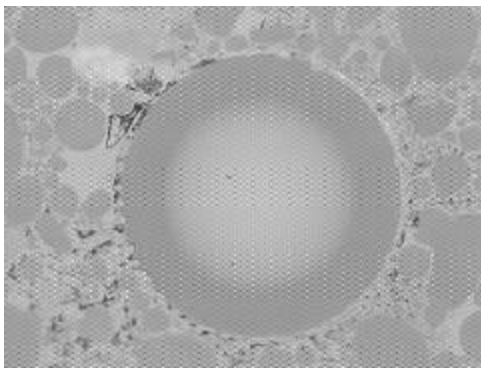


Figure B6: Cable set DUT B, Side B, Channel 3 before and after the vibration and thermal testing sequence.

Before

After

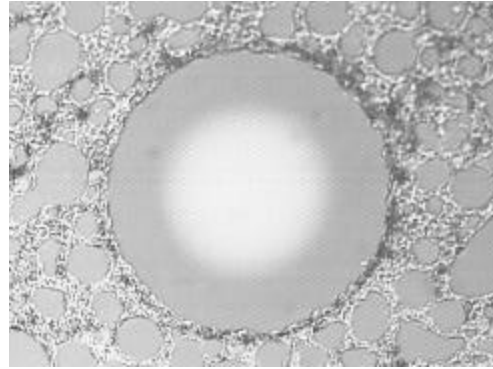
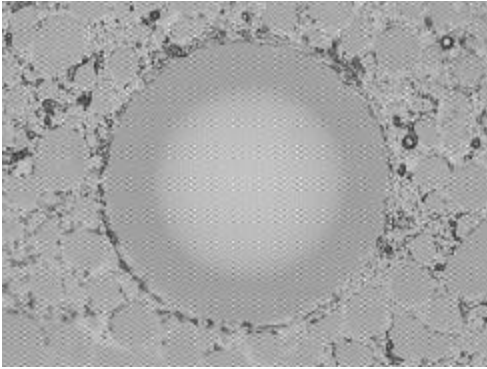


Figure B7: Cable set DUT B, Side A, Channel 4 before and after the vibration and thermal testing sequence.

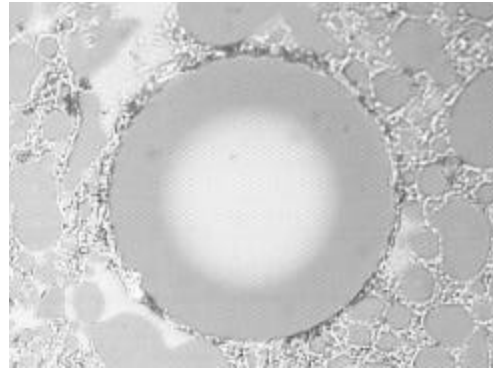
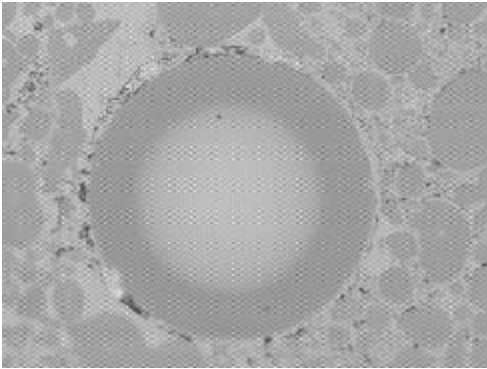


Figure B8: Cable set DUT B, Side B, Channel 4 before and after the vibration and thermal testing sequence.

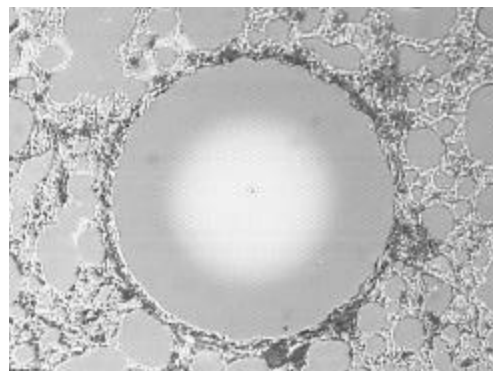
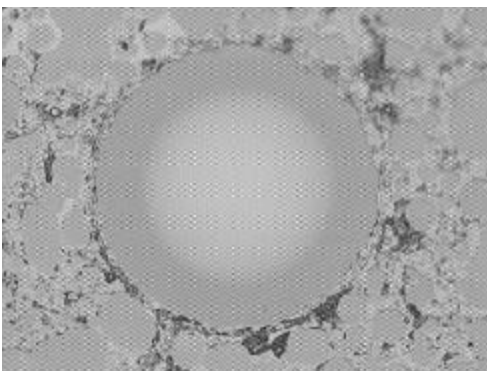


Figure B9: Cable set DUT B, Side A, Channel 5 before and after the vibration and thermal testing sequence.

Before

After

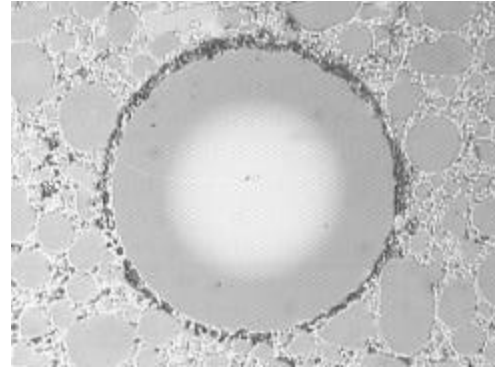
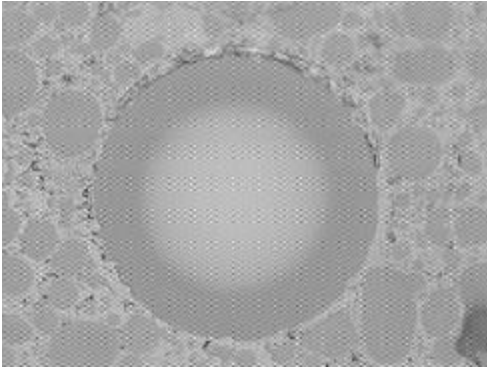


Figure B10: Cable set DUT B, Side B, Channel 5 before and after the vibration and thermal testing sequence.

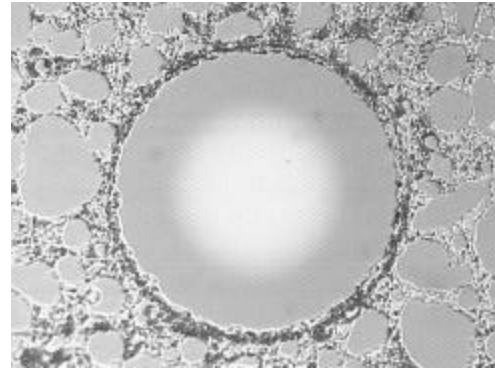
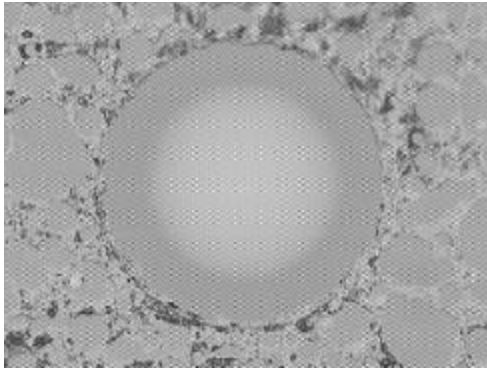


Figure B11: Cable set DUT B, Side A, Channel 6 before and after the vibration and thermal testing sequence.

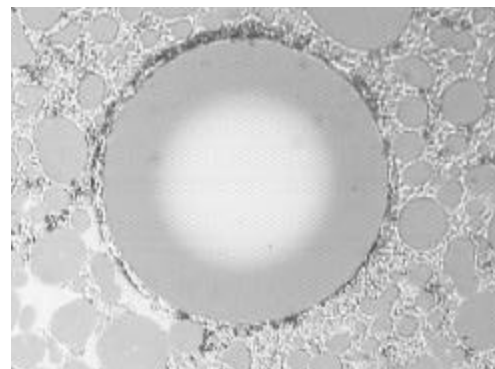
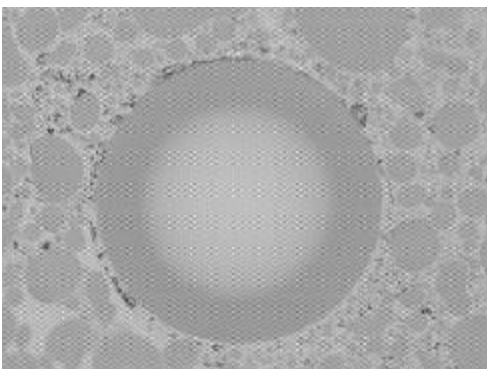


Figure B12: Cable set DUT B, Side B, Channel 6 before and after the vibration and thermal testing sequence.

Before

After

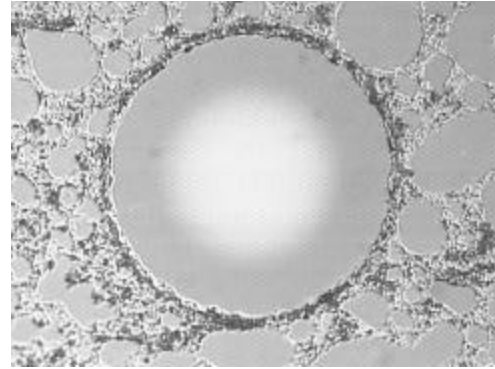
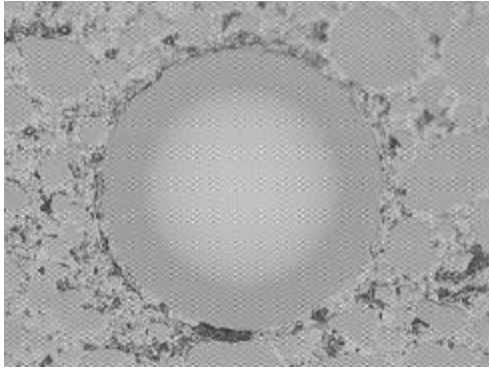


Figure B13: Cable set DUT B, Side A, Channel 7 before and after the vibration and thermal testing sequence.

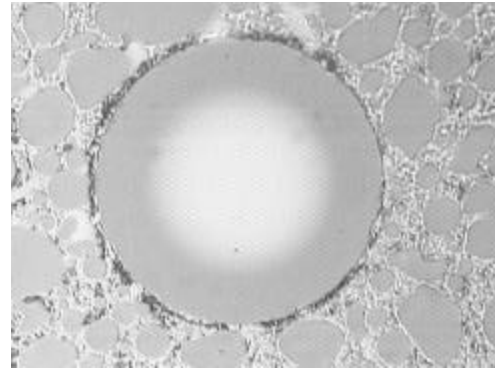
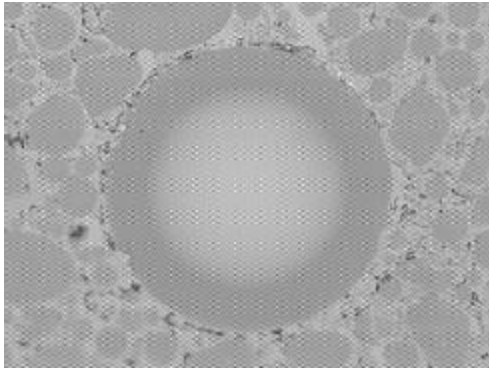


Figure B14: Cable set DUT B, Side B, Channel 7 before and after the vibration and thermal testing sequence.

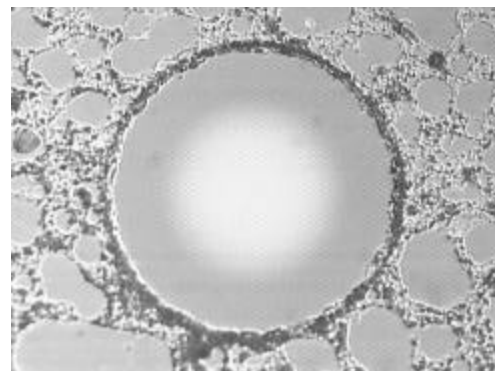
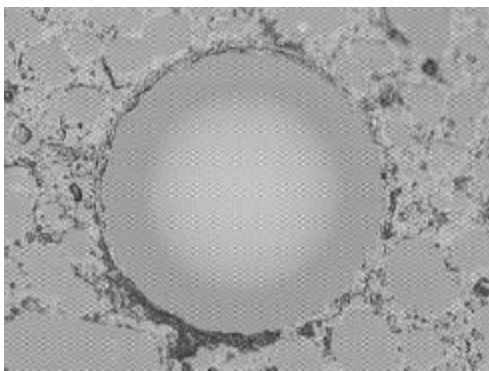


Figure B15: Cable set DUT B, Side A, Channel 8 before and after the vibration and thermal testing sequence.

Before

After

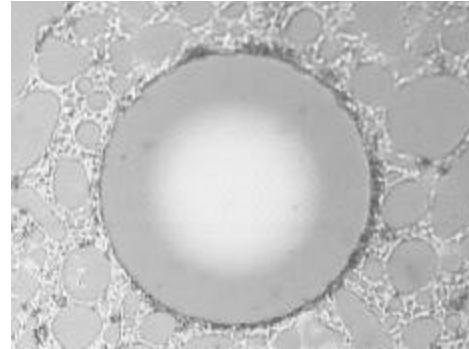
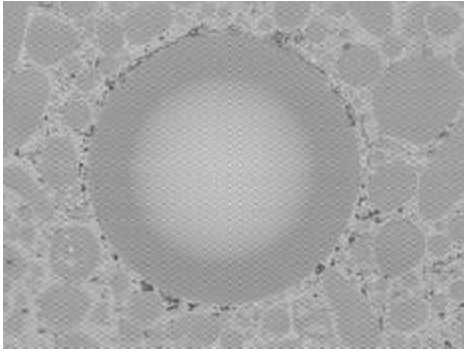


Figure B16: Cable set DUT B, Side B, Channel 8 before and after the vibration and thermal testing sequence.

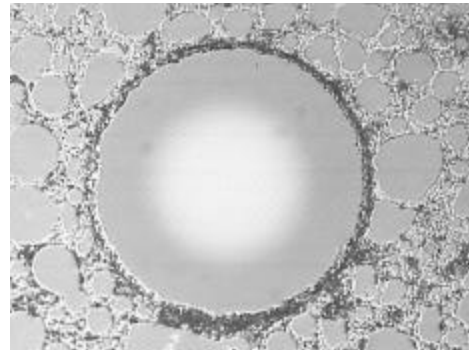
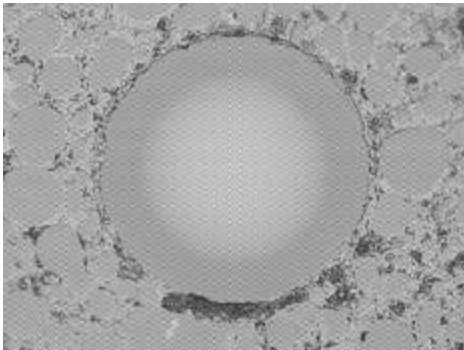


Figure B17: Cable set DUT B, Side A, Channel 9 before and after the vibration and thermal testing sequence.

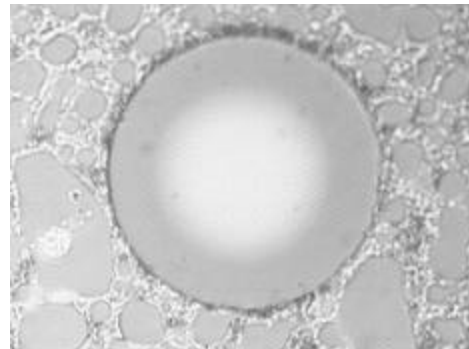
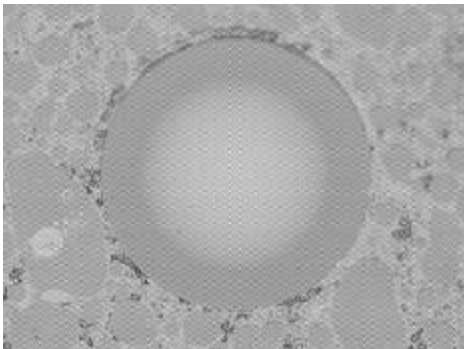


Figure B18: Cable set DUT B, Side B, Channel 9 before and after the vibration and thermal testing sequence.

Before

After

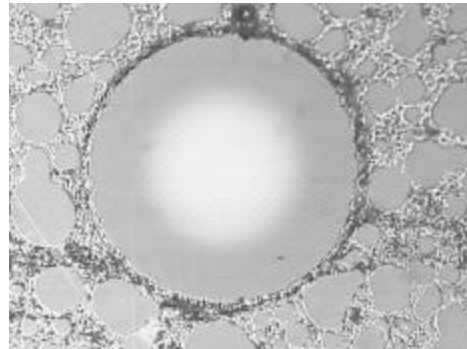
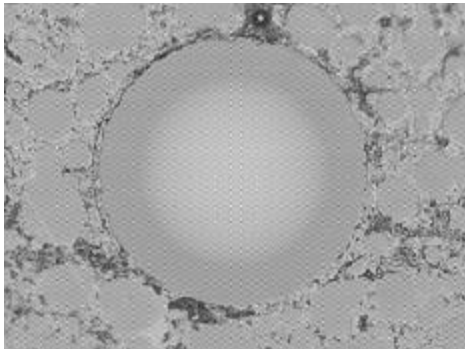


Figure B19: Cable set DUT B, Side A, Channel 10 before and after the vibration and thermal testing sequence.

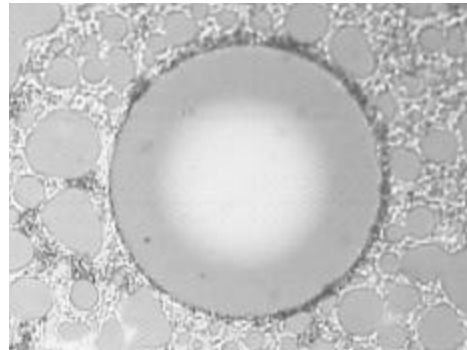
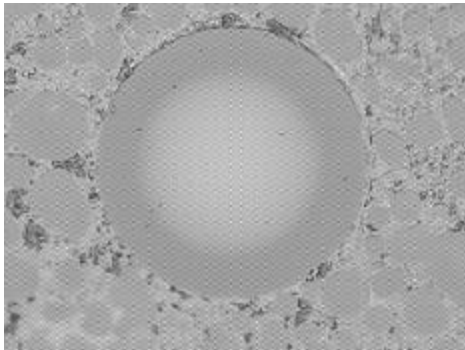


Figure B20: Cable set DUT B, Side B, Channel 10 before and after the vibration and thermal testing sequence.

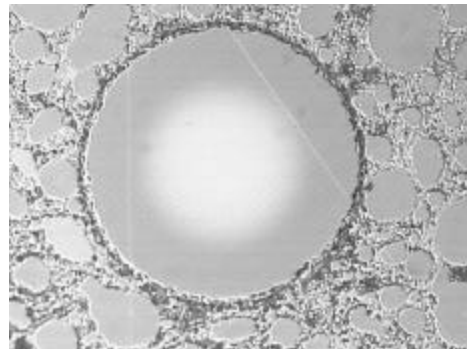
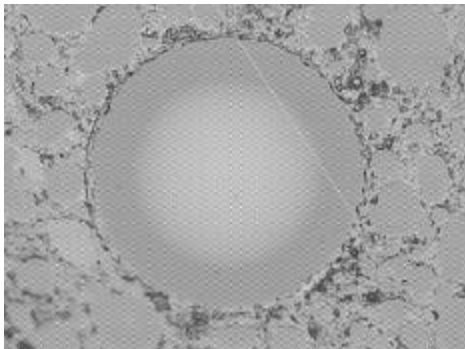


Figure B21: Cable set DUT B, Side A, Channel 11 before and after the vibration and thermal testing sequence.

Before

After

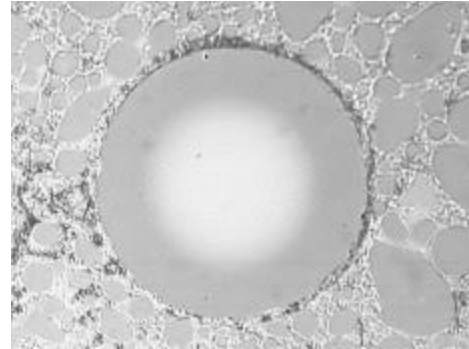
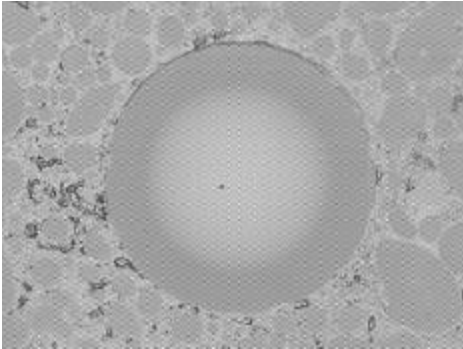


Figure B22: Cable set DUT B, Side B, Channel 11 before and after the vibration and thermal testing sequence.

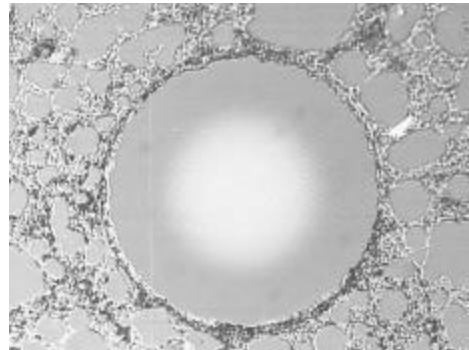
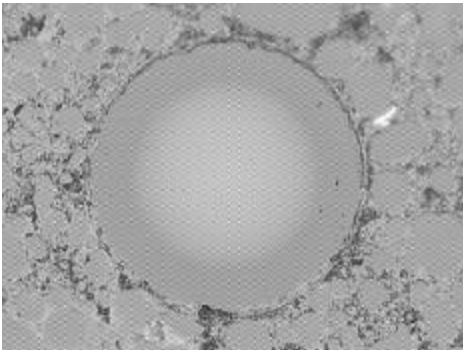


Figure B23: Cable set DUT B, Side A, Channel 12 before and after the vibration and thermal testing sequence.

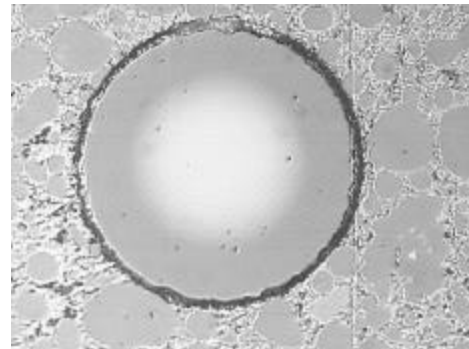
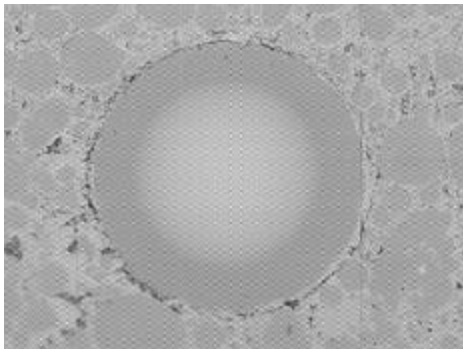


Figure B24: Cable set DUT B, Side B, Channel 12 before and after the vibration and thermal testing sequence.

Appedix C
MTP optical fiber end face visual inspection images before and after environmental testing (vibration and thermal).

Before

After

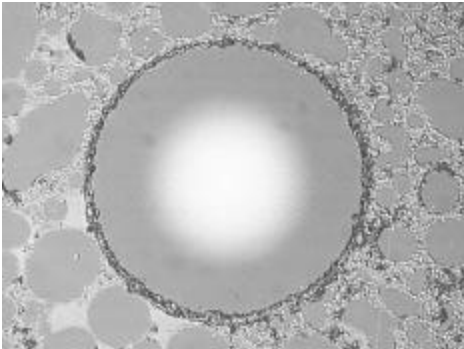
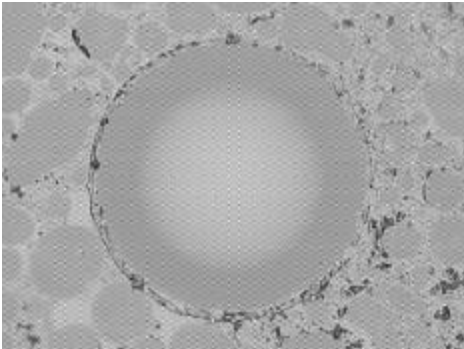


Figure C1: Cable set DUT C, Side A, Channel 1 before and after the vibration and thermal testing sequence.

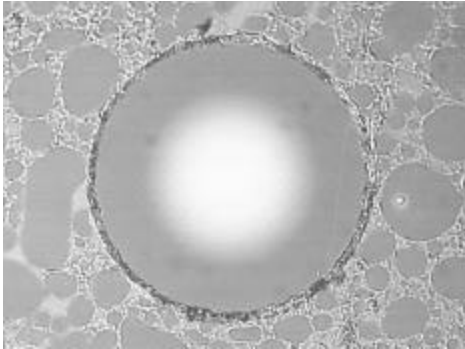
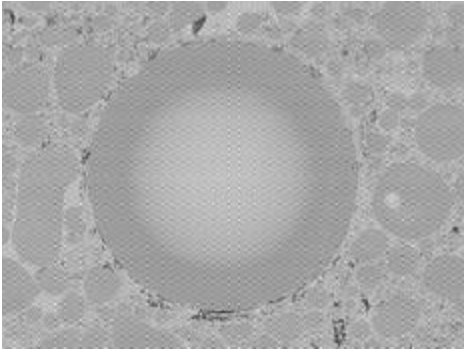


Figure C2: Cable set DUT C, Side B, Channel 1 before and after the vibration and thermal testing sequence.

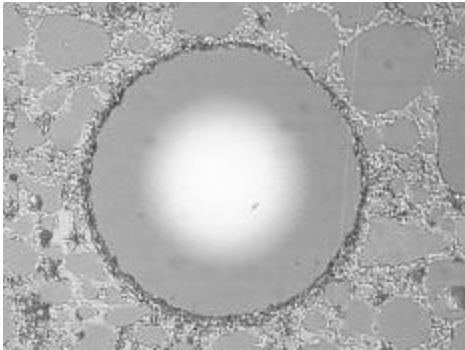
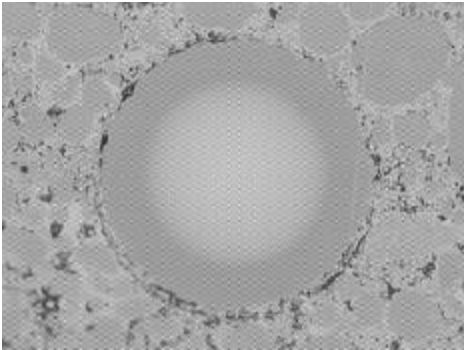
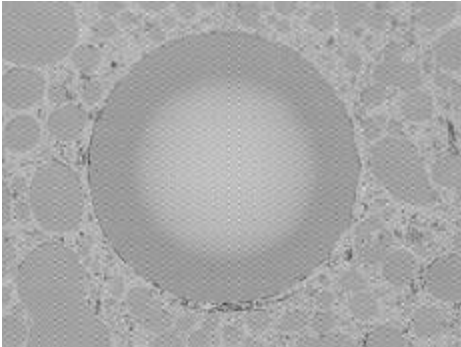


Figure C3: Cable set DUT C, Side A, Channel 2 before and after the vibration and thermal testing sequence.

Before



After

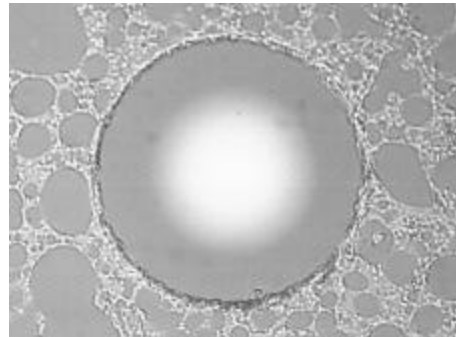


Figure C4: Cable set DUT C, Side B, Channel 2 before and after the vibration and thermal testing sequence.

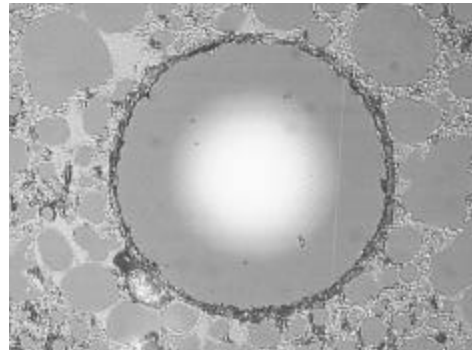
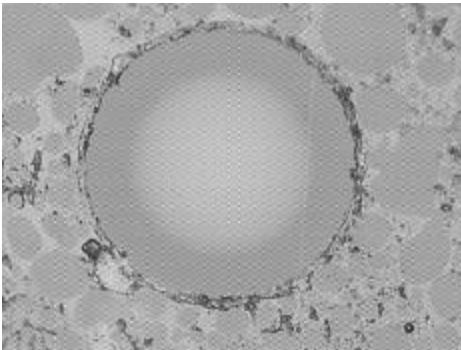


Figure C5: Cable set DUT C, Side A, Channel 3 before and after the vibration and thermal testing sequence.

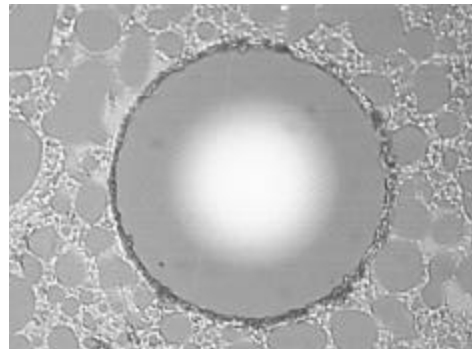
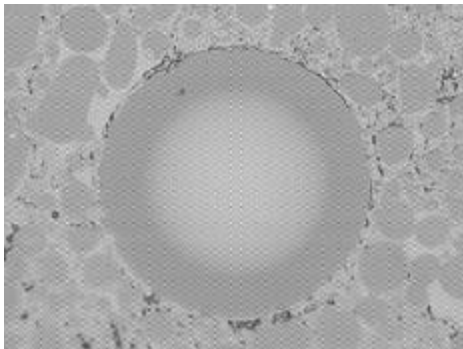


Figure C6: Cable set DUT C, Side B, Channel 3 before and after the vibration and thermal testing sequence.

Before

After

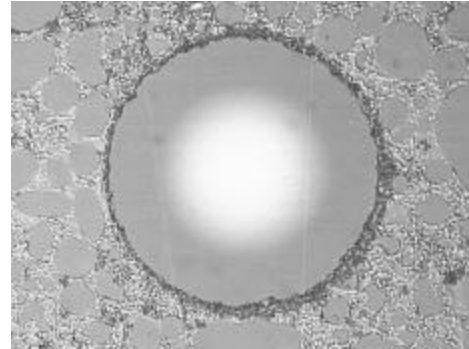
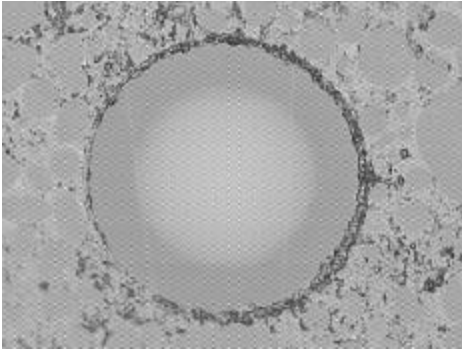


Figure C7: Cable set DUT C, Side A, Channel 4 before and after the vibration and thermal testing sequence.

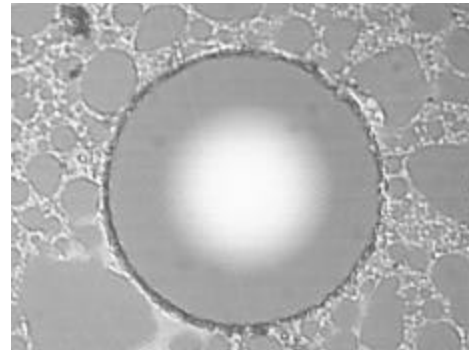
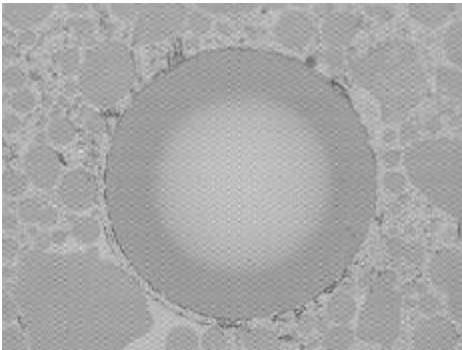


Figure C8: Cable set DUT C, Side B, Channel 4 before and after the vibration and thermal testing sequence.

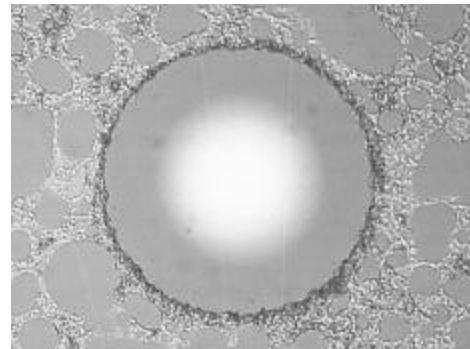
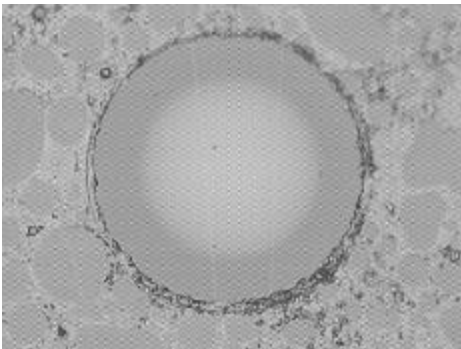


Figure C9: Cable set DUT C, Side A, Channel 5 before and after the vibration and thermal testing sequence.

Before

After

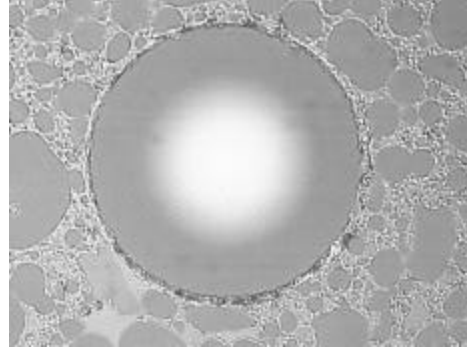
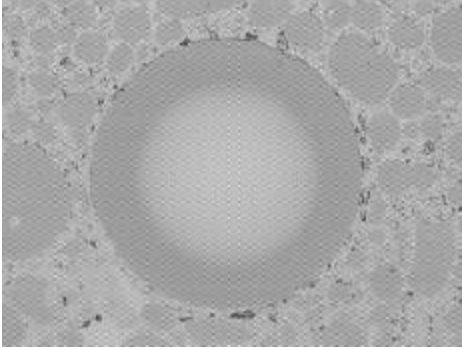


Figure C10: Cable set DUT C, Side B, Channel 5 before and after the vibration and thermal testing sequence.

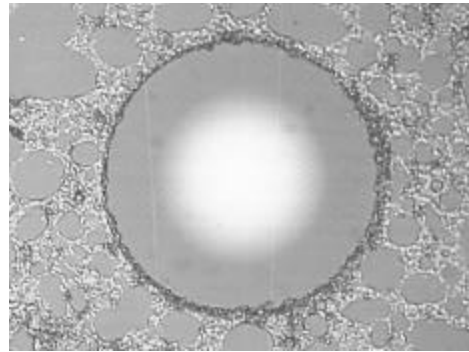
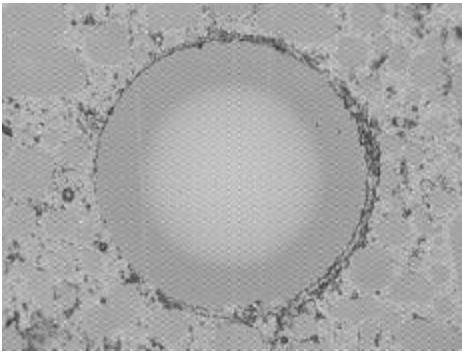


Figure C11: Cable set DUT C, Side A, Channel 6 before and after the vibration and thermal testing sequence.

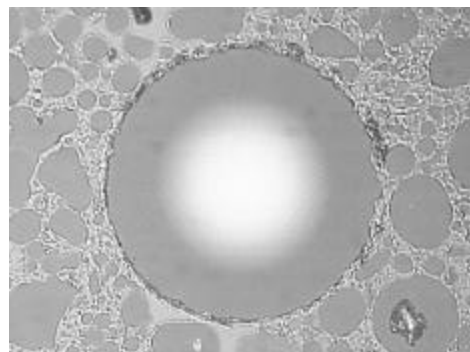
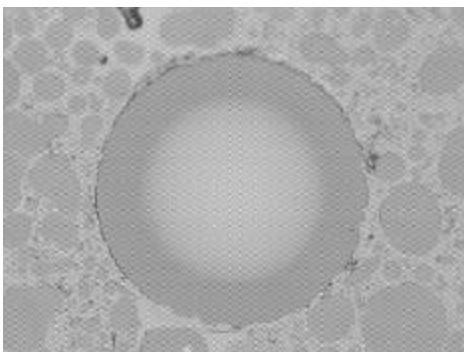


Figure C12: Cable set DUT C, Side B, Channel 6 before and after the vibration and thermal testing sequence.

Before

After

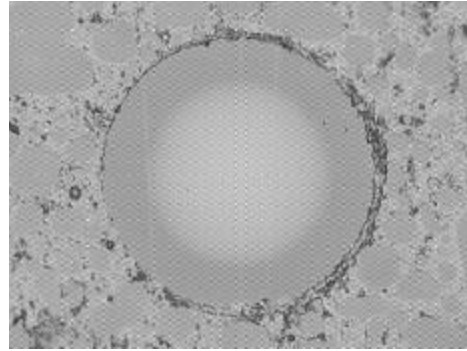
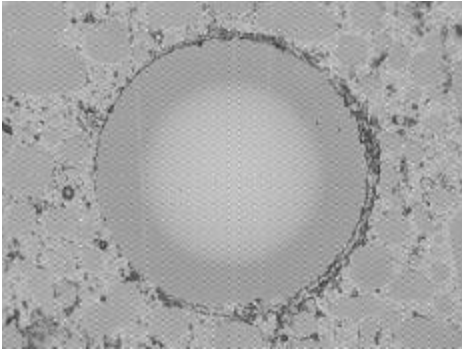


Figure C13: Cable set DUT C, Side A, Channel 7 before and after the vibration and thermal testing sequence.

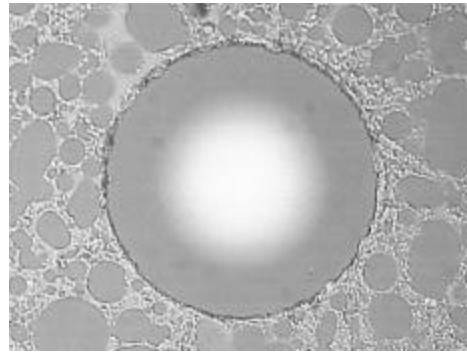
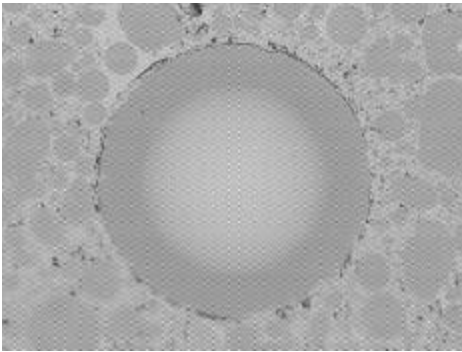


Figure C14: Cable set DUT C, Side B, Channel 7 before and after the vibration and thermal testing sequence.

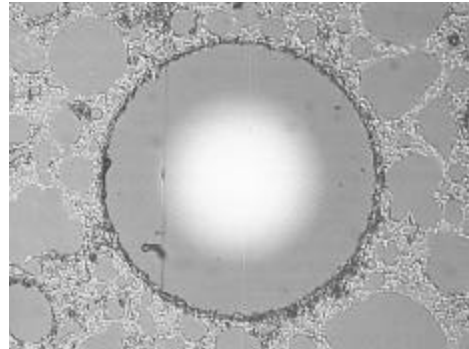
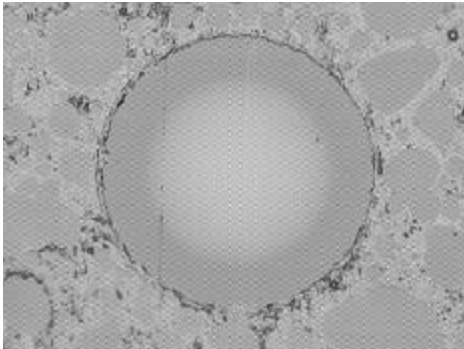


Figure C15: Cable set DUT C, Side A, Channel 8 before and after the vibration and thermal testing sequence.

Before

After

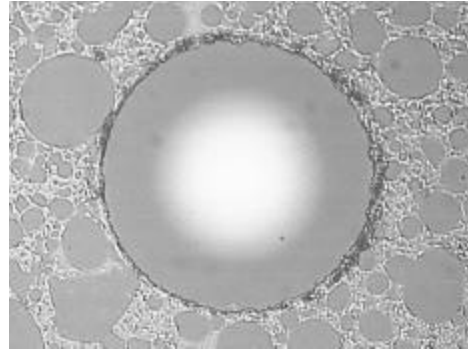
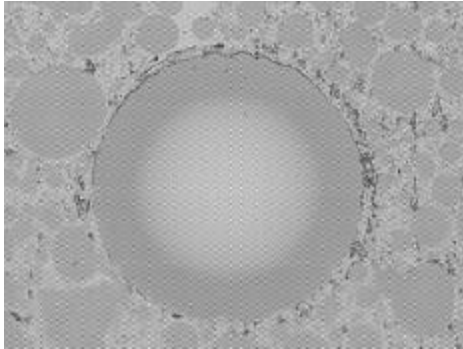


Figure C16: Cable set DUT C, Side B, Channel 8 before and after the vibration and thermal testing sequence.

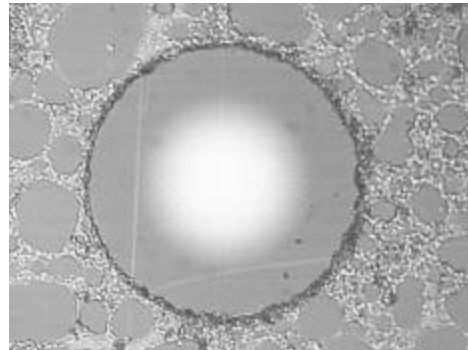
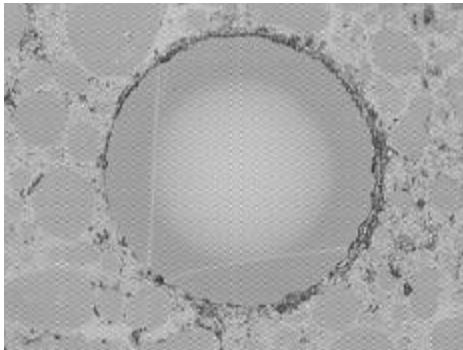


Figure C17: Cable set DUT C, Side A, Channel 9 before and after the vibration and thermal testing sequence.

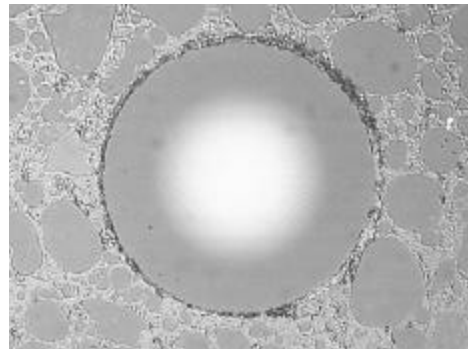
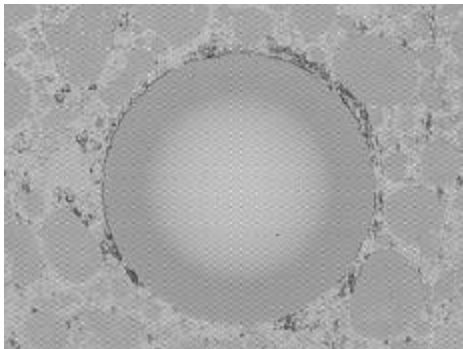


Figure C18: Cable set DUT C, Side B, Channel 9 before and after the vibration and thermal testing sequence.

Before

After

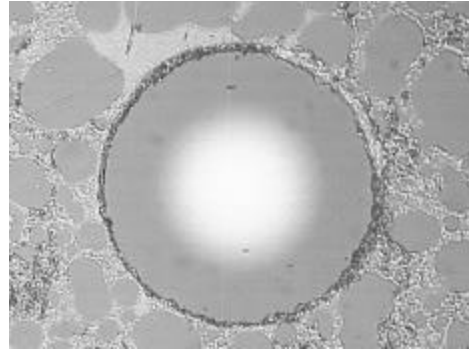
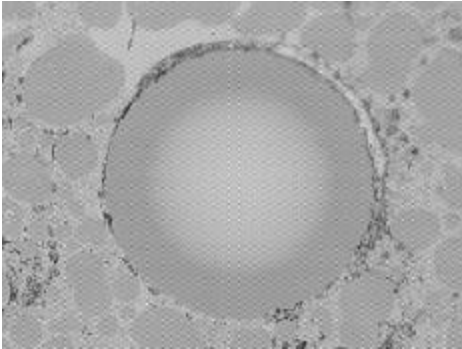


Figure C19: Cable set DUT C, Side A, Channel 10 before and after the vibration and thermal testing sequence.

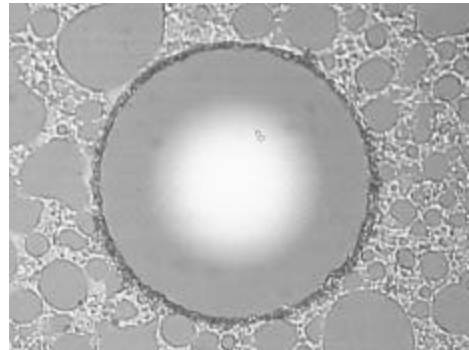
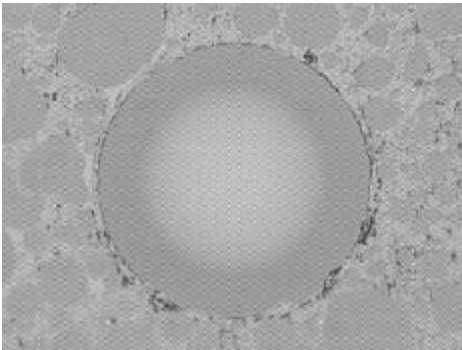


Figure C20: Cable set DUT C, Side B, Channel 10 before and after the vibration and thermal testing sequence.

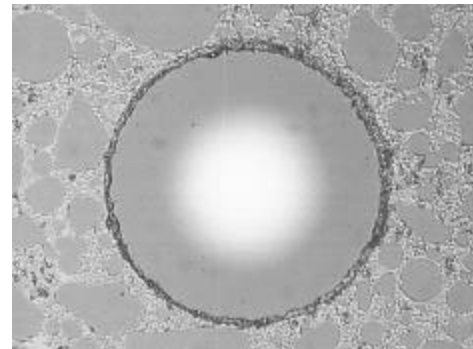
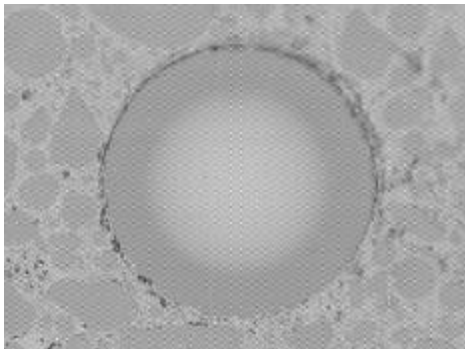


Figure C21: Cable set DUT C, Side A, Channel 11 before and after the vibration and thermal testing sequence.

Before

After

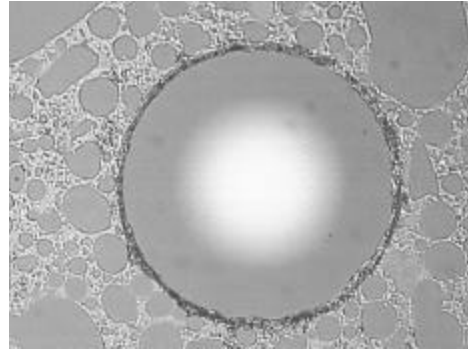
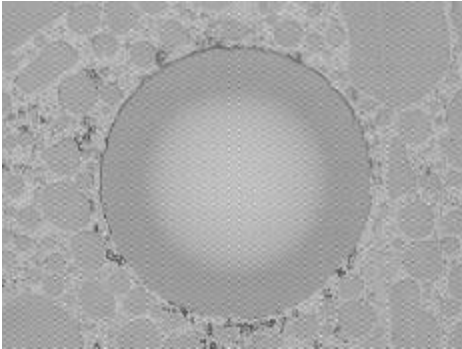


Figure C22: Cable set DUT C, Side B, Channel 11 before and after the vibration and thermal testing sequence.

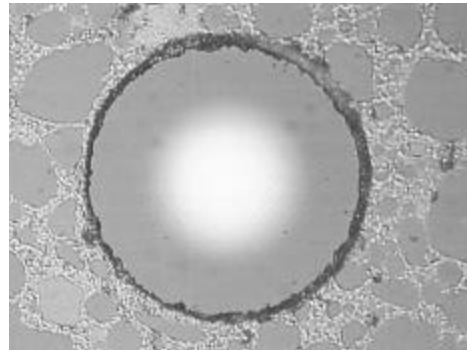
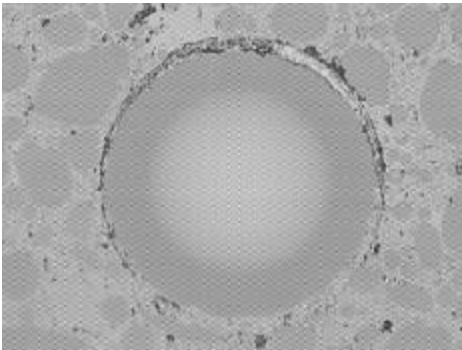


Figure C23: Cable set DUT C, Side A, Channel 12 before and after the vibration and thermal testing sequence.

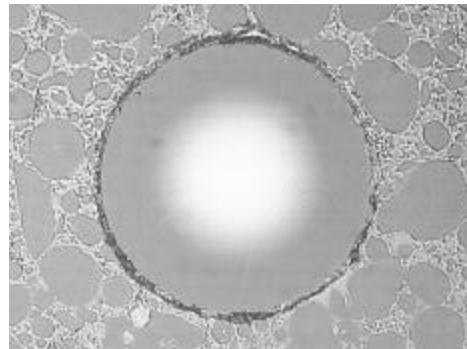
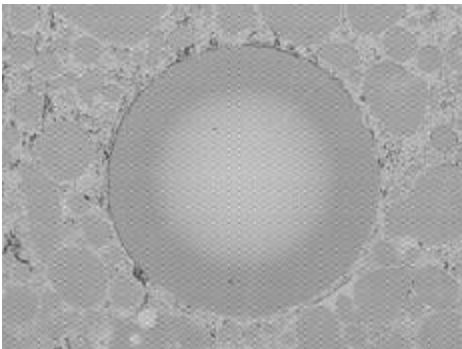


Figure C24: Cable set DUT C, Side B, Channel 12 before and after the vibration and thermal testing sequence.



**Goddard Space
Flight Center**

National Aeronautics and
Space Administration



Radiation Testing of Commercial off the Shelf 62.5/125/250 Micron Optical Fiber for Space Flight Environments

Melanie Ott, Shawn Macmurphy, Matthew Dodson

Sigma Research and Engineering
NASA Goddard Space Flight Center
Code 562

Component Technology and Radiation Effects Branch
Greenbelt MD 20771

melanie.ott@gsfc.nasa.gov

301-286-0127

Abstract

The 62.5/125/250 micron optical fiber manufactured by Lucent SFT was tested for gamma radiation resistance at the NASA Goddard Space Flight Center Cobalt⁶⁰ chamber. The fiber was tested with 1300 nm light, at 20.7 rads/min and 5 rads/min at -25°C and at 32.3 rads/min and 5 rads/min at $+25^{\circ}\text{C}$. Data was recorded during exposure until the attenuation reached levels below that of the optical detection data acquisition system. All gathered data is presented here along with extrapolation equations for other dose rates.

Background

In the past for space flight applications, 100/140 micron optical fiber was used for optical communication purposes. This fiber has been characterized for space flight environments under various conditions.[1-2] For several years, there has more interest in usage of commercial optical fiber products because of the limited availability of 100/140 micron optical fiber. Over seven years ago, Corning ceased manufacturing the 100/140 fiber and since then Lucent SFT (formerly Spectran Specialty Fiber) has been the only manufacturer of this fiber. NASA has been asked to look into other options for purposes of providing alternatives to the 100/140 micron graded index fiber for space flight environments. Specifically, the question has been asked: how does 62.5/125 perform in a space radiation environment? The dopants used in the 62.5/125 micron optical fiber are different from those used in the radiation hardened 100/120/172 micron fiber being used currently. Therefore, it was expected that there would be a difference in the radiation performance but until now, answering the question about how much of a difference in performance there would be, was based on speculation with no data.

Experimental Set-up

The radiation exposure was conducted at Goddard Space Flight Center's Cobalt⁶⁰ gamma radiation chamber. Four tests total were conducted to assess the performance of the 62.5/125 micron commercial fiber using two dose rate conditions for each thermal condition. In each case the fiber was tested until light could no longer be detected with the optical detection system used for in-situ monitoring throughout exposure. Table 1 summarizes the tests conducted.

Table 1: Summary of experiments conducted

Designation	Test Length	Temperature	Dose Rate	Total Dose*	Input Level
Spool A	100 m	-25°C	20.7 rads/min	33.12 Krads	.84 μwatt
Spool B	100 m	-25°C	5 rads/min	26.0 Krads	.84 μwatt
Spool C	100 m	+25°C	32.3 rads/min	45.22 Krads	.65 μwatt
Spool D	100 m	+25°C	5 rads/min	35.0 Krads	.65 μwatt

* Total dose is based on the last detectable transmission through each of the fiber spools.

In Table 1 the details of the experiments are shown with the designation for each spool under test. The last column is the input light level registered prior to the 100 m spool or the output of the lead in cables coupling the source to the spools themselves. The level used for monitoring the transmission of light through the fiber during exposure is required to be below 1 microwatt to limit photobleaching effects.[2] Two of the spools of 62.5/125 micron fiber were tested at -25°C and tested at two different dose rates; 20.7 rads/min for spool A and 5 rads/min for spool B. With typical germanium doped multimode fiber, this thermal environment represents a harsher scenario than room temperature since the lower temperatures inhibit thermal annealing of the radiation induced attenuation. At room temperature or +25°C, the other two spools were tested at 32.3 rads/min for spool C and 5 rads/min for spool D.

For all spools tested, data was recorded prior to testing and every minute during exposure. All spools were placed inside of lead boxes (to eliminate secondary low energy level reflections) and remained there through the duration of the test. Lead in and lead out cables were used to couple the source and detection equipment, through the chamber wall, to where the spools were located in the chamber. A thermal chamber (with enough room for one spool) was used in addition, to maintain a temperature of -25°C during and after the radiation exposure.

The RIFOCS 752L dual wavelength LED source was used at 1300 nm. The signal was attenuated with the JDS HA9 optical attenuator such that all incoming light to the spools was less than 1 microwatt of optical power. The HP8166 multichannel optical power meter was used for detection of the output signal from the spools.

Experimental Results

Two exposure sessions were conducted to collect data for the two thermal and dose rate condition combinations, since the thermal chamber could only be used to test one spool at a time. The results of all testing conducted are graphed in Figure 1.

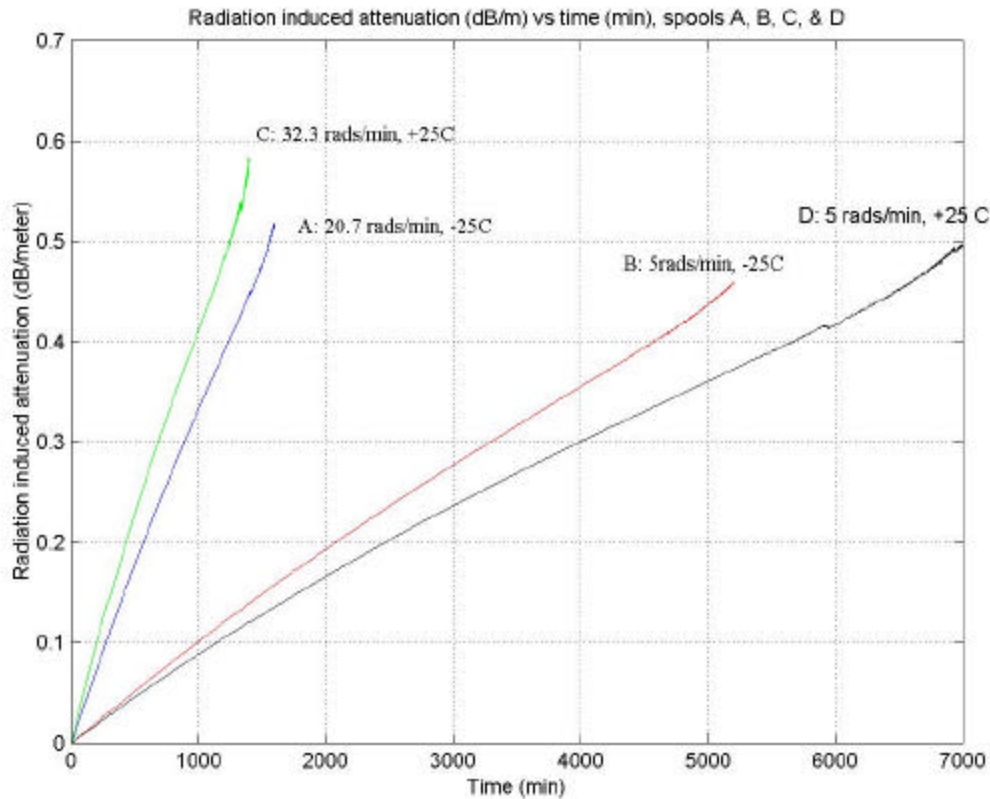


Figure 1: Complete data set of radiation induced attenuation recorded for each spool in units of dB/m vs. time .

It is evident by Figure 1 that all the spools experienced large radiation induced attenuation. The data has been scaled such that it is represented in dB/m units. Typical space flight applications will use 3 to 10 m of fiber when connecting instruments on a spacecraft for communication purposes. This would result in 1.5 to 5 dB for the short cables at the largest total dose registered here of ~ 25-40 Krads. However, the dose rates used for this testing are not exactly the dose rates expected for space flight. They may represent some periods of time but it is not usually the case that high dose rates such as these are maintained for any long duration over a few hours. The exposure at high dose rate in this testing was maintained for 3.5 to 4.5 days depending on the dose rate. The purpose of this was to collect enough data to formulate an extrapolation equation for other dose rates.

In Figure 1, it is evident that when held at the same dose rate but at different temperatures, the fiber performs as expected for germanium doped multimode where the colder thermal environment represents a harsher case for a fiber during radiation exposure. Spool B and spool D are both exposed at 5 rads/min but spool B experiences more induced attenuation since the temperature is much colder at -25°C .

For analysis the data was categorized into two segments by thermal condition and an extrapolation equation for each condition was formulated to make predictions for losses using other dose rates and total doses.[3]

Results of radiation exposure at -25°C :

Data set one is the radiation induced attenuation gathered at -25°C for spools A and B. The data for spool A and spool B is shown in Figure 2.

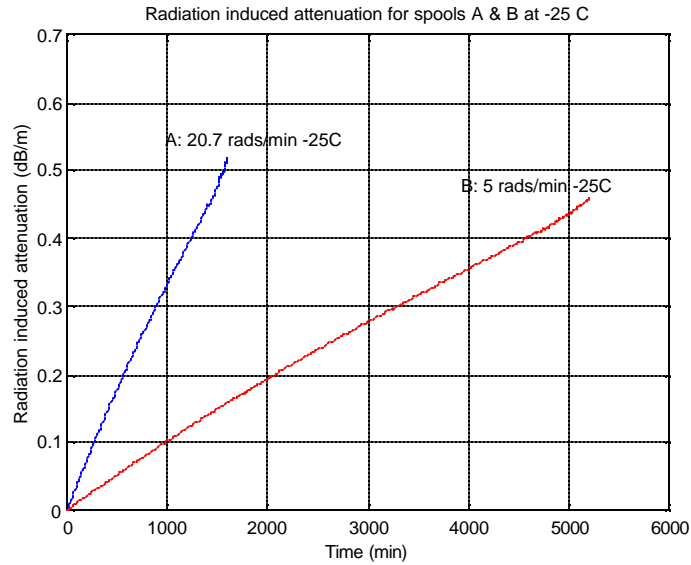


Figure 2: Radiation induced attenuation of spools A & B at -25°C .

With curve fitting, an equation to describe the induced attenuation can provide more information on how the attenuation would proceed if the test were continued with greater sensitivity of detection equipment. Figure 3 is a graph of the data from spool A and the corresponding model to fit the data.

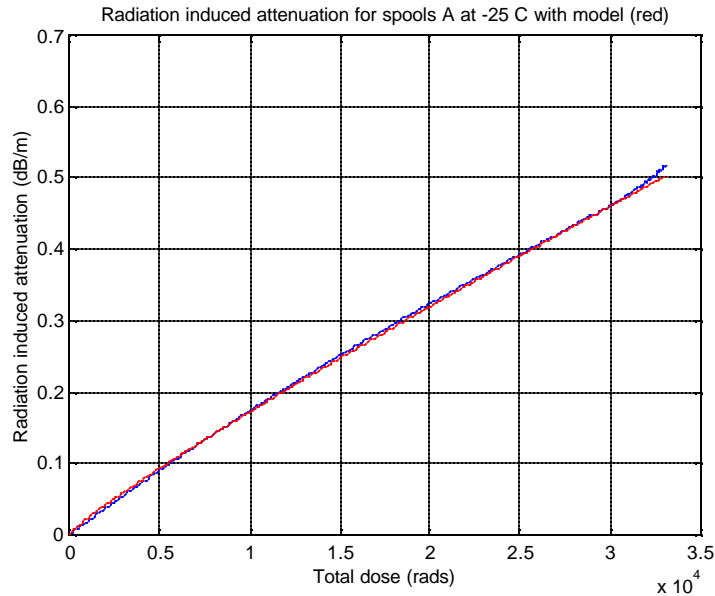


Figure 3: Radiation induced attenuation (dB/m) vs. Total dose (rads) for spool A (blue) at 20.7 rads/min and the curve fit equation (red).

The equation that fits the data, for spool A (shown in red in Figure 3) is:

$$A(D) = .43 \cdot 10^{-4} D^{.90} \text{ (dB/m)} \quad (1)$$

where $A(D)$ is radiation induced attenuation and D is the total dose.

The same analysis was performed on the data set for spool B and is shown in Figure 4.

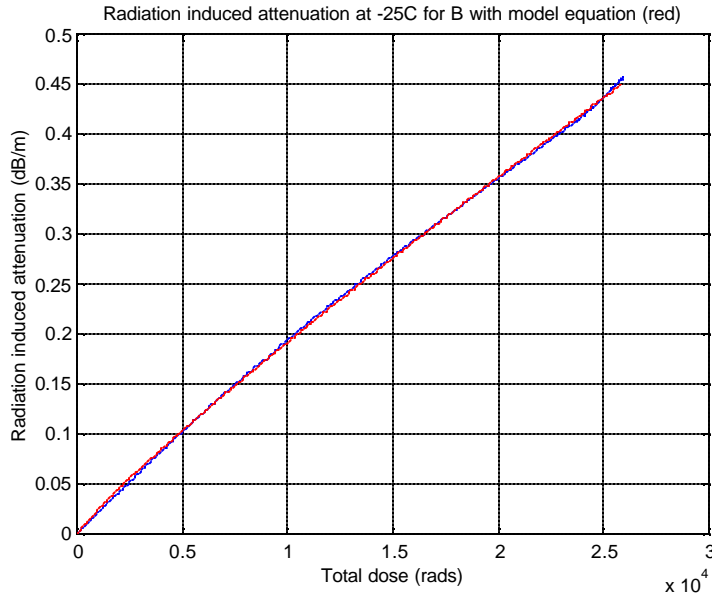


Figure 4: Radiation induced attenuation (dB/m) vs. Total dose (rads) for spool B (blue) at 5 rads/min and the curve fit equation (red).

The equation that fits the data, for spool B (shown in red in Figure 4) is:

$$A(D) = .48 \cdot 10^{-4} D^{.90} \text{ (dB/m)} \quad (2)$$

Equation 1 and 2 appear to be very similar which is typical of germanium doped fiber and allows for an extrapolation equation to be determined. Using the results of both equations, the general model at -25°C for radiation induced attenuation of this fiber can be expressed as:

$$A(D) = 3.64 \cdot 10^{-5} \phi^{.1} D^{.90} \text{ (dB/m)} \quad (3)$$

where $A(D)$ is radiation induced attenuation, ϕ is the dose rate of exposure, D is the total dose of exposure, and the constant $C_0 = 3.64 \cdot 10^{-5}$. [3] There is some error involved in predicting the exact numerical value of attenuation using equation 3 due to the slight difference in the constants generated from equations 2 and 1. The error for equation 3 can be represented by $C_0 = 3.64 \cdot 10^{-5} \pm 0.45 \cdot 10^{-5}$. Figure 5 is the extrapolation equation 3 plotted for 1 rad/min, .1 rads/min and .01 rads/min dose rates. Figure 5 represents more realistic background radiation dose rates that can be expected for typical space flight environments.

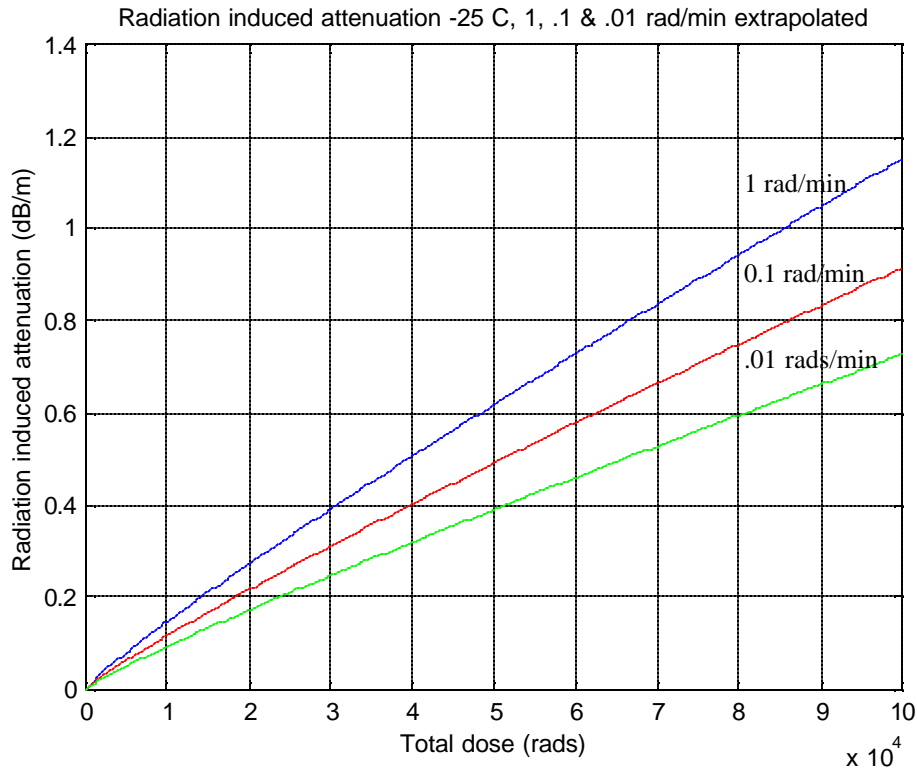


Figure 5: Radiation induced attenuation for -25°C extrapolated for 1 rad/min (blue), .1 rad/min (red) and .01 rads/min (green) to a total dose of 100 Krads.

In Table 2 the induced attenuation values at -25°C are summarized for the actual and extrapolated dose rate values.

Table 2: Summary of radiation induced attenuation for various dose rates and total doses both from actual data and extrapolated predictions at -25°C .

Dose Rate	Total Dose	Attenuation (dB/m)	Attenuation (dB/3m)	Attenuation (dB/10m)	Comment
20.7 rads/min	35.65 Krads	.517	1.55	5.17	Actual Data
20.7 rads/min	100 Krads	1.55	4.65	15.5	Extrapolated
20.7 rads/min	10 Krads	.173	.519	1.73	Actual Data
5.0 rads/min	29.0 Krads	.459	1.38	4.59	Actual Data
5.0 rads/min	100 Krads	1.35	4.05	13.5	Extrapolated
5.0 rads/min	10 Krads	.193	.579	1.93	Actual Data
1.0 rad/min	100 Krads	1.15	3.45	11.5	Extrapolated
1.0 rad/min	10 Krads	.145	.435	1.45	Extrapolated
0.1 rad/min	100 Krads	.914	2.74	9.14	Extrapolated
0.1 rad/min	10 Krads	.115	.345	1.15	Extrapolated
0.01 rad/min	100 Krads	.726	2.18	7.26	Extrapolated
0.01 rad/min	10 Krads	.091	.278	.910	Extrapolated

In Table 2, the numerical values for radiation induced attenuation at -25°C are listed for lower dose rates that represent more realistic values for background radiation dose rates in typical space flight environments. The attenuation is listed for total doses of both 10 Krads and 100 Krads, again, typical total dose requirements for space flight fiber optics. The lengths used for calculation of these attenuation values are also typical space flight cable lengths of 3 m or 10 m. Space Station uses lengths of 30 m or more and because of these long lengths the radiation induced losses are too high for this fiber to be considered without making other efforts to compensate for the huge transmission losses. Space Station also has a -125°C requirement and a point where the dose rate would be as high as 42 rads/min for two hours. This would further increase the predicted losses. However, for other missions where the background radiation is close to .1 rad/min maximum with a 100 Krad requirement and lengths of fiber usage at 3 m, the extrapolated attenuation is 2.74 dB. This value is high in comparison to radiation hardened fiber but could still be tolerated with some compensation depending on the power budget requirements of the mission for optical transmission

Results of radiation exposure at $+25^{\circ}\text{C}$:

Data set two is the radiation induced attenuation gathered at $+25^{\circ}\text{C}$ for spools C and D. The data for spool C and spool D is shown in Figure 6. Spool C was exposed to 32.3 rads/min and spool D was exposed to 5 rads/min radiation at room temperature.

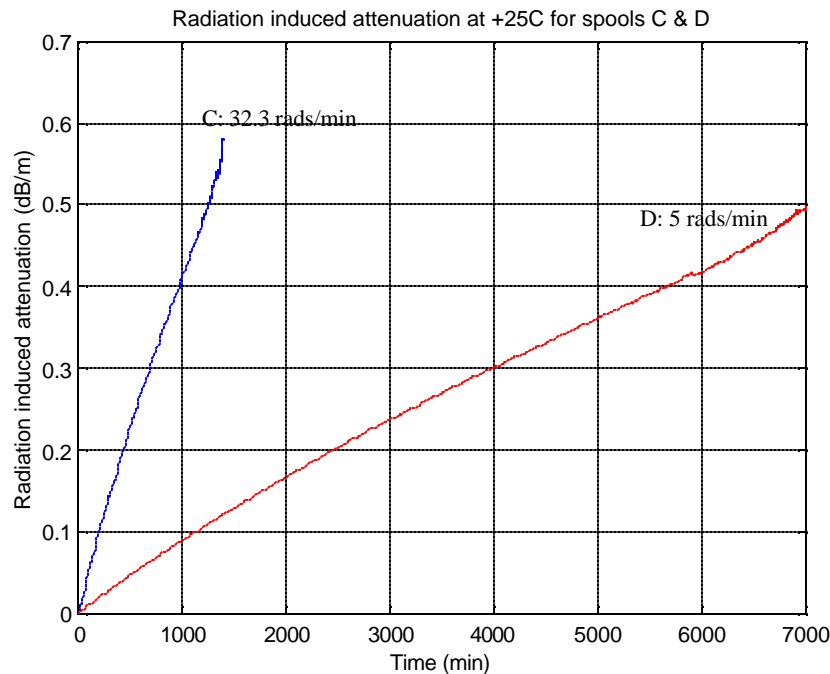


Figure 6: Radiation induced attenuation at $+25^{\circ}\text{C}$ for spools C (blue) and D (red).

Figure 7 shows the curve fitting equation graphed along with the actual data for spool C.

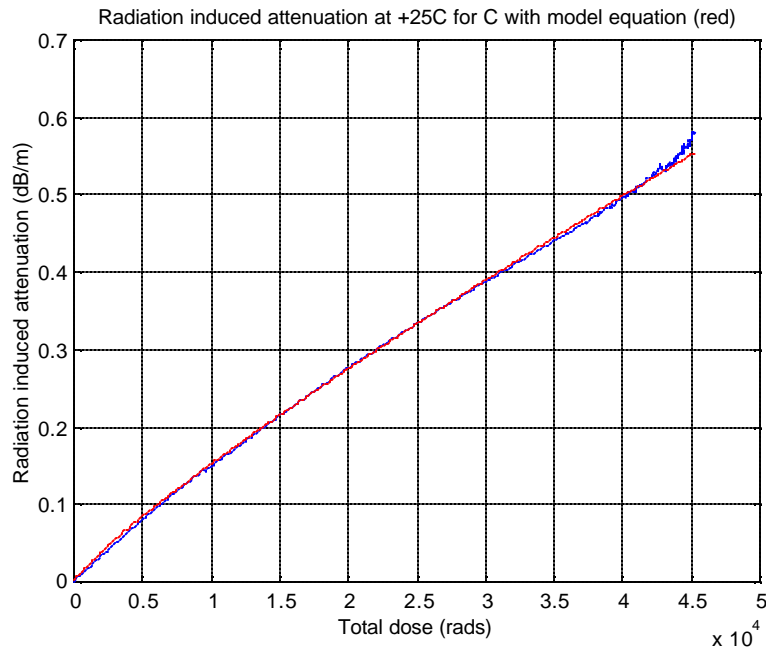


Figure 7: Radiation induced attenuation (dB/m) vs. Total dose (rads) for spool C (blue) at 32.3 rads/min and the curve fit equation (red).

The equation represented in Figure 7 in red, for radiation induced attenuation on spool C is:

$$A(D) = .55 * 10^{-4} D^{.86} \text{ (dB/m)} \quad (4)$$

where A(D) is again radiation induced attenuation given a total dose of D.

The same analysis was performed on the data for spool D and the results are in Figure 8.

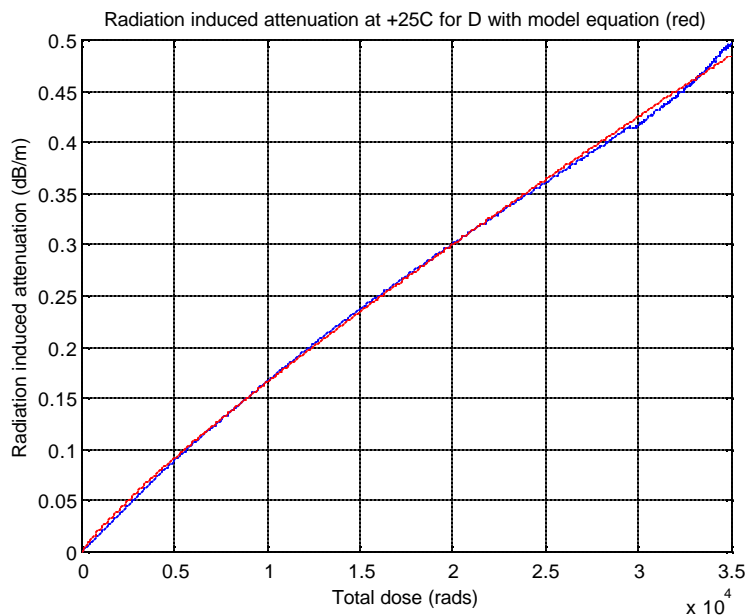


Figure 8: Radiation induced attenuation at +25°C for spool D at 5 rads/min with curve fit (red).

In Figure 8 the equation for the curve fit can be expressed as

$$A(D) = .60 \cdot 10^{-4} D^{.86} \text{ (dB/m)} \quad (5)$$

Both equations 4 and 5 are similar as expected. Using both equations and their respective data to generate the extrapolation model for radiation induced attenuation at room temperature the resulting expression is:

$$A(D) = 4.10 \cdot 10^{-5} \phi^{.14} D^{.86} \text{ (dB/m)} \quad (6)$$

Where ϕ is any dose rate, D is total dose and A(D) is radiation induced attenuation. This is the extrapolation equation for +25°C gamma exposure. The uncertainty associated with the constant in equation 6 is $C_0 = 4.1 \cdot 10^{-5} \pm .71 \cdot 10^{-5}$. Equation 6 is graphed in Figure 9 for three different dose rates, 1.0 rad/min, 0.1 rad/min, & .01 rad/min.

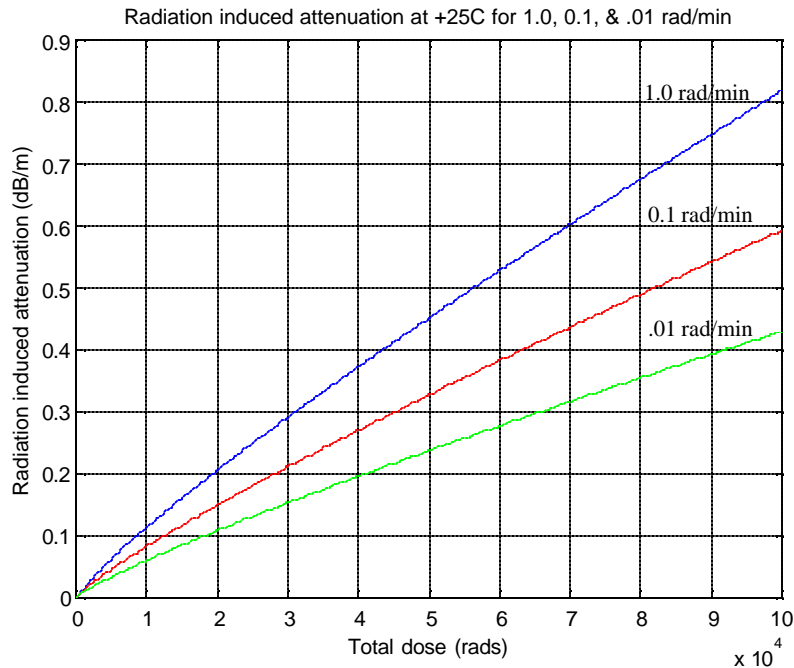


Figure 9: Radiation induced attenuation in dB/m using the extrapolation equation 6, +25°C exposure for 1.0 rad/min, 0.1 rad/min, & .01 rad/min vs. total ionizing dose.

Table 3 contains the summary and some extrapolated values given dose rate and total dose for room temperature exposure or exposure at +25°C.

Table 3: Summary of radiation induced attenuation for various dose rates and total doses both from actual data and extrapolated predictions for +25 ° C.

Dose Rate	Total Dose	Attenuation (dB/m)	Attenuation (dB/3m)	Attenuation (dB/10m)	Comment
32.3 rads/min	46.8 Krads	.581	1.74	5.81	Actual Data
32.3 rads/min	100 Krads	1.33	3.99	13.3	Extrapolated
32.3 rads/min	10 Krads	.148	.444	1.48	Actual Data
5.0 rads/min	37.1 Krads	.498	1.49	4.98	Actual Data
5.0 rads/min	100 Krads	1.02	3.06	10.2	Extrapolated
5.0 rads/min	10 Krads	.166	.498	1.66	Actual Data
1.0 rad/min	100 Krads	.818	2.45	8.18	Extrapolated
1.0 rad/min	10 Krads	.113	.339	1.13	Extrapolated
0.1 rad/min	100 Krads	.593	1.78	5.93	Extrapolated
0.1 rad/min	10 Krads	.082	.246	.820	Extrapolated
0.01 rad/min	100 Krads	.429	1.29	4.29	Extrapolated
0.01 rad/min	10 Krads	.059	.177	.590	Extrapolated

Even at room temperature exposure, the losses are still very high for a low dose rate environment such as .1 rad/min. At 10 Krads the losses for a 3 m length of fiber is .246, but at 100 Krads the losses increase to 1.78 dB. To make a comparison to the performance at -25°C, this attenuation is about 1 dB lower.

Conclusions:

In previous papers the results of testing 100/140 micron optical fiber were presented.[1-2] The Spectran 100/140/500 micron acrylate coated fiber was tested at +25°C and resulted in losses less than .007 dB/m when tested at a dose rate of 34 rads/min to a total dose of 100 Krads. Testing the Lucent SFT radiation hardened 100/140/172 fiber at -125°C to a total dose of 5 Krads with a dose rate of 28.3 rads/min the losses were approximately .15 dB/m and would have been .21 dB/m if the test were continued to 10 Krad. These facts are mentioned to make a comparison to the results presented here. The performance of a radiation hardened fiber under very severe thermal and radiation environments performed similarly to how the 62.5/125 micron optical fiber would in a moderately benign space environment of 1 rad/min for 10 Krads at -25°C (attenuation was .113 dB/m).

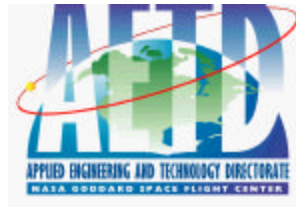
Answering the question as to whether the Lucent SFT 62.5/125/250 micron acrylate coated commercial off the shelf product would be suitable for a space flight environment depends on how much attenuation can be tolerated over short lengths. It is obvious from the data presented that for lengths greater than 10 m this fiber is not the best choice for applications that rely on high performance. However, at low dose rates, total doses and short lengths this fiber can perform with less than 1 dB of losses. For .1 rad/min at 10 Krads the losses at -25°C for 3 meters of fiber (typical length used) is less than .5 dB and at +25°C the losses with these same conditions is less than .3 dB. So in benign radiation environments the commercial 62.5/125 micron fiber can provide a suitable solution in lengths less than 10 m.

References:

1. Melanie N. Ott, "Fiber Optic Cable Assemblies for Space Flight II: Thermal and Radiation Effects," Photonics For Space Environments VI, Proceedings of SPIE Vol. 3440, 1998.
2. Melanie N. Ott, Patricia Friedberg, "Technology validation of optical fiber cables for space flight environments," Optical Devices for Fiber Communication II, Proceedings of SPIE Vol. 4216, 2001.
3. E. J. Friebele, M.E. Gingerich, D. L. Griscom, "Extrapolating Radiation-Induced Loss Measurements in Optical Fibers from the Laboratory to Real World Environments", 4th Biennial Department of Defense Fiber Optics and Photonics Conference, March 22-24, 1994.



Goddard Space
Flight Center
National Aeronautics and
Space Administration



Fiber Optic Epoxy Outgassing Study for Space Flight Applications

NASA/GSFC Component Technology
and Radiation Effects Branch

October 4, 2001

Matthew Bettencourt, Sigma Research and Engineering

Melanie Ott, Sigma Research and Engineering,
NASA Goddard Space Flight Center
Code 562

Advanced Photonic Interconnection Manufacturing Lab
&
Technology Validation Assurance Laboratory for Photonics
(301)-286-0127
melanie.ott@gsfc.nasa.gov

ABSTRACT: Fiber Optic Epoxy Outgassing Study for Space Flight Applications

Presently there are very few epoxies qualified for space flight and even fewer qualified for space flight optical fiber cable assemblies. Currently, Goddard Space Flight Center uses Tra-Con Bipax, Tra-Bond BA-F113AMP for all fiber optic space flight cable harnesses. During this study two epoxies from AngstromBond were tested for their outgassing characteristics inside and outside of a cable configuration. The two test epoxies used in the experiment were the AngstromBond AB9119 and the AngstromBond 9112 fiber optic epoxies.

To test the fiber optic epoxy in cable configuration, the test epoxies were used in lieu of Tra-Con Bipax Tra-Bond BA-F113AMP epoxy in the preparation of the fiber optic cables. The cables were assembled using Goddard Space Flight Center's standard procedure for space flight fiber optic cable. After assembly the cables were tested for their optical performance and inspected for the physical integrity of the fiber endface. Following the performance testing and visual inspection the cables underwent the outgas testing in a CAHN Microbalance. After the testing, the cable were tested again for performance and inspected for damage.

Upon completion of outgas testing in cable configuration it was apparent that two of the cables were damaged. The damage found in the cables made it necessary for the testing outside of cable configuration to be performed. Failure analysis of the damaged cables revealed that the failure was due to the small size of the cables and not the outgassing of the epoxies.

The testing of the fiber optic epoxy when outside of a cable configuration was conducted using the standard procedures for an ASTM-E595 outgassing test. The epoxy samples were cured in separate aluminum dishes and given to material engineers. The engineers cut the sample into the necessary size and shape and conducted the outgas testing. After the completion of the testing, values for Total Mass Loss and Collected Volatile Condensable Materials were received from the material engineers.

When tested in cable configuration the cables prepared with both the AB9119 and 9112 passed the outgas testing with TML values below 1 percent. However, when the epoxies were tested out of configuration the AB9119 epoxy passed and the 9112 failed. Therefore, the conclusion was made that the AB9119 epoxy qualified for space flight use and the 9112 did not.

Introduction

The issue of epoxy used for a fiber optic cable assembly or termination is very significant to the reliability of the system and even more crucial in a space flight environment. The epoxy is needed to ensure the precise alignment of the fiber core within the connector. If the integrity of the epoxy's bond of the fiber to the connector is damaged, then the performance of the fiber optic cable will be affected. The integrity of the bond can be affected by contaminants within the epoxy, improper mixing of the epoxy, air bubbles present when the epoxy is injected into the connector, and the outgassing of the epoxy in a vacuum environment (for space flight applications).

To prevent the epoxy from becoming contaminated, especially for space flight applications, fiber optic technicians must wear gloves and other protective clothing. They are also required to perform all termination and curing procedures within a clean room. To combat the adverse effects that improper mixing of the epoxy can create, the epoxies are mixed using an automatic timed mixer that runs on compressed air. The mixer runs for a set period of time and ensures the proper mixing of the epoxy. Air bubbles within the epoxy when the epoxy is injected into the connector can also affect the integrity of the epoxy's bond. Technicians are required to keep air bubbles from affecting the fiber performance by spinning the mixed epoxy in a centrifuge and injecting the epoxy upward into a connector so that all the air escapes before the epoxy is injected. There is no way to prevent the outgassing of an epoxy from occurring. In order to prevent the outgassing of the epoxy from affecting the integrity of the bond, the engineers must conduct outgas testing on the epoxy. The purpose is to demonstrate how much of the epoxy is released and whether or not this outgassing is significant enough to cause shifts in the fiber such that the optical performance or the reliability of the terminated system is compromised.

The outgas testing of an epoxy is significant because it is the only validation that the epoxy and the terminated system can withstand a vacuum environment. It is very important to make sure that the integrity of the bond and termination is kept, especially in space flight applications where the fiber optic cables cannot be easily replaced. Also any materials released by the epoxy in a vacuum environment could block the transmission of light through contamination of the optical endface or place a stress on the fiber that could result in breaks and cracks. These events could cause a major failure in those components that are using the fiber for communication and data transmission and potentially result in loss of equipment or loss of life if used on a critical system in a manned space craft. The potential for such a great impact on other systems makes the outgas testing of the epoxy such an essential test.

Background

Most of the outgas testing is conducted by materials engineers for Goddard Space Flight Center using a system that is a "diffusion pumped facility" with "a glass cylindrical bell jar containing the outgassing test apparatus specified in ASTM E595-93." (Illustration 1)



Illustration 1

This testing system is known as an "ASTM E595" test. However, this system does not accurately depict the behavior of the amount of epoxy used in the manufacturing of a fiber optic cable. The ASTM E595 test uses 100 to 300 milligram samples during the testing, but an actual fiber optic cable uses far less than the 100 to 300 milligrams used in the ASTM E595 test. To better simulate the behavior of the epoxy when it outgasses within a fiber optic cable assembly a different testing system was used. Instead of testing with the typical ASTM E595 system, the epoxy was evaluated in the termination of a fiber optic cable assembly and the entire assembly (Illustration 2) was tested using another system known as a CAHN recording vacuum balance (Illustration 3).

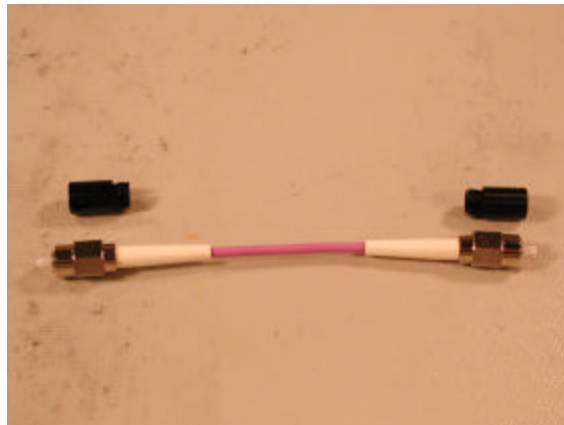


Illustration 2

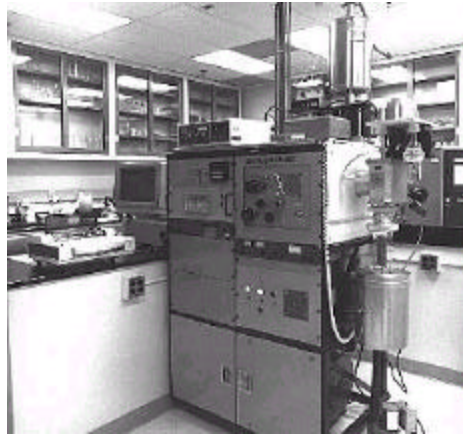


Illustration 3

The use of the CAHN balance system allowed for the observation of the position of the fiber's core within the connector and the presence of any voids that may have occurred in the ferrule filled with epoxy. The CAHN system, while allowing for the testing of the whole cable assembly, still was used to determine the amount of material that was outgassed by the epoxy or the percent contribution of the epoxy material to the materials collected from the cable assembly in a vacuum environment.

Experimental procedure

The experimentation completed in this study was completed in three phases: termination of the samples for testing, configuration testing and epoxy testing in a vacuum environment, and data analysis of the results.

The first phase of the experimentation was the assembly and preparation phase. This phase of the experimentation ensured that each cable met set space flight cable requirements and that the cabling and connectors did not interfere with the data collection within the outgas testing. This phase also ensured that the epoxy samples used in the ASTM E595 test would be an accurate representative of any sample of the test epoxies. The fiber optic cables were prepared and terminated using the standard space flight procedures and the epoxy samples were prepared using the procedures set by the manufacturer and modified with space flight required procedures. Before the prepared cables underwent outgas testing they were inspected visually for faults within the connector and ferrule and then tested for adequate levels of insertion loss.

The second phase of the experimentation was the testing phase. In this phase the fiber optic epoxy underwent the outgas testing and the values for the epoxy's outgas characteristics were collected. The epoxy was tested in cable configuration and out of cable configuration. The in cable configuration testing was conducted using the CAHN recording vacuum balance and the out of cable testing was conducted using the ASTM E595 system. The CAHN recording vacuum balance system measures weight loss of specimens versus time while in vacuum. Temperatures

of up to 125°C can be applied to the specimen. Initially, the sample is weighed manually and inserted in the balance, where a vacuum is produced. As the sample loses weight, the weight loss is automatically recorded with digital interface software that runs on a IBM PC Computer. If the weight change exceeds the recording range on the recorder, it will automatically rescale itself. The system will perform this operation until a maximum of 10g is lost from the sample. Weight loss is monitored until equilibrium is reached. The chamber cycles the temperature from 25°C to 75°C over twenty-four hours at a constant rate. The vacuum chamber is 2 inches in diameter by 20 inches long. The sample fiber optic cable assembly was hung vertically within the chamber. The ASTM E595 system used at GSFC is a micro-CVCM apparatus. The apparatus presented in ASTM E 595-77/84/90 has a number of critical dimensions to ensure that similar systems should produce similar results. These critical dimensions are described in E 595-77/84/90. A number of samples can be tested at one time in the vacuum system. Each sample, of 100 to 300 milligrams mass - nominally 250 milligrams - is placed into a pre-weighed aluminum foil boat, which has been thoroughly cleaned and dried. Following a 24-hour pre-conditioning at 25° C, 50% relative humidity and standard atmospheric pressure to ensure that the samples receive a common preliminary treatment, the individual samples are weighed. The samples are then loaded into individual compartments in a solid copper bar that can be heated. Each compartment is closed by a solid copper cover, requiring that all volatile materials escape only through a 6.3-mm (0.25-in.) diameter exit port. The copper heater bar, having 12 sample compartments, is heated to 398 K (125° C) for 24 hours. The sample is also heated to 398 K (125° C) by conduction and radiation. This causes the volatile materials to be driven off, with their only escape being through the exit port. At a distance of 12.7 mm (0.5 in.), a chromium-plated collector is in direct line of sight of the exit port and is maintained at 298 K (25° C). A significant portion of the escaping volatiles collects on the chromium-plated disk if the condensation temperature is 298 K (25° C) or above. Barriers are near the collector plate to prevent cross-contamination between adjacent samples. The mass loss of the sample is determined from the weights before and after the 398 K (125° C) exposure, and the percentage loss is calculated to provide the TML. In a similar manner, the difference between the weight of a clean collector and of the collector having condensed materials will provide the mass of condensables. This mass of condensables is calculated as a percentage of the starting mass of the sample, and stated as CVCM. During the outgas testing with both systems the values for Total Mass Loss (TML) were collected. Additionally, when the epoxy was tested using the ASTM E595 system values for Collected Volatile Condensable Materials (CVCM) were obtained.

The third phase of the experimentation was the analysis phase. In this phase the fiber optic cables were again inspected for faults, voids, or damages caused by the releasing of the materials in the vacuum environment using a high powered microscope. The cables were also tested again for insertion loss values to ensure that there was no damage to the fiber that could not be seen.

The termination procedure for Phase One is documented below.

Cable Configuration Test Samples

- Cable Preparation
 1. Cut required length of fiber, 6.3 inches, off of the spool for each cable.
 2. Cut outer jacket to required length, 3.9 inches, for each cable.

3. Use stripper (Claus No-Nik) to remove 0.4 inches of outer jacket from each end of cable to expose strength members.
 4. Cut inner buffer tubing to 0.12 inches away from outer jacket.
 5. Inspect fiber for any nicks or cuts.
- Cable Stripping
 1. Pour stripping formula of Sulfuric Acid (95-98%) into 100mL beaker.
 2. Place beaker on hot plate and heat up to 142°C (+5°C, -2°C).
 3. Fill 3 100mL beakers with Deionized water.
 4. Fill 1 100mL beaker with 2-Propanol alcohol
 5. Place fiber end into acid for 1 minute when reaches 142°C.
 6. Remove carefully and place fiber end in each beaker of Deionized water for 30 seconds.
 7. Place fiber end into 2-Propanol beaker and swish around for 1 minute.
 8. Wipe dry with small kim-wipe.
 9. Repeat as necessary.
 - Cable Cleaning
 1. Wipe all beakers down with clean solvent prior to use.
 2. Wipe all tweezer surfaces with cleaning solvent and place on large, clean dry wipe.
 3. Fill two labeled beakers with cleaning solvent as follows: 100ml to beaker #1 and beaker #2
 4. Place epoxy syringes in beaker #1
 5. Operate ultrasonic cleaner for five minutes and place syringes on clean dry towel.
 6. Place one packet of connector parts into beaker #2.
 7. Operate ultrasonic cleaner for five minutes using beaker #1 and placed syringes on clean dry towel
 8. Repeat for number of desired connectors using beaker #2 (one packet per connector).
 - Epoxy Mixing
 1. Open epoxy packaging and remove middle separation clip.
 2. Squeeze the package to start mixing.
 3. Place the package on pad inside the TraCon automatic timed mixer.
 4. Turn on the automatic mixer and wait 5 minutes.
 5. Place epoxy package in the centrifuge and turn on for 3 minutes
(making sure that centrifuge is balanced).
 6. Cut package open and poured into pre-cleaned syringe.
 7. Insert syringe piston and pushed piston until all trapped air is expelled.
 - Termination
 1. Clean the entire stripped cable end and allow to dry for five minutes.
 2. Place pre-cleaned connector boot and crimp sleeve on fiber.
 3. Insert syringe into back of the connector body until it butted against the ferrule and squeeze enough in until a small bead appeared at the ferrule tip.

4. Slowly remove the syringe while ensuring that the rear barrel is kept full of epoxy as the tip is withdrawn.
 5. Blot excess epoxy from the ferrule face.
 6. Insert the fiber into the connector using a vertical rotation and push the fiber gently down until the fiber emerged from the ferrule and can not be inserted farther.
 7. Put a thin coat of epoxy in the outside threads of the rear connector body.
 8. Slide the crimp sleeve up against the connector body and crimp the sleeve around the rear barrel of the connector.
 9. Place the connector into the curing oven for 35 minutes at 120° C.
 10. Once cured, scribe the fiber with the scribe using a gentle motion.
 11. Gently grasp the fiber and pull the excess away from the ferrule face.
 12. Repeat for 2nd connector for each cable needed.
- Polishing
 1. Use the Buehler Fibermet Polisher to polish the connector end face in the following sequence:
 - a. Use wet 3 micron diamond film polish for 10 arm cycles or 50 seconds and clean end with alcohol.
 - b. Use wet 1 micron diamond film polish for 10 arm cycles or 50 seconds and clean end with alcohol.
 - c. Use dry 0.5 micron diamond film polish for 10 arm cycles or 50 seconds and clean end with alcohol.
 - d. Use dry 0.1 micron diamond film polish for 5 arm cycles or 25 seconds and clean end with alcohol.
 - e. Use 0.05 micron aluminum oxide film polish for ½ wet and ½ dry arm cycles or 5 seconds.
 - f. After completing polishing sequence clean the fiber end with alcohol.
 - Inspection
 1. Using the Buehler Fiberskope inspect the fiber end at a magnification of 200x.
 2. Ensure that the connector face is free from cracks, scratches, edge chips, hackles, pits and other anomalies.
 3. If any anomalies are present re-polished the endface using a half time procedure starting with the 0.5 micron diamond film.
 4. If no anomalies are present cover endface with a dust cap and place aside for testing.
 5. After polishing is complete, use multimeter, power sensor, and laser source to conduct insertion loss testing and record data for each cable.

Out of Configuration Test Samples

- Epoxy Sample Preparation
 1. Open epoxy packaging for AB9119 and remove middle separation clip.
 2. Squeeze the package to start mixing.
 3. Place the package on pad inside the TraCon automatic timed mixer.
 4. Turn on the automatic mixer and wait 5 minutes.
 5. Place epoxy package in the centrifuge and turn on for 3 minutes

- (making sure that centrifuge is balanced).
6. Cut open epoxy package and pour approximately half of 2.5 package into precleaned aluminum foil boat.
 7. Place aluminum boat on curing oven and cure for 30 minutes at 120°C
 8. Repeat steps for other epoxy sample, 9112, and cured at 90°C for 30 minutes.

The procedures used for Phase Two are documented below:

- CAHN Recording Vacuum Balance system
 1. Place one terminated cable into testing cylinder of MOLIDEP CAHN Vacuum Balance
 2. Start the outgas program of the MOLIDEP as specified in NASA Directive No. 541-WI-5330.1.14
 3. After completion of the testing compile the data and analyze.
 4. Compare results to specification values of space flight materials.
 5. Repeat for each additional cable.
- ASTM E595 system
 1. Place epoxy sample within E-595 testing apparatus.
 2. Begin procedures specified in ASTM E-595-90.
 3. Remove sample and compile data.
 4. Compare results to specification values of space flight materials.
 5. Repeat for second epoxy sample.

The procedures for Phase Three were:

1. Re-inspect fiber ends using Buehler Fiberskope and check for any changes in the fiber's position or condition.
2. Use multimeter, power sensor, and laser source to conduct insertion loss testing and record data.
3. Use OTDR to determine if the cable has experienced any damages due to the outgassing of the epoxy

Instrumentation

Each phase of the experimentation required specific equipment.

Equipment used during Phase One:

- Curing Oven, OFCI # 08-0028-OFC, 24 port for ST/FC/SMA/SC
- Clauss No-Nik, NN023
- Ideal Jacket Stripper, 45-164
- 3M Diamond angled Scribe, 05-00010
- Clauss Scissors, 925C
- Tec Cut Strength Member Shears, 702SC023
- Clauss Fiber Trash Can, FS200

- Molex Syringe & Tip, 86710-0023
- Lint Free Kim Wipes
- Alcohol Reservoir Bottle
- 95-98% Sulfuric Acid
- Buehler Fibermet Optical Fiber Polisher, B-0273
- 3, 1, 0.5, 0.1, and 0.05 micron polishing paper
- Tracon Roller & pad, MXR-1001

Equipment used during Phase Two:

- NASA/GSFC MOLIDEP CAHN Vacuum Balance
- E-595 Outgas testing apparatus outlined in ASTM E-595-90

Equipment used during Phase One & Three:

- Noyes Testing Kit, with 850 nm Power Meter, 850 nm Light Source, MLP4-2
- Buehler Fiber Termination Inspection Fiberskope Zoom 200-400X, Buehler #0801-0504
- Nikon SMZ High Powered Microscope
- Nikon Digital Camera
- HP 8153A Lightwave Multimeter
- HP 81532A Power Source
- HP 81551MM Laser Source
- OPTO Electronics Inc. Optical Fiber Monitor, Model OFM130

Data and Results

All the samples underwent outgas testing in a vacuum environment for Total Mass Loss (TML) and/or Collected Volatile Condensable Materials (CVCM). The values for TML and CVCM were then analyzed and specific characteristics of each of the epoxies were revealed. Before the outgas testing, the fibers underwent visual inspections (Table 1) for detection of shifts or unwanted movement of the fiber's core and optical testing (Table 2) to monitor the performance values of the test cables. After completing the outgas testing, the fibers again underwent visual inspections (Table 1) to detect shifts or unwanted movement of the fiber's core and optical testing (Table 2) to monitor the optical performance values of the test cables.

The original hypothesis of the experimentation was that all the epoxies would qualify for use in space flight components. Each of the epoxy would share the standard characteristics that other space flight qualified epoxies have, such as cure time, cure temperature, Total Mass Loss, and Collected Volatile Condensable Materials. The values for Total Mass Loss (Table 3 & 4) and Collected Volatile Condensable Materials (Table 5) for each of the epoxies would be under 0.1 percent. The epoxies would experience no shifts in shape and no reduction in performance values after testing in the vacuum environment.

The testing was conducted using a CAHN Microbalance, an E-595 outgas testing apparatus, optical sources and receivers, an optical fiber monitor, and high-powered microscopes. The microbalance and outgas testing apparatus held the sample fiber optic cable in a vacuum environment and recorded the mass of the material that was released by the epoxy and cable. The mass of the material released was compared to the total mass of the cable before and after the testing. The comparison resulted in values for Total Mass Loss and Collected Volatile

Condensable Materials for each of the epoxies. These values were compared to the standards for outgas testing, TML of less than one percent and CVCM of less than 0.01 percent. It was determined whether or not the epoxies met these standards and then conclusions were drawn.

The results from the testing from the ASTM E595 testing can be seen in Tables 7&8.

Visual Inspection		
Cable	Before	After
9112 Cable # 1 End A	PASS	FAIL (no back light present)
9112 Cable # 1 End B	PASS	PASS
9112 Cable # 2 End A	PASS	PASS
9112 Cable # 2 End B	PASS	PASS
AB9119 Cable # 1 End A	PASS	PASS
AB9119 Cable # 1 End B	PASS	PASS
AB9119 Cable # 2 End A	PASS	PASS
AB9119 Cable # 2 End B	PASS	FAIL (no back light present)

Table 1

Insertion Loss For Fiber Optic Cables (in dB)		
Cable	Before Testing	After Testing
9112 Cable # 1	0.02 dB	No Light
9112 Cable # 2	0.01 dB	0.18 dB
AB9119 Cable # 1	0.01 dB	0.01 dB
AB9119 Cable # 2	0.01 dB	No Light

Table 2

Total Mass Loss While in Cable Configuration (in percentage of total mass)	
9112 Cable # 1	0.06545 %
9112 Cable # 2	0.03106 %
AB9119 Cable # 1	0.01934 %
AB9119 Cable # 2	0.03045 %

Table 3

Average Total Mass Loss of Epoxy Alone (in percentage of total mass)	
Epoxy (9112)	4.33%
Epoxy (AB9119)	0.64%

Table 4

Average Collected Volatile Condensable Materials of Epoxy (in Grams, when tested alone)	
Epoxy (9112)	1.34%
Epoxy (AB9119)	0.00%

Table 5

MICRO VCM TEST REQUEST AND DATA SHEET PER ASTM E-595-93

(Requestor please read, then furnish all information above asterisks.)

Requested by: **Matt Bettencourt**

Phone: **6-8311**

Date: **4/12/01**

Material Identification (product name, number, description, classification, etc.)

Angstrom Bond 9119 Fiber Optic Epoxy

Manufacturer of Material (Name, City and State Address): **Fiber Optic, Inc., 23 Center Street, New Bedford, MA**

Material application (general usage, i.e. adhesive, coating, potting, etc.): **Fiber Optic Epoxy**

J. O. Number/Project Name: **EOS/PM**

Request Infra-Red Spectra? YES NO

Originator Source/Code (other than Code 541): **562**

Indicate processing required by GSFC Materials personnel. Include the recipe, cure(s), and special instructions to be performed.

None

If material is to be tested in the "as received" condition, without further processing required, indicate in full the past history, recipe, cure(s), post cure(s), nomenclature of components, etc.

Cured @ 120 degrees C for 10 minutes after automatic mixing and 3 minutes in centrifuge

CVCM test specimen preparation and description: **cut up & put in boats**

Bar Position-CVCM Test Number	25607 (7)	25608 (9)	25609 (9)
Initial mass, holder and specimen, gm	0.264538	0.250444	0.273846
Mass of holder, gm	0.035022	0.035010	0.034572
Initial specimen mass @ 50 %RH, gm	0.229516	0.215434	0.239274
Final mass, holder & specimen, gm	0.263006	0.249102	0.272339
Total mass loss, specimen, gm	0.001532	0.001342	0.001507
Percent TML, specimen	0.67%	0.62%	0.63%
Average value TML	*****	0.64%	*****
Mass after 50 %RH re-soak, 23 C, 24hr, gm	0.263812	0.249870	0.273074
Total mass, water vapor regain, gm	0.000806	0.000768	0.000735
Percent water vapor regain	0.35%	0.36%	0.31%
Average value WVR @ 50 %RH	*****	0.34%	*****
Initial mass, collector, gm	1.730079	1.735126	1.738126
Final mass, collector, gm	1.730096	1.735134	1.738126
Collected mass – CVCM, gm	0.000017	0.000008	0.000000
Percent CVCM	0.01%	0.00%	0.00%
Average Value CVCM	*****	0.00%	*****

Remarks: CVCM (unweighable) on separator plate to _____ mm diameter. CVCM appearance as follows: _____ is not detectable on collector plates.

thin; _____ heavy; **smoke** color; _____ transparent; _____ colored liquid;

opaque; matte; interference fringes; foggy; distorts eye reflection; smooth; smoky; splotchy; partially opaque;

clear liquid; liquid runs in excess; Deposit covers **15** % of collector disc.

Specimen appearance after test:

No Visible Change

Test started 4/18/01
Pascal

Test completed: 4/19/01

Period 24 Hrs.

Pressure 5.6×10^{-5}

Specimen Temp. 124.3 °C

Collector Temp. 24.8 °C

Analyst Dewey Dove & Debbie Thomas

VCM REV 14 25 JAN 2001

Table 7

MICRO VCM TEST REQUEST AND DATA SHEET PER ASTM E-595-93

(Requestor please read, then furnish all information above asterisks.)

Requested by: **Matt Bettencourt**

Phone: **6-8311**

Date: **4/12/01**

Material Identification (product name, number, description, classification, etc.)

Angstrom Bond 9112, Fiber Optic Epoxy

Manufacturer of Material (Name, City and State Address): **Fiber Optic, Inc., 23 Center Street, New Bedford, MA**

Material application (general usage, i.e. adhesive, coating, potting, etc.): **Fiber Optic Epoxy**

J. O. Number/Project Name: **EOS/PM**

Request Infra-Red Spectra? YES NO

Originator Source/Code (other than Code 541): **562**

Indicate processing required by GSFC Materials personnel. Include the recipe, cure(s), and special instructions to be performed.

None

If material is to be tested in the "as received" condition, without further processing required, indicate in full the past history, recipe, cure(s), post cure(s), nomenclature of components, etc.

Cured @ 90 degree C for 15 minutes after automatic mixing and 3 minutes in centrifuge

CVCM test specimen preparation and description: **cut up & placed in boats**

Bar Position-CVCM Test Number	25610 (10)	25611 (11)	25612 (12)
Initial mass, holder and specimen, gm	0.233235	0.239087	0.257544
Mass of holder, gm	0.033617	0.032973	0.033130
Initial specimen mass @ 50 %RH, gm	0.199618	0.206114	0.224414
Final mass, holder & specimen, gm	0.224238	0.230013	0.248400
Total mass loss, specimen, gm	0.008997	0.009074	0.009144
Percent TML, specimen	4.51%	4.40%	4.07%
Average value TML	*****	4.33%	*****
Mass after 50 %RH re-soak, 23 C, 24hr, gm	0.225476	0.231431	0.249450
Total mass, water vapor regain, gm	0.001238	0.001418	0.001050
Percent water vapor regain	0.62%	0.69%	0.47%
Average value WVR @ 50 %RH	*****	0.59%	*****
Initial mass, collector, gm	1.746686	1.746588	1.739651
Final mass, collector, gm	1.749516	1.749360	1.742468
Collected mass - CVCM, gm	0.002830	0.002772	0.002817
Percent CVCM	1.42%	1.34%	1.26%
Average Value CVCM	*****	1.34%	*****

Remarks: CVCM (unweighable) on separator plate to _____ mm diameter. CVCM appearance as follows: _____ is not detectable on collector plates.

_____ thin; _____ heavy; **blue** color; transparent; _____ colored liquid;
 opaque; matte; interference fringes; foggy; distorts eye reflection; smooth; smoky; splotchy; partially opaque;

clear liquid; liquid runs in excess; Deposit covers **100** % of collector disc.

Specimen appearance after test:

gummy

Test started 4/18/01
Pascal

Test completed: 4/19/01

Period 24 Hrs.

Pressure 5.6×10^{-5}

Specimen Temp. 124.3 °C

Collector Temp. 24.8 °C

Analyst Dewey Dove & Debbie Thomas

VCM REV 14 25 JAN 2001

Table 8

Discussion

The fiber optic cables met the necessary space flight termination specifications. After termination each prepared cable was inspected visually, mechanically and optically. If any flaws were present the cables were re-terminated. None of the cables failed initial inspections (Illustration 4). The cables were polished properly and met all criteria for space flight termination.

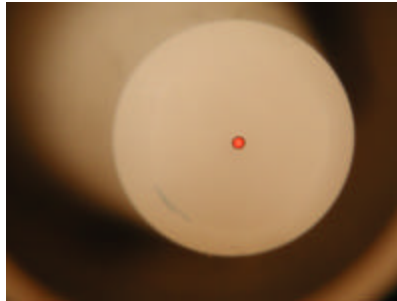


Illustration 4

The fiber optic cables were required to have adequate performance levels before and after the outgas testing. Before and after the outgas testing the test cables were tested for their insertion loss. This testing showed the amount of light, or information, that was lost within the cable. The standard accepted value for insertion loss is 1 dB. All of the test cables had insertion loss values below this value prior to outgas testing (Table 2). However, after outgas testing, two of the cables did not have values for insertion loss within the accepted range (Table 8). The 9112 Cable # 1 and the AB9119 Cable # 2 had no light visible for the insertion loss reading. The light loss of these cables showed that some type of damage had occurred during the outgas testing of each of these cables. After failure analysis, it was learned that the short length of the test cables did not allow for the adequate amount of flex needed to prevent the fiber from breaking during the thermal expansion and contraction of the outer jacket. The post visual inspection showed no voids present around the ferrule and the fiber core on any of the cables (Illustration 5), but no light passed through 9112 cable #1 and AB9119 cable #2 so they failed final visual inspection and optical performance testing.

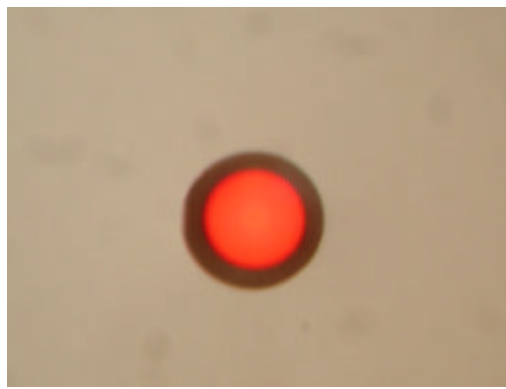


Illustration 5

The data for each epoxy during outgas testing are required to be compared to the standard values for space flight hardware. The standards for outgassing of materials during outgas testing are a TML of less than 1 percent and a CVCM of less than 0.10 percent. In the outgas testing of the epoxy in cable configuration each cable had a TML that was within the standards for outgassing (Table 4). However, when the two epoxies were tested alone in the E-595 testing apparatus the values showed different results (Table 4&5, 7&8). The AB9119, had a TML of 0.64 percent. This percentage is within the standards for outgassing of materials. The 9112, had a TML of 4.33 percent. This percentage was above the accepted value for TML. The values for CVCM were only taken during the testing of the epoxy alone. The AB9119 had a CVCM value of 0.00 percent. This value was well within the standards. The 9112, however, had a CVCM value of 1.34 percent. This value was significantly above the standards for the CVCM of outgas testing.

Conclusions

The outgas testing of the fiber optic epoxy allowed for specific values to be documented that represent the epoxy's outgas characteristics. By ensuring that the fiber optic cables that were prepared for testing met the standards for space flight terminations and that each cable had an adequate performance level, the validity of the outgas characteristics was maintained. The values acquired during the outgas testing demonstrated that the AngstromBond 9119, epoxy had outgas characteristics that were within the acceptable ranges for flight qualified fiber optic epoxies. Yet, the values acquired for the, AngstromBond 9112, epoxy had characteristics that were not within the acceptable values. Both of the epoxies did not meet the requirements for space flight qualified epoxies thereby voiding the hypothesis that both epoxies would pass the outgas testing with acceptable characteristics. One epoxy passed, one did not.

The AngstromBond 9119 epoxy has the necessary outgassing characteristics to qualify for use in a space flight environment. The epoxy produced no adverse effects on the fiber optic cable's performance and did not shift due to the presence of a vacuum environment.

The AngstromBond AB9112 epoxy did not have the necessary outgassing characteristics needed to qualify for use in a space flight environment. While the epoxy did not have any adverse effects on the performance of the fiber optic cable or produce any shifts of the core while in the vacuum environment, the values for TML and CVCM obtained during the outgas testing were not within the needed standards that warrant qualification.

The testing of fiber optic epoxies in cable configurations should be performed with adequate length of fiber within the cabling to withstand the stresses caused by the expansion and contraction of the outer jacket. The results of the configuration testing were inconclusive although none of the optical fiber interfaces appeared to be affected by the outgassing of epoxy out of the ferrule when verified by visual inspection.

References

1. Designers Guide to Fiber Optics. (1982) Harrisburg, Pennsylvania: AMP Inc.
2. Larson, W.J., & Wertz J.R..(1992). "Spacecraft Manufacture and Test", In Space Mission Analysis and Design, Second edition. California: Microcosm, Inc., & Boston: Kluwer Academic Publishers.
3. Mahlke, G., & Gössing, P.. (1997). Fiber Optic Cables, Third Revised and Enlarged Edition. Berlin: Siemens Aktiengesellschaft.
4. Powers, J.. (1997) An Introduction To Fiber Optic Systems, Second Edition. Boston: Irwin.
5. Trehwella, J.M., DeCusatis, C.M., Fox, J.. "Performance comparison of small form factor fiber optic connectors". Advanced Packaging, IEEE Transactions. Volume: 23 Issue: 2 , May 2000
6. Hikita, M., Tomaru, S., Enbutsu, K., Ooba, N., Yoshida, R., Usai, M., Yoshida, T., Imamura, S.. "Polymeric optical waveguide films for short-distance optical interconnects". Selected Topics in Quantum Electronics, IEEE Journal on , Volume: 5 Issue: 5, Sept.-Oct. 1999
7. Takeuchi, Y., Mitachi, S., Nagase, R.. "High-strength glass-ceramic ferrule for SC-type single-mode optical fiber connector". IEEE Photonics Technology Letters , Volume: 9 Issue: 11 , Nov. 1997
8. National Aeronautics and Space Administration Goddard Space Flight Center. Total Mass Loss (TML) and Collected Volatile Condensable Materials (CVCM) from Outgassing in a Vacuum Environment (Publication No.E 595-77/84/90). Greenbelt, Md: U.S. Government Printing Office.
9. Kihara, M., Nagasawa, S., Tanifuji, T.. "Return loss characteristics of optical fiber connectors". Lightwave Technology, Journal of , Volume: 14 Issue: 9 , Sept. 1996
10. Broadwater, K., Mead, P.F.. (2000). "Experimental and numerical studies in the evaluation of epoxy-cured fiber optic connectors". Paper presented at Electronic Components & Technology Conference.
11. Liu, J.G., Andersen, B.M., Bergmann, E.E., Fairchild, S.K.. (2000). Epoxy adhesives for optical element attachment in planar passive optical components". Paper presented at Electronic Components & Technology Conference, 2000.
12. National Aeronautics and Space Administration Goddard Space Flight Center. Outgassing Data for Selecting Spacecraft Materials Online. (2000, Oct 15). Available: <http://epims.gsfc.nasa.gov/og/>.
13. National Aeronautics and Space Administration Goddard Space Flight Center.
14. Instructions For EEE Parts Selection, Screening, and Qualification. (2000) Available : http://misspiggy.gsfc.nasa.gov/ctre/parts/inst/rev_a/311insta.pdf

Evaluation of VCSEL Mounted on CVD Diamond Substrates

Home

Current Projects

Past Topics in...

TVA Library

Validation Methods

TVA Group Members

Links

Site Index

Harry C. Shaw

301-286-6616

Associate Branch Head

Component Technology and Radiation Effects Branch

Goddard Space Flight Center

harry.c.shaw@gsfc.nasa.gov

Melanie N. Ott

301-286-0127

Director, Advanced Photonic Interconnection Manufacturing
Laboratory

Director, Technology Validation Laboratory for Photonics

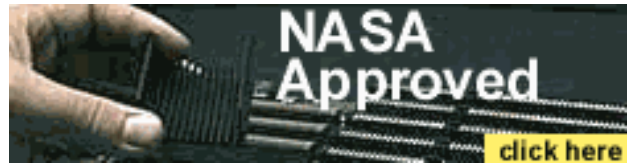
Sigma Research and Engineering

Goddard Space Flight Center

Melanie.Ott@gsfc.nasa.gov

Evaluation of Vertical Cavity Surface Emitting Lasers (VCSEL) mounted on CVD Diamond Substrates

- [Part 1 of Report](#)
- [Part 1B of Report](#)
- [Part 2 of Report](#)
- [Conclusion of Report](#)



Tailoring Cores of Optical Fibers by a Sol-Gel Method

Core dopants can be tailored for specific photonic applications.

Discuss this and other technologies with colleagues at the [Reader Forum](#)

Goddard Space Flight Center, Greenbelt, Maryland

A method of tailoring the cores of optical fibers to obtain optical properties needed for specific photonic applications exploits the sol-gel process. The method is expected to open new avenues of development of fiber-optic sensors for measuring strain, temperature, intensity of ionizing radiation, concentrations of chemicals, and numerous other quantities.

Heretofore, the optically active dopants that constitute the transducer materials of fiber-optic sensors have generally been incorporated into films deposited on the exterior surfaces of optical fibers. In some cases that are particularly relevant to the present development, the exterior films have been doped sol-gels. The operation of such a sensor depends on evanescent-wave coupling of light between core of the fiber and the dopant(s) in the coating film. However, the inherent weakness and large optical loss of evanescent-wave coupling are obstacles to the attainment of adequate sensor response.

If the dopant(s) could be incorporated into the core, the optical coupling would be much stronger and the sensory light could propagate to the detection equipment with very little loss. In addition, given the limit of solubility of the dopants in the sol-gel reaction mixture and the wave-propagation geometry, the optically effective quantity of dopant that could be contained in the bulk of the core would be much greater than the optically effective quantity of dopant that can be contained in an exterior sol-gel sensory film. The net effect of incorporating the dopant into the core would be to make the sensor much more sensitive. The present method exploits this effect.

A fiber-optic sensor fabricated by this method offers an additional advantage (beyond direct vs. evanescent-wave coupling) over a comparable prior-art sensor that comprises an optical fiber coated with a doped sol-gel film. This advantage arises in connection with the fact that to prevent thermal degradation of dopants in the prior art, it is necessary to deposit the sol-gel film first, then diffuse the dopants into the pores of the film. As a result, there is a tendency for the dopants to leach out of the pores of the sol-gel film in some sensor operating environments. In the present method, there is little or no tendency for the

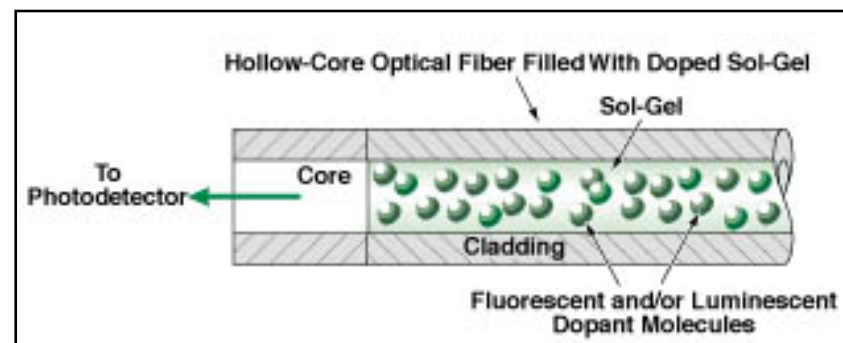
dopants to leach out because the dopants are incorporated deep within the sol-gel core, which, in turn, is protected from the environment by the cladding layer of the fiber.

In the present method, the dopants are dissolved and incorporated as ingredients in a sol-gel reaction mixture, which is injected into an initially hollow optical fiber. The sol-gel is then polymerized, forming a monolithic solid core that comprises a porous sol-gel with the dopants occupying its pores (see figure).

One main obstacle that had to be overcome in the development of the present method was the tendency of sol-gels to shrink and crack during polymerization. In fiber-optic sensors, cracks cannot be tolerated because they cause large optical losses. Moreover, the extreme temperatures and pressures

often used for processing sol gels will cause fatigue and damage to optical fibers and preclude the use of many biochemical dopants. The success of the present method stems from the development of sol-gel formulations that can contain adequate amounts of sensory dopants and can be polymerized while managing the shrinkage in a near-room-temperature process.

The process for fabricating the tetraethyl orthosilicate (TEOS) based sol gels employs a number of agents to reduce the process problems inherent in the condensation-polymerization process. A variety of configurations of sensors is being evaluated, including sensors utilizing intrinsic and extrinsic sol-gels. Fluorescent sensing experiments with sol-gels doped with fluorescence derivatives and calcofluor derivatives are underway. Both substances have a wide variety of potential applications in biochemistry and monitoring of metabolic reactions at the cellular level.



A **Monolithic Core** of sol-gel material with dopant molecules in its pores is formed in an initially hollow optical fiber.

*This work was done by Harry C. Shaw and Michele V. Manuel of **Goddard Space Flight Center** and Melanie N. Ott of Sigma Research and Engineering. For further information, access the Technical Support Package (TSP) **free on-line** at www.nasatech.com under the [Materials category](#).*

This invention is owned by NASA, and a patent application has been filed. Inquiries concerning nonexclusive or exclusive license for its commercial development should be addressed to the Patent Counsel, Goddard Space Flight Center; (301) 286-7351. Refer to GSC-13913.

[Download detailed Technical Support Package for this Brief](#)

[SEARCH](#) | [HOME](#) | [ABOUT NTB](#) | [LINKS](#) | [CONTACT US](#) | [FEEDBACK](#) | [PRIVACY](#)

All information property of ABP International

Technology validation of optical fiber cables for space flight environments

Melanie N. Ott^{*a}, Patricia Friedberg^b

^a Sigma Research and Engineering/ NASA Goddard Space Flight Center

^b NASA Goddard Space Flight Center

Component Technologies and Radiation Effects Branch, Code 562, Greenbelt, Maryland 20771

ABSTRACT

Periodically, commercially available (commercial off the shelf, COTS) optical fiber cable assemblies are characterized for space flight usage under the NASA Electronic Parts and Packaging Program (NEPP). The purpose of this is to provide a family of optical fiber cable options to a variety of different harsh environments typical to space flight missions. The optical fiber cables under test are evaluated to bring out known failure mechanisms that are expected to occur during a typical mission. The tests used to characterize COTS cables include: vacuum exposure, thermal cycling and radiation exposure. Presented here are the results of the testing conducted at NASA Goddard Space Flight Center on COTS optical fiber cables over this past year. Several optical fiber cables were characterized for their thermal stability both during and after thermal cycling. The results show how much preconditioning is necessary for a variety of available cables to remain thermally stable in a space flight environment. Several optical fibers of dimensions 100/140/172 microns were characterized for their radiation effects at -125°C using the dose rate requirements of International Space Station. One optical fiber cable in particular was tested for outgassing to verify whether an acrylate coated fiber could be used in a space flight optical cable configuration.

Keywords: fiber optic, radiation effects, thermal effects, communications, harsh environments, multimode, testing, cable, preconditioning.

1. INTRODUCTION

This is the fifth paper in a series of publications on the subject of characterization of commercial optical fiber and optical cables for space flight.¹⁻⁴ The objective of these publications is to provide information on the correct environmental usage of commercial cables for space flight through characterization testing to typical space flight environmental parameters. Several tests are used as a technology validation method to determine if an optical cable is suitable for a typical space flight environment. Included in this validation testing is outgassing testing, thermal testing and radiation testing. Vibration testing is also used as a technology validation test but data from this type of testing is not included in this paper.

In most cases, all materials used on space flight hardware are evaluated for outgassing characteristics in a vacuum environment to ASTM 595 (% Total Mass Loss, %TML must be less than 1%).⁵ If a material passes the ASTM 595 test then the material is considered acceptable for usage in a vacuum environment. A comprehensive database is available via a NASA GSFC website.⁵ In some cases when a material is known to outgas in a vacuum environment, the potential for usage still exists if the outgassing occurs in an area of the unmanned portion of a space craft such that these materials could not degrade the performance of any existing systems. Acrylate coatings used as protection on optical fiber are well known as "outgassers" and therefore are usually prohibited from space flight missions. However, acrylate coating used inside of a cable configuration was evaluated by Lockheed Martin to verify whether the acrylate coating added to the collected materials or mass loss. The testing showed that this configuration was acceptable by ASTM-595. The result of this testing was never verified at GSFC until now.

Thermal stability of optical cables is examined in two ways. The first is to examine the optical stability of fiber optic cable configuration given a changing thermal environment or during thermal cycling. The second is to examine the total amount of cable component shrinkage after exposure to a changing thermal environment or after thermal cycling. Both tests are used to determine if a cable is suitable for space flight. Presented here are results from testing using a generic thermal environment of -55°C to +125°C.

* melanie.ott@gsfc.nasa.gov, 301-286-0127, misspiggy.gsfc.nasa.gov/tva/photronics.html

Lastly, of the subjects presented here, total ionizing dose radiation testing is used as a technology validation method of determining which fiber cable is suitable for space flight environment usage. The data presented is from testing using the International Space Station environment at two different dose rate exposures while at a temperature of -121°C. In most cases, low temperature during radiation exposure, represents the worst case for radiation induced attenuation for cable configurations containing typical germanium doped 100/140 micron optical fiber. At colder temperatures optical fiber is less likely to anneal and recover from the color centers generated as a result of radiation exposure. The test results from cold temperature radiation exposure of three optical fibers are discussed here.

2. THERMAL CHARACTERIZATION OF CABLES

2.1 Discussion of experiments on thermal characterization

For this thermal characterization, five fiber optic cable configurations were tested: one from W.L. Gore, two from Brand Rex, and two from RIFOCS (manufacturer Northern Lights). All cables chosen for testing, were chosen based on the intention that these cables would be used for space flight applications. These cables were designed to be commercially available (all but the OC1614 which was made for space station) but also space flight ruggedized cable configurations. One of the Brand Rex cables, the OC1008, included in this study is actually a discontinued item but was included for comparison purposes since this cable was used for both the TRMM and XTE missions. The W.L. Gore cable was designed to be used in the -55°C to +125°C thermal environment and the Brand Rex space station cable OC1614 was designed for the -100°C to +75°C, but most of the other candidates have a smaller thermal range for performance. It is important to note that the OC1614 is based on the configuration described in Table 1, which includes a polyimide coated fiber and it is very likely that the cable could be operated all the way to +200°C. Brand Rex does confirm that although the OC1614 was made to the SSQ-21654 specification, it could be capable of temperatures well beyond the upper limit of +75°C. Table 1 describes the configurations of the cables tested with some details about their dimensions and specified thermal ratings. The cables listed in Table 1 with the exception of the OC1008 are in fact available or will be available if not already, with other types of optical fiber. Brand Rex, W.L. Gore and RIFOCS have communicated the intention of using these configurations to manufacture for various different applications that require other fiber diameters that are the standard outer diameter of 125 microns or the 140 micron nonstandard fiber with acrylate and polyimide coatings. Therefore, the products listed here are only an example of the family of cables that are available using these configurations and these cables were chosen based on availability at the time of this testing.

Table 1: Summary of cable configurations thermally characterized for length shrinkage and optical performance.

Vendor Cable Part #	Cable Configuration	Fiber Type	Secondary Buffer	Strength Members/ Jacket	Outer diameter	Thermal rating
W.L. Gore FON1004	Tight Tube with Metal braid over GoreTex buffer	Single mode, 1310/1550 nm acrylate buffer	Gore Tex Expanded PFA	Kevlar/FEP	2.5 mm	-55°C to +125°C
Brand Rex OC1614 (SSQ-21654 Rev. B)	Tight tube	Multimode 100/140/170 hermetic seal/ polyimide buffer	FEP Teflon	Teflon impregnated fiber glass/FEP	2.1 mm	-100°C to +75°C
Brand Rex OC1008	Loose tube	Multimode 100/140/500 acrylate buffer from corning now discontinued	Hytrell	Teflon impregnated fiber glass/ETFE	2.77 mm	- 55°C to +85°C
RIFOCS H06	Tight tube	Multimode 62.5/125/250	Hytrell	Kevlar/Tefzel	2.4 mm	-40°C to +95°C
RIFOCS HL1	Tight tube	Single mode, 1310/1550 nm acrylate buffer	Hytrell	Kevlar/Tefzel	2.4 mm	-40°C to +95°C

Most of the tested cables are not rated for the extremes of -55°C to +125°C, and it is usually due to the rating of the acrylate coating on the fiber itself which is +85°C. However, this testing was conducted to determine the amount of thermally induced shrinkage of the cable components and the optical performance in general so the thermal limits were extended to -55°C to +125°C. Because of this, it is important to note that all the optical cable candidates with the exception of the W.L. Gore FON1004 were taken beyond their rated thermal specifications. The ramp rates for all of the thermal testing was 2°C/min with dwells of 28 minutes per temperature extreme.

When monitoring the cables actively for optical transmission changes, each cable was placed inside the chamber with terminated ST connectors, positioned just outside the feed-through hole to the oven. There were reference cables connected

to the sources and detectors with the cable under test in between the two sets inside of the oven. Insertion loss of the cable assembly was not the issue of concern. Instead it was the change in transmitted optical power during the thermal cycling.

The sources used for transmission of optical power through the cables were the RIFOCS 252A and the RIFOCS 752L both used at 1300 nm. The detector used to convert the optical signal to an electrical signal was the HP8153A with HP81532A power sensor modules. For the insitu testing, a Labview program was written to acquire data and store it in a text file. One cable of each type was tested for optical transmittance changes before, during, and after thermal cycling to a total of 48 cycles.

2.2 Results of thermal characterization

The thermal testing was conducted in two parts. During part one of the testing, all cables were cycled and measured after each 8 cycle session for dimensional shrinkage in the longitudinal direction only. Some optical measurements were made. Part two of this testing focused on the optical performance of these cables (with most of them being taken well outside of their thermal specifications) during thermal cycling. The overall optical fluctuations that occur during the cycling are used as a characterization of the thermal expansions and contractions due to the CTE of materials used in the configuration. The data for part one of this thermal characterization is presented in Figure 1.

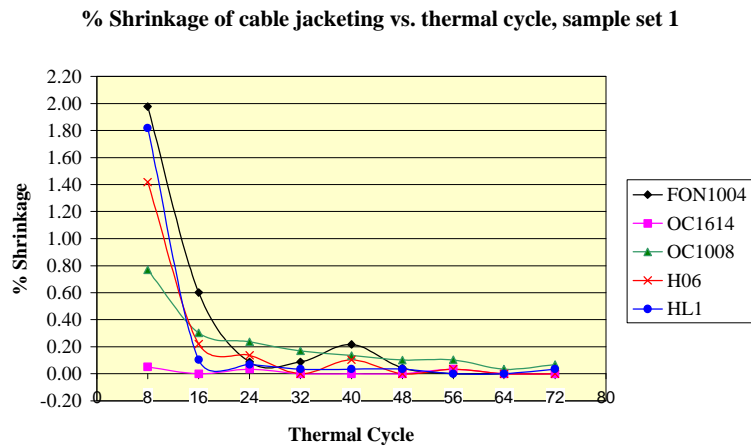


Figure 1: Cable configuration shrinkage in length for five different cables up to a total of 72 thermal cycles.

There was no visible damage that occurred as a result of taking most of the cables outside of their respective thermal specifications. It is interesting to note that the FON1004 and both RIFOCS cables had jacket shrinkage but the kevlar and other buffer materials did not shrink back. In the thermal tests conducted and reported in reference 2, this was not the case. All cable components would shrink back exposing only the coated optical fiber.

2.3 Summary of thermal characterization experiment

Table 2 summarizes the results of the thermal characterization study. The total % shrinkage in cable component length after 72 thermal cycles is in column two where both data sets are included; the second data set is in parenthesis. In the third column, the total % shrinkage after 24 cycles is presented. The purpose for showing the results after 24 cycles, is that in many cases 20 to 24 cycles is used to "precondition" optical cables such that they will cease to shrink in length during further thermal cycling. Column four lists the numbers of thermal cycles that it took for the cables to shrink less than .1% as compared to the cable length after the previous 8 cycle session. The optical transmission changes that occurred as a result of thermal cycling were monitored during thermal cycling at 1300 nm, and are listed in column five. The comments on those transmission changes are listed in the last column of Table 2. Since only one 3 meter length was tested of each type of cable, there is only one set of data presented as a result of insitu monitoring of the optical transmission during thermal cycling. The data for the optical transmission changes were normalized to match a 3 meter length exactly since each cable was approximately, but not exactly 3 meters in length.

Table 2: Summary of results from thermal testing both length shrinkage and insitu optical transmission monitoring.

Cable	Total % Shrinkage	Total % Shrinkage after 24 cycles	Cycles to < 0.1%	Insitu transmission changes, 3m	Comments on transmission
W.L. Gore FON1004	2.94 (2.99)	0.75 (0.24)	56 (40)	< .05 dB	After 2 cycles, steady below .05 dB
Brand Rex OC1614	0.12 (0.13)	0.03 (0.0)	< 8 (< 8)	< .10 dB	Increased from less < .025 dB upto .10 dB as test progresses
Brand Rex OC1008	1.90 (1.80)	0.44 (0.44)	56* (56)	< .50 dB	Increases from .05 dB to .45 dB as test progresses
RIFOCS H06	1.90 (1.87)	0.14 (0.17)	24 (24)	< .10 dB	After 2 cycles steady below .10 dB
RIFOCS HL1	2.12 (2.13)	0.10 (0.17)	16* (16)	< .40 dB	After 13 cycles drops to below .05 steady for the rest of test

The optical power transmission transients were calculated by comparing adjacent optical power peaks and losses within a thermally induced cycle. In this way, the LED output power drift was eliminated. The total optical power transmission change, which is presented in these figures, is calculated by comparing the optical power maximum to the optical power minimum in a given cycle. Although the intention was to collect data for a total of 48 thermal cycles, in some cases not all data was captured due to operation error.

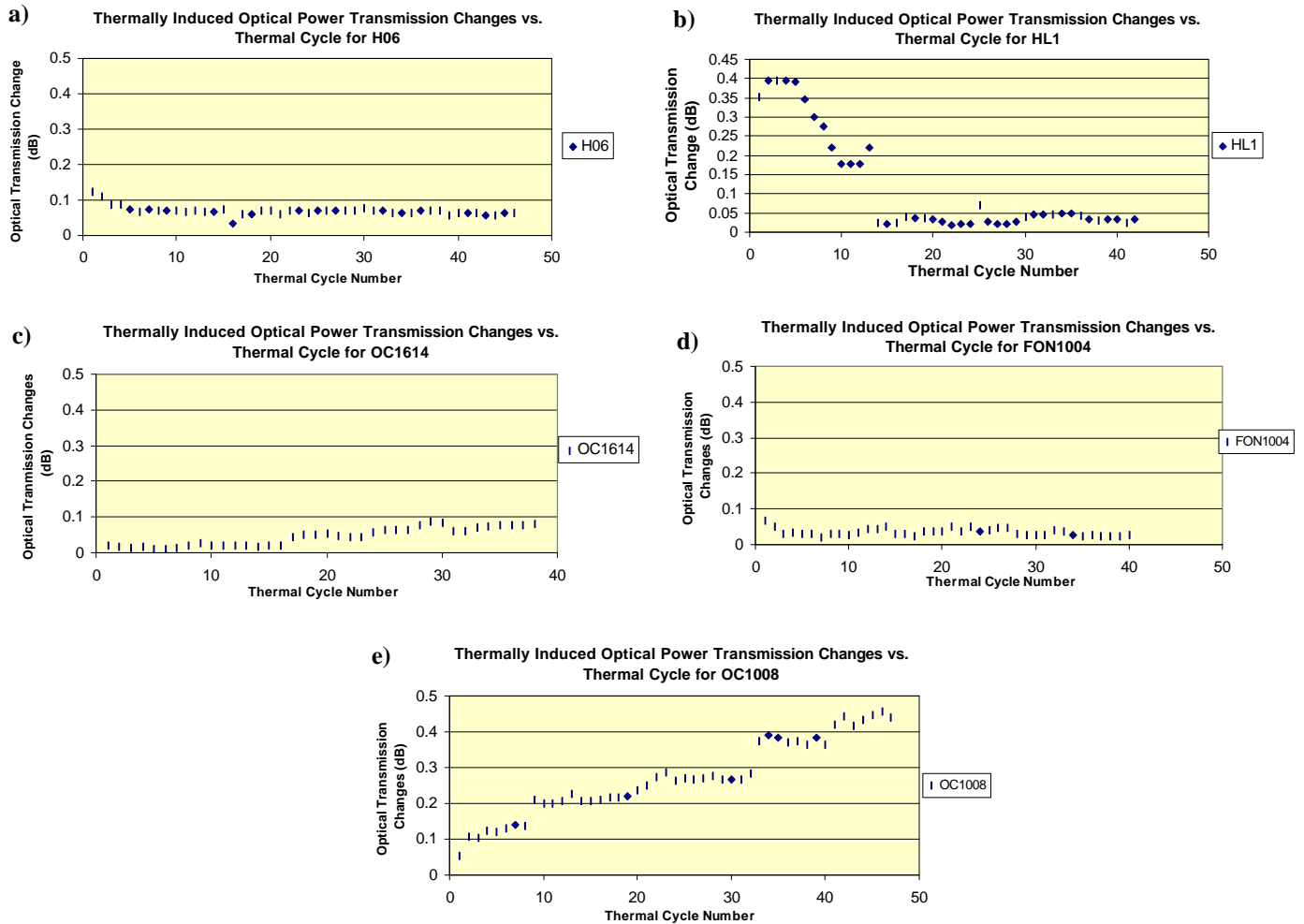


Figure 2: Optical transmission changes monitored during thermal cycling a) H06, b) HL1, c) OC1614, d) FON1004 and e) OC1008.

The optical transmission changes for the H06 were less than 0.1 dB (Figure 2a) for the duration of the testing on a length of cable 3 meters long. The optical transmission changes for HL1 (Figure 2b) decrease considerably after 13 thermal cycles down to less than .05 dB. The FON1004, (Figure 2d) for the duration of the testing had oscillations less than .05 dB. The OC1614 (Figure 2c) and the OC1008 (Figure 2e) both had increased power fluctuations during thermal cycling as the cycling

progressed. This was most likely due to the fact that both cables have a loose tube construction. It would make sense that shrinking cable would force the fiber into a tighter helix and make the fiber more sensitive to the expansion and contraction caused by the materials CTE. The OC1614 shrinks very little and even though there is a slight increase in the thermally induced transmission transients, the total swing never reach more than 0.1 dB/3 m.

During this testing, it was expected that the single mode cables would perform better than the multimode cables in terms of stability due to the short lengths used and that indeed was the case. Launch conditions were not regulated such that the multimode fiber would reach its equilibrium point for power distribution across the traveling modes. In typical space flight applications, launch conditions are not always controlled or at optimal levels and therefore they were not regulated here.

It was expected that during insitu testing that when the temperature was at a maximum, the optical power transmission of the cable under test would be at a maximum as well and that during a low thermal extreme, the power would reach its minimum value. In most cases this was true except for the OC1614. Just the opposite appeared to occur. Two more additional tests were conducted on cables from another source to confirm that for cable OC1614, the optical maximum would be reached during the soak at -55°C and during the +125°C soak, the optical transmission would reach a minimum.

2.4 Conclusions on thermal characterization

The overall rankings of how the cable candidates performed are in Table 3. The ranking is somewhat subjective for the optical tests in that multimode cables are being compared to single mode cables. It is expected that the highest ranking cables for optical performance should be the FON1004 and the HL1. For the most part these do appear to be more optically stable than the multimode cables. Comparing the HL1 and the FON1004 to each other the FON1004 slightly outperforms the HL1 for the optical testing. The difference here could be that the HL1 was being cycled at a temperature +30°C above and -15°C below the temperatures for which it is rated. The HL1 did have large thermally induced transmission transients during the first 13 cycles but decreased after the 13th cycle and remained at a level less than .05 dB. This again may be due to the fact that the cable is being taken well above its rated thermal limit. In addition, it is also interesting to note where the majority of the linear cable component shrinkage becomes less than 0.1%, and that it is after the 16th thermal cycle. It may be that the reduction in shrinkage actually occurred after the 13th cycle but that during this testing the thermal effects were only measured after 8 cycle sessions. The data here indicates the H06 is a good performer once the 13th cycles have been completed. This gives an indication of how much "preconditioning" the HL1 requires to reach a thermal stability, given these thermal cycle extremes of -55°C to +125 °C. There is a RIFOCS preconditioning procedure that once performed, should allow the cable to remain thermally stable. Verification of the preconditioning procedure was conducted in addition to this testing. The shrinkage was measured after the procedure was used and then again after every 4 thermal cycles using the range -40°C to +95°C for which the cable is rate by specification. The test results showed that although the majority of the shrinkage occurred from the preconditioning process as expected, the shrinkage did not decrease to less than .1% until an additional 16 cycles. The thermal cycling performed using the temperature extremes -40°C to +95°C was conducted using a 30 minute dwell and a ramp rate of 2°C/min.

The FON1004 cable ranks the lowest in the total amount of thermally induced shrinkage although the shrinkage did stabilize somewhere after 48-56 cycles. Optically, this cable performed very well even with the large amount of cable component shrinkage. Again, we see that preconditioning for this cable is absolutely necessary for up to 50 cycles to reach less than 0.1% shrinkage.

Table 3: Ranking summary of cables in terms of best performance, rank 1 being the best.

Test	Total Length Shrinkage	Cycles to less than .1% Shrinkage	Insitu transmission stability
Rank 1	OC1614	OC1614	FON1004
Rank 2	H06	HL1	OC1614
Rank 3	OC1008	H06	H06
Rank 4	HL1	FON1004	HL1
Rank 5	FON1004	OC1008	OC1008

Of the multimode cables the OC1614 is by far the best performer for all testing conducted when compared to the multimode cables. The H06 appears to be second when compared to the OC1614. However, where preconditioning through thermal

cycling may not be necessary for the OC1614 it is necessary for the H06. The majority of the linear shrinkage for H06 occurs in the first 32-40 thermal cycles. It may or may not be the case that the configuration materials in the HL1 and the H06 are identical. If the assumption is that they are in fact the same, then the variability from lot to lot with respect to the lengthwise component shrinkage could be a factor of 2. This could explain why for the HL1 the bulk of the length shrinkage occurred around 13-16 cycles and for the H06 the bulk of the shrinkage occurred after 32-40 cycles. Without a large number of cable samples from different lots this can not be verified.

For most of the testing conducted, the available cables perform better than the vintage OC1008 optical fiber cable currently used in space flight. Since the thermal induced transients become larger as the loose tube configuration cables, OC1008 and OC1614 are cycled, preconditioning to eliminate the bulk of the shrinkage must be conducted prior to termination of the optical connectors. In fact, in all cases preconditioning should be performed prior to termination to avoid reliability hazards from the fiber being pulled out of the ferrule from the stress or leaving exposed fiber between the cable components and the connector itself.

The OC1614 was the superior performer throughout the testing and was taken well beyond its specification level. Just as this testing was completed, the International Space Station Mission reported failures on their space flight cable, which is the OC1614. The root cause report is now available.⁶

3. RADIATION CHARACTERIZATION OF OPTICAL FIBER

3.1 Background

The testing of Lucent SFT optical fiber was conducted to characterize several types of the Lucent SFT 100/140/172 carbon coated product for use in a harsh space flight environment. The environmental parameters used in this testing were extracted from the new International Space Station (ISS) specification 21657 Revision N/C.⁷ The environmental parameters include a constant temperature of -121°C for a maximum of six days during which the fiber is exposed to total ionizing radiation exposure as a result of solar flare events, passes through the South Atlantic Anomaly, and background radiation. The ISS specification requirement includes testing of cable to three different levels of the expected total ionizing dose (TID) in a cold environment. The objective of this testing was to simulate the worst of the actual conditions during a six day cold temperature exposure without over testing. In order to accomplish this, two dose rates were to be used for estimating the radiation induced attenuation performance of the cable, 42 rads/min for two hours to simulate the solar flare activity and .5 rads/min to simulate passes through the South Atlantic Anomaly, SAA and background radiation. The specification requires a TID radiation exposure on the optical fiber cable for a total of six days at a constant temperature of -121°C +/- 4°C. This test was then to continue at the second dose rate of exposure, but at room temperature for an additional 48 hours or once a saturation level had been reached for radiation induced attenuation.

3.2 Discussion of experiment on radiation characterization

In order to use the TID cobalt 60 chamber at NASA Goddard Space Flight Center with a thermal chamber and necessary shielding, the highest dose rate attainable for exposure on an optical fiber reel was 28.3 rads/min. Therefore, two tests had to be conducted at different dose rates. It was expected that the highest radiation induced attenuation would occur after an exposure to 5.1krads at 42 rads/min. That being the case, it was considered adequate to use two different dose rates for testing and extrapolate to obtain the actual required radiation induced attenuation values.

Table 4: Lucent SFT optical fiber DUTs.

Fiber ID for Test	Part Number	Lot #, Test 1 (96 meters)	Lot #, Test 2 (100 meters)	Description
F3	BF05202	CD0712XA	CD0712XB	SL BASE Prem, Flightguide 100/140/172 micron, Ge- B- doped, natural silica deposition tube, carbon coated
F2	BF05202	CD0892XC	CD0892XC	New Flight guide, Ge- B- doped, synthetic silica deposition tube, carbon coated
F1	CF04530-04	CD0266XA	CD0266XA	standard fiber, carbon coated Ge- P- doped, synthetic silica deposition tube

The optical fibers under test (devices under test, DUTs) are described in Table 1. Optical fiber F3 is the "rad hard" fiber most space flight projects have used when a 100/140/172 micron hermetic fiber was required. F2 is the same fiber as F3, but manufactured a different way using a synthetic silica deposition tube. Both F2 and F3 are doped with germanium and boron. F1 is a commercially available non "rad hard" optical fiber that is doped with germanium and phosphorous. F1 was included

in this study to determine if in fact, a non radiation hardened optical fiber could be used in a harsh space flight environment such as the ISS specification illustrates.

The Cobalt 60 chamber housed the nitrogen tanks and thermal chamber set to operate at -121°C , with the spool holding approximately 100 m of each type of fiber F1, F2, and F3 inside the thermal chamber. The fiber spool was shielded by a 62.5 milli-inches lead box and a 62.5 milli-inches aluminum plate to limit secondary X-rays and reflections that could lead to other types of radiation damage not included in this study. The terminated FC connector ends of each fiber DUTs were fed through the thermal chamber feed-through hole. The fiber DUTs were mated to 25 meter lead out cables that were fed through the chamber feed through conduit and led to the source and detector setups outside of the chamber.

A light emitting diode (LED) source was connected to a reference cable, which was mated to a mandrel wrap and then to an attenuator. In the first test the 1300 nm LED source was the EXFO FLS-2100 which included an attenuator and in this case the mandrel wrap was connected between the output of the source and the input coupler. For Test 2, the RIFOCS 752L dual wavelength source was used with the JDS FITEL HA9 optical variable attenuator and in this case the mandrel wrap was connected between the source and the attenuator. The purpose of the attenuator was to reduce the power to the DUTs such that the input optical power was equal to or less than 1 microwatt at 1300 nm. The input coupler was connected to the output of the attenuator for Test 2. The input coupler was connected to the input "lead-in" cables that were fed through the radiation chamber feed through wall conduit. The input lead-in cables were then connected to the fiber DUTs and mounted to the top of the thermal chamber. The fiber spooled onto the reel, was very closely spooled on one side of the reel and filled a space of less than 1 inch along the reel width. This was to insure that each fiber was getting the same radiation exposure. All fiber on the spool was unjacketed and spooled such that the leads in and out were not considered part of the 100 m.

The chamber lead-out cables were connected to HP8153A power meters with HP81532A power sensor modules. The system was operated at 1300 nm. Labview software via a Dell laptop computer controlled the data acquisition from the HP detectors. Data was logged once per minute, time stamped and stored in a text file with the first data point recorded prior to radiation exposure. All lead and reference cables contained 100/140 micron optical fiber.

Two tests were conducted for the purpose of data extrapolation to 42 rads/min for two hours and .5 rads/min for a total of six days (including the two hours) at a constant temperature of -121°C . The thermal chamber was positioned in front of the radiation source shutter to achieve the maximum radiation dose rate at the location of the fiber spool. The largest dose rate achieved was 28.3 rads/min. Therefore, the second dose rate was scaled proportionally from the actual lower dose rate to .34 rads/min. The first test involved exposing the fiber, while at -121°C , to 28.3 rads/min for three hours, which was approximately a total dose of 5.1 Krads. Following the high dose rate exposure, a low dose rate exposure of .34 rads/min was used for the rest of the six-day duration. The dose rate for Test 2 was scaled by a factor of two and therefore a dose rate of 14.2 rads/min was used for the initial 5.1 Krads (six hours). This was followed by a six-day exposure of .17 rads/min at -121°C after which the exposure continued at room temperature, 25°C for two additional days.

The attenuators on both test set-ups were used to limit the input power to the DUTs to either 1 microwatt or less. This was done as a precaution to avoid most of the photobleaching effects of the source on the radiation performance of the optical fiber. Typically, the higher the optical power is, the more aid is lent to fiber in annealing due to this effect known as photobleaching, although germanium doped DUTs show little dependence on the amount of optical power injected.⁸ Regardless, the optical power was limited to between .5 and 1 microwatt. Throughout testing, the temperature of the thermal chamber was monitored and logged into a text file. The measured temperature throughout each experiment was -125°C .

3.3 Results of radiation characterization

The radiation exposure test conditions for total dose and dose rates of each test are represented in Table 5.

Table 5 Radiation Test Conditions

Test	High dose rate condition (5.1 Krads)	Low dose rate condition (~6.3 Krads)
1	28.3 rads/min, 3 hours	.34 rads/min, 141 hours
2	14.2 rads/min, 6 hours	.17 rads/min, 138 hours

The data was separated into high dose rate and low dose rate sections for ease of analysis. The actual data for the high and low dose rate sections of test 1 and 2 for each fiber are in Figures 3, 4 and 5. For Figures 3 through 5, the graphs in a) are the

high dose rate segments of the radiation induced attenuation data, for F1, F2 and F3 respectively. The plots in b) of Figures 3 through 5 are the low dose rate segments of the radiation induced attenuation data collected for F1, F2 and F3 respectively. The data from Test 1 was normalized to 100 m such that the lengths would be consistent with Test 2.

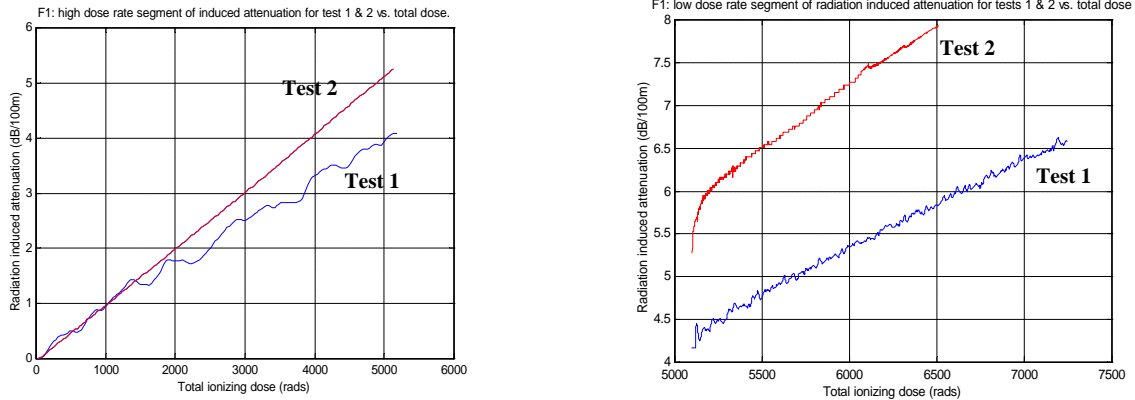


Figure 3: Optical fiber F1, a) high dose rate segment of radiation induced attenuation for Test 1 and 2 at -125 °C with a total dose of 5.1 Krads. b) low dose rate segment of radiation induced attenuation for Test 1 and 2 at -125 °C to a total dose of 6.5 Krads for Test 2 and 7.25 Krads for Test 1.

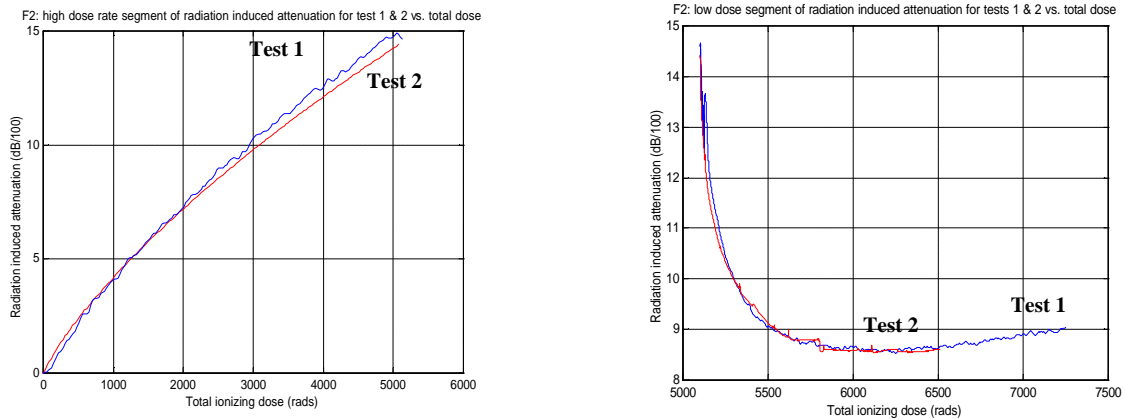


Figure 4: Optical fiber F2, a) High dose rate segment of radiation induced attenuation for Tests 1 and 2 at -125 °C with a total dose of 5.1 Krads, b) low dose rate segment of radiation induced attenuation for Tests 1 & 2 at -125 °C to a total dose of 6.5 Krads for Test 2 and 7.25 Krads for Test 1.

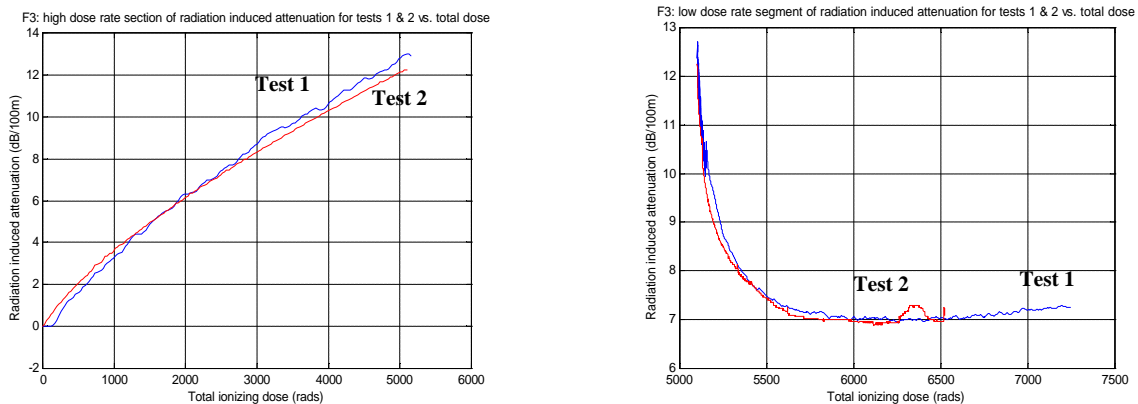


Figure 5: Optical fiber F3 a) high dose rate segment of the radiation induced attenuation data for Test 1 at 28.3 rads/min and Test 2 at 14.2 rads/min; b) low dose rate segment of the radiation induced attenuation data for Test 1 at .34 rads/min and Test 2 at .17 rads/min to total dose of 5.1 Krads at -125°C.

The data for F2 and F3 illustrated behavior typical for germanium doped fiber. In contrast, the data for F1 showed data atypical of germanium doped fiber. It is surmised that F1's behavioral deviation was due to the phosphorous doping of the optical fiber (phosphorous is typically used to raise index of refraction while boron is used to lower the index of a silica fiber). For F2 and F3, once the dose rate was lowered to .34 rads/min and to .17 rads/min during Test 1 and 2 respectively, the radiation induced attenuation levels off and saturates. Figures 4b and 5b show this behavior as expected from germanium doped optical fiber. This behavior indicates that even at an elevated dose rate of .5 rads/min both optical fibers will saturate at the same attenuation in which they saturated for both .34 rads/min and .17 rads/min. This simplifies the extrapolation necessary to allow us to focus on only the high dose rate segments of the tests for F2 and F3 to answer how these fibers would act in the ISS space radiation environment. This is not the result for F1 however, it does continue to attenuate even after the dose rate is lowered, just about linearly.

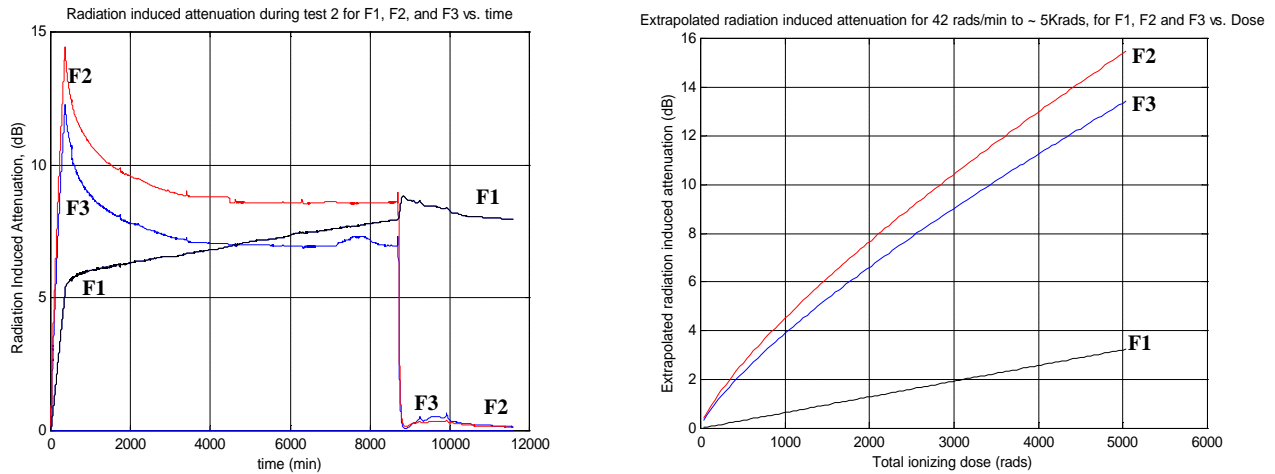


Figure 6 a) Complete data set for radiation induced attenuation of all fibers during Test 2 vs. time, b) extrapolation of radiation induced attenuation data to 42 rads/min for all fibers tested.

The entire data set for fibers F1, F2 and F3 are graphed in Figure 6a for Test 2. This plot illustrates how the optical fibers behave in comparison to one another once the temperature is elevated to +25°C after being at a constant -125°C for six days. Again F2 and F3 behave identical while F1 continues to increase and begin to perhaps saturate. The radiation exposure for test 2 continued at .17 rads/min after the temperature was elevated to +25 °C. The plots for each fiber in Figure 6a are marked by name at the beginning and end of the corresponding data plot.

The high dose rate data from each test was used to extrapolate to the ISS dose rate of 42 rads/min and the results of this extrapolation are in Figure 6b. The model $A=CD^f$ is used to describe the high dose rate behavior of all three fibers, where C is a constant related to dose rate, D is the total ionizing dose and f is less than one.⁹ The equations that govern the behavior of F1, F2 and F3 at 42 rads/min up to a total dose of 5.04 Krads while at -125°C are in Table 6 along with the values of attenuation for the different dose rates.

Table 6: Summary of radiation induced attenuation and extrapolated attenuation for all optical fibers.

Dose & Temperature Condition	Radiation Induced Attenuation F1	Radiation Induced Attenuation F2	Radiation Induced Attenuation F3
28.3 rads/min 5.1 Krads, -125°C	4.1 dB/100m $A=8.1*10^{-4}D^{.999}$	14.9 dB/100m $A=23*10^{-3}D^{.76}$	12.9 dB/100m $A=19*10^{-3}D^{.765}$
14.2 rads/min 5.1 Krads, -125°C	5.3 dB/100m $A=1.02*10^{-3}D^{.999}$	14.4 dB/100m $A=22*10^{-3}D^{.76}$	12.3 dB/100m $A=18*10^{-3}D^{.765}$
.34 rads/min (Test 1) 6.5 Krads, -125°C	5.8 dB/100m	8.6 dB/100m	7.0 dB/100m
.17 rads/min (Test 2), 6.5 Krads, -125°C	7.9 dB/100m	8.6 dB/100m	7.0 dB/100m
> 6.5 Krads 25°C, Test 2 (.17 rads/min)	8.0 dB/100m	0.15 dB/100m	0.15 dB/100m
42 rads/min , 5.1 Krads, -125°C	6.1 dB/100m $A=6.5*10^{-4}D^{.999}$	15.7 dB/100m $A=23.75*10^{-3}D^{.76}$	13.4 dB/100m $A=19.75*10^{-3}D^{.765}$
.5 rads/min, 6.5 Krads, -125°C	ND	8.6 dB/100m	7.0 dB/100m
> 6 Days at -125°C, .5 rads/min (@ 25 °C)	ND	~ 0.2 dB/100m	~0.2 dB/100m

The values in Table 6 are based on the final induced attenuation upon reaching the total dose at the specified dose rate and temperature. The equations that govern the attenuation behavior as a result of exposure are in terms of total dose, D. The objective of the testing was to determine the equations and values in rows seven, eight and nine for the ISS environmental parameters listed in column one. The equations that governed the attenuation behavior of each fiber were deduced through curve fitting techniques using the software program MATLAB.

From Table 6 as well as previous plots, it is evident that the radiation induced attenuation for fiber F1 actually increased as the fiber was tested at a lower dose rate. This is contrary to how F2 and F3 perform. In both tests for the fibers F2 and F3 as the dose rate decreased, so did the amount of radiation induced attenuation. For F1 at 28.3 rads/min to a total dose of 5.1 Krads at -125°C, the total attenuation at the completion of this segment of the test was 4.1 dB/100m. To clarify, this implies that the dose of 5.1 Krads at a dose rate 28.3 rads/min the signal at the output of the optical fiber was down by 4.1 dB for the 100 meters under test. At a lower dose rate, under the same conditions of 14.2 rads/min, this attenuation increased to 5.3 dB/100m. So by decreasing the dose rate by a factor of 2, this resulted in an increase of attenuation by 1.2 dB/100m down from the previous attenuation at the higher dose rate. This result was unexpected.

The radiation induced attenuation of optical fiber F2 decreased with decreasing dose rate. At the 28.3 rads/min to a total dose of 5.1 Krads the induced attenuation was 14.9 dB/100m. By reducing the dose rate by a factor of two to 14.2 rads/min (to a TID of 5.1 Krads), the induced attenuation decreases by .5 dB/100m; from 14.9 dB/100m to 14.4 dB/100m. The same is true for F3 where after reducing the dose rate by a factor of two the radiation induced losses decrease by .6 dB/100m. These fibers perform as expected for typical germanium doped silica. Fibers F2 and F3 perform similarly and only differ by 2 dB in performance under exposure. Where F2 is only slightly more sensitive than F3 to radiation effects.

Both fibers F2 and F3 saturate after a long exposure at the lower dose rates, however they saturate at attenuation values that differ by almost 2 dB. The lower dose rates used in the second segment of this testing, differ by a factor of two (.34 rads/min for Test 1 and .17 rads/min for Test 2) but have no difference in effect on fibers F2 and F3. For F2, both low dose rate data sets show that the fiber saturates at 8.6 dB/100m and for F3 the saturation point for both low dose rates is at 7.0 dB/100m. In contrast, the attenuation continues to increase on fiber F1 showing no effects related to lowering the dose rate. It is also interesting that even when the temperature returns to 25°C after six days prior at -125°C and it is expected that the transmission for all optical fibers would return to a nearly nonexistent attenuation, F1 continues to attenuate as if the conditions had not changed. It is possible that after a few days, F1 would begin to recover such that it would eventually reach a much lower attenuation value, but that was not yet evident from the 48 hours it was monitored at room temperature. When F2 and F3 return to 25°C the losses decrease to less than 0.2 dB/100m and would probably decrease over a long period of time at this exposure. From viewing the data more closely during the last two days it does in fact appear that fibers F2 and F3 would have continued the downward trend even while being exposed to .17 rads/min.

Overall, the losses for F1 (for the high dose rate segment of the testing) are much less than that of both F2 and F3. The loss for F1, after the first 5.1 Krads, is more than 10 dB less than the induced attenuation for F2. After the low dose rate testing, even then, F1 is still registering lower losses than F2 and F3 in the case of the higher low dose rate exposure. At the .17 rads/min dose rate exposure F1 is rating between the performance of F2 and F3. This in itself would be promising for the usage of this non rad hard fiber in a space environment. The only unknown is what the fiber F1 will do after constant exposure of .17 rads/min at room temperature. Would it continue to attenuate until it reached values for radiation induced attenuation much larger than those final values in the high dose rate data of F2 and F3, or would it eventually saturate and then recover to a much smaller attenuation value? Because this fiber behaves so differently than typical germanium doped optical fiber, it is impossible to make any conclusions without conducting more testing. Additional testing would answer the question of whether there is a predictable pattern to the radiation induced attenuation, and whether the fiber would eventually have recovered or continued to attenuate over prolonged low dose radiation exposure.

The extrapolated data in rows seven through nine of Table 6, contains the answer to the question "how will this fiber perform in the ISS environment?". The data was extrapolated to a high dose rate of 42 rads/min with a low dose rate value of .5 rads/min for all fibers. The largest radiation induced attenuation is seen from fiber F2 at 15.7 dB/100m, and the lowest for F1 at 6.1 dB/100m assuming that the fiber F1 has lower losses for a greater dose rate. The data for F1 indicated this was so under the same -125 °C thermal conditions.

It is safe to assume that both F2 and F3 will perform similarly at a low dose rate of .5 rads/min (ISS environmental requirement) to the way they performed during this testing. Therefore, a conclusion can be made based on this available data that the values for attenuation after this low dose rate exposure of .5 rads/min are the same for both the fibers as shown in

Table 6. More data would need to be available to make conclusions on how F1 would perform under the .5 rads/min dose rate following a high dose rate exposure of 42 rads/min. The only assumption that can be made based on available data is that the radiation induced attenuation would linearly increase regardless of the decrease in radiation dose rate.

3.4 Conclusions on radiation characterization

Three types of Lucent SFT optical fiber were tested for radiation effects using two different sets of conditions towards the goal of extrapolating to the ISS radiation requirements. For both Test 1 and Test 2 the temperature remained at -125°C for a total of six days and at 25°C for two days following. The two dose rate combinations used were chosen to make the extrapolation to a higher dose rate combination, simpler. In both tests, the first dose rate of exposure was approximately two orders of magnitude higher than the second dose rate, to match the radiation environmental requirement of the ISS specification for space flight cable. The collected data for radiation induced attenuation using two dose rate combinations of 28.3 rads/min and .34 rads/min for Test 1, and 14.2 rads/min and .17 rads/min for Test 2, was used to extrapolate to a dose rate combination of 42 rads/min and .5 rads/min. Under the conditions of 42 rads/min to a total dose of 5.1 Krads at -125°C, the fiber F1 would reach an attenuation of 6.1 dB/100m, F2 would reach an attenuation of 15.7 dB/100m, and F3 would experience radiation induced losses of 13.4 dB/100m. After a total dose exposure of 5.1 Krads at 42 rads/min, it was concluded based on available data that the induced loss for F1 could not be predicted, but the losses for F2 and F3 would be 8.6 dB/100m and 7.0 dB/100m respectively. After completion of the six days at -125°C, it is expected that both F2 and F3 would return to less than 0.2 dB/100m during low dose rate exposure of .5 rads/min over a prolonged exposure. The ISS requirement states that the total dose should be 50.4 Krads at the lower dose exposure and requires a low dose rate of .24 rads/min. It is expected that even up to a total dose of 50.4 Krads that the losses for F2 and F3 would still be less than -0.2 dB/100m. The low dose extrapolation was performed for a dose rate of .5 rads/min but by available data the results show that the effects are the same regardless of a factor of 2 decrease in dose rate. This conclusion was made based on the low dose rate data for both F2 and F3. It was not apparent that a recovery would occur for F1 and for now it can only be assumed that the radiation induced attenuation for F1 would only continue to increase even at a low dose rate of .5 rads/min while at 25°C.

4. RESULTS OF OUTGASSING TESTS

The FLEX-LITE® 1.2 mm type optical fiber cable manufactured by W.L. Gore can contain optical fiber with an acrylate coating. This configuration can be ordered with a variety of optical fibers inside. The FON8383 part number is specific to the selection of an acrylate coated fiber rated for 980 nm and the part number FON1008 is a multimode version with a 62.5/125 optical fiber inside. This cable configuration with an acrylate coated fiber was tested in configuration by the Materials Engineering Branch at NASA Goddard Space Flight Center. Two 1.5 meter samples of the cable with fiber inside were tested at 80°C and at 125°C in a vacuum environment of 10^{-6} Torr for 24 hours. The cables were open on both ends, unterminated. The results state that the amount of %TML was .24% and .34% respectively. Both results show that acrylate coated fiber can in fact, be used inside of a "non outgassing" cable configuration such as the 1.2 mm FLEX-LITE® series configuration made by W.L. Gore. It was also verified by other data that the %TML did not change with a change in length of the cable. This cable with acrylate fiber inside, passes the requirement of the ASTM-595 outgassing test in a configuration.

5. CONCLUSION

Examined here were several optical fiber cables and optical fiber for their suitability in typical space flight environments. The W.L. Gore FON1008 cable was tested with acrylate fiber inside for its suitability in a thermal vacuum environment. The W.L. Gore FON1004, the Brand Rex OC1614 and OC1008 and the Northern Lights H06 and HL1 made for RIFOCS were examined for thermal stability for the parameters of length shrinkage and optical stability. Lastly three 100/140/172 polyimide, carbon coated optical fibers made by Lucent SFT were tested for their suitability of use in the ISS space radiation environment at -125 °C.

6. ACKNOWLEDGEMENTS

Most endeavors of this magnitude are accomplished by a team effort. We would like to acknowledge the following people of our team who made this work a success: Claude Smith, QSS/ NASA GSFC, John Slonaker, QSS/ NASA GSFC , Steve Brown, NASA GSFC, Harry Shaw, NASA GSFC, Michelle Manuel, NASA GSFC, Shawn Macmurphy, Sigma Research and Engineering/ NASA GSFC, Jesse Frank, Swales Aerospace/ NASA GSFC, Matt Bettencourt, Sigma Research and Engineering / NASA GSFC, Faruq Sabur, NASA GSFC, Jeff Frazier, Swales Aerospace / NASA GSFC, Ken LaBel, NASA

GSFC, Doug Hardy, W.L.Gore, Joe Gallo, W.L. Gore, Dennis Horwitz, RIFOCS, Dr. Jie Li, Lucent SFT, and Dr. Henning Leidecker, NASA GSFC.

7. REFERENCES

1. Melanie N. Ott, Jeannette Plante, Jack Shaw, M. Ann Garrison-Darrin, "Fiber Optic Cable Assemblies for Space Flight Applications: *Issues and Remedies*," Paper 975592 SAE/AIAA 1997 World Aviation Congress, October 13-16, Anaheim, CA.
2. Melanie N. Ott, "Fiber Optic Cable Assemblies for Space Flight II: Thermal and Radiation Effects," Photonics For Space Environments VI, Proceedings of SPIE Vol. 3440, 1998.
3. Melanie N. Ott, Joy Bretthauer, "Twelve Channel Optical Fiber Connector Assembly: from Commercial off the Shelf to Space Flight Use," Photonics For Space Environments VI, Proceedings of SPIE Vol. 3440, 1998, pp 57-68.
4. Melanie N. Ott, "Electron Induced Scintillation Testing of Commercially Available Optical Fibers for Space Flight," 1999 IEEE Radiation Effects Data Workshop, IEEE Nuclear and Space Radiation Effects Conference, July 1999.
5. Outgassing Data for Selecting Spacecraft Materials Online, URL is <http://epims.gsfc.nasa.gov/og/>
6. ISS Fiber Optic Failure Investigation Root Cause Report, August 1, 2000 WWW URL <http://issfoc.gsfc.nasa.gov/final.htm>
7. International Space Station Specification SSQ 21657, WWW URL, <http://misspiggy/tva/issfo/spec/issnewspec.html>
8. H. Henschel, O. Kohn, H.U. Schmidt, "Radiation Induced Loss Measurements of Optical Fibres with Optical Time Domain Reflectometers (OTDR) at High and Low Dose Rates," IEEE 1992.
9. E. J. Friebele, M.E. Gingerich, D. L. Griscom, "Extrapolating Radiation-Induced Loss Measurements in Optical Fibers from the Laboratory to Real World Environments", 4th Biennial Department of Defense Fiber Optics and Photonics Conference, March 22-24, 1994.

Technology Validation of Optical Fiber Cables for Space Flight Environments

posted 11/20/00

[Click here to start](#)

[Table of Contents](#)

Author: Melanie Ott, Patricia Friedberg

[Technology Validation of Optical Fiber Cables for Space Flight Environments](#)

Home Page:

<http://misspiggy.gsfc.nasa.gov/tva>

[Outline](#)

[Background](#)

[Optical Fiber Cable Definitions](#)

[PPT Slide](#)

[Thermal Testing of COTS cables](#)

[Thermal Optical Cable Testing Description and % Shrinkage Summary, 3m lengths, -55°C to +125°C, 20 min dwell,](#)

[Thermal Cycling Test Results COTS and Space Flight Cables](#)

[Thermal Cycling Length Shrinkage and Optical Performance Summary, -55°C to +125°C, 72 cycles](#)

[Radiation Effects on Optical Fiber](#)

[TID Test Parameters](#)

[Optical Fiber TID Tested](#)

[Test Results](#)

[High Dose Rate Section of Testing, F1](#)

[Low Dose Rate Section of Testing, F1](#)

[High Dose Rate Section of Testing, F2](#)

[Low Dose Rate Section of Testing, F2](#)

[High Dose Rate Section of Testing, F3](#)

[Low Dose Rate Section of Testing, F3](#)

[High Dose Rate Data Extrapolated to 42 rads/min -125 degrees C](#)

[Summary of TID Testing](#)

[Conclusion](#)

[For a copy of this presentation and other related reports please see the photonics website located at the URL: \[http://misspiggy.gsfc.nasa.gov/tva/authored/fo_photonics.htm\]\(http://misspiggy.gsfc.nasa.gov/tva/authored/fo_photonics.htm\)](#)

TID Radiation Induced Attenuation Testing at 1300 nm Using ISS Requirements on Three Optical Fibers Manufactured by Lucent SFT

Melanie Ott

NASA Goddard Space Flight Center/ Sigma Research and Engineering

Component Technologies and Radiation Effects Branch

September 2000

Objective

The testing of Lucent SFT optical fiber was conducted to characterize several types of the Lucent SFT 100/140/172 carbon coated product for use in a harsh space flight environment. The environmental parameters used in this testing were extracted from the new International Space Station (ISS) specification 21657 Revision N/C.[1] The environmental parameters include a constant temperature of -121°C for a maximum of six days during which the fiber is exposed to total ionizing radiation exposure as a result of solar flare events, orbital passes through the South Atlantic Anomaly, and background radiation. The ISS specification requirement includes testing of cable to three different levels of the expected total ionizing dose (TID) in a cold environment. The objective of this testing was to simulate the worst of the actual conditions during a six day cold temperature exposure without over testing. In order to accomplish this, two dose rates were to be used for estimating the radiation induced attenuation performance of the cable, 42 rads/min for two hours to simulate the solar flare activity and .5 rads/min to simulate passes through the South Atlantic Anomaly, SAA and background radiation. The specification requires a TID radiation exposure on the optical fiber cable for a total of six days at a constant temperature of -121°C +/- 4°C. This test was to continue at the second dose rate of exposure, but at room temperature for an additional 48 hours or once a saturation level had been reached for radiation induced attenuation.

Background

In order to use the TID cobalt 60 chamber at NASA Goddard Space Flight Center with a thermal chamber and necessary shielding, the highest dose rate attainable for exposure on an optical fiber reel was 28.3 rads/min. Therefore, two tests had to be conducted at different dose rates. It was expected that the highest radiation induced attenuation would occur after an exposure to 5.1 krads at 42 rads/min. That being the case, it was considered adequate to use two different dose rates for testing and extrapolate to obtain the actual required radiation induced attenuation values.

The optical fibers under test (DUTs) are described in Table 1. Optical fiber F3 is the "rad hard" fiber most space flight projects have used when a 100/140/172 micron hermetic fiber was required. F2 is the same fiber as F3, but manufactured a different way using a synthetic silica deposition tube. Both F2 and F3 are doped with germanium and boron. F1 is a commercially available non "rad hard" optical fiber that is doped with germanium and phosphorous. F1 was included in this study to determine if in fact, a non radiation hardened optical fiber could be used in a harsh space flight environment such as the ISS specification illustrates.

Table 1: Lucent SFT optical fiber DUTs.

Fiber ID for Test	Part Number	Lot Number Test 1 (96 meters)	Lot Number Test 2 (100 meters)	Description
F3	BF05202	CD0712XA	CD0712XB	SL BASE Prem, Flightguide 100/140/172 micron, Ge- B- doped, natural silica deposition tube, carbon coated
F2	BF05202	CD0892XC	CD0892XC	New Flight guide, Ge- B- doped, synthetic silica deposition tube, carbon coated
F1	CF04530-04	CD0266XA	CD0266XA	SL TCU-MC100H, standard fiber, carbon coated Ge- P- doped, synthetic silica deposition tube)

Experimental Setup

The Cobalt 60 chamber housed the nitrogen tanks and thermal chamber operating at -121°C , with the spool holding approximately 100 m of each type of fiber F1, F2, and F3 inside the thermal chamber. The fiber spool was shielded by a 62.5 milli-inches lead box and a 62.5 milli-inches aluminum plate to limit secondary X-rays and reflections that could lead to other types of radiation damage not included in this study. The terminated FC connector ends of each fiber DUTs (devices under test) were fed through the thermal chamber feed-through hole. The fiber DUTs were mated to 25 meter lead out cables that were fed through the chamber feed through conduit and led to the source and detector setups outside of the chamber.

A light emitting diode (LED) source was connected to a reference cable, which was mated to a mandrel wrap and then to an attenuator. In the first test the 1300 nm LED source was the EXFO FLS-2100 which included an attenuator and in this case the mandrel wrap was connected between the output of the source and the input coupler. For Test 2, the RIFOCS 752L dual wavelength source was used with the JDS FITELE HA9 optical variable attenuator and in this case the mandrel wrap was connected between the source and the attenuator. The purpose of the attenuator was to reduce the power to the DUTs such that the input optical power was equal to or less than 1 microwatt at 1300 nm. The input coupler was connected to the output of the attenuator for Test 2. The input coupler was connected to the input "lead-in" cables that were fed through the radiation chamber feed through wall conduit. The input lead-in cables were then connected to the fiber DUTs and mounted to the top of the thermal chamber. The fiber spooled onto the reel, was very closely spooled on one side of the reel and filled a space of less than 1 inch along the reel width. This was to insure that each fiber was getting the same radiation exposure. All fiber on the spool was unjacketed and spooled such that the leads in and out were not considered part of the 100 m.

The chamber lead-out cables were connected to HP8153A power meters with HP81532A power sensor modules. The system was operated at 1300 nm. Labview software via a Dell laptop computer controlled the data acquisition from the HP detectors. Data was logged once per minute, time stamped and stored in a text file with the first data point recorded prior to radiation exposure. All lead and reference cables contained 100/140 micron optical fiber.

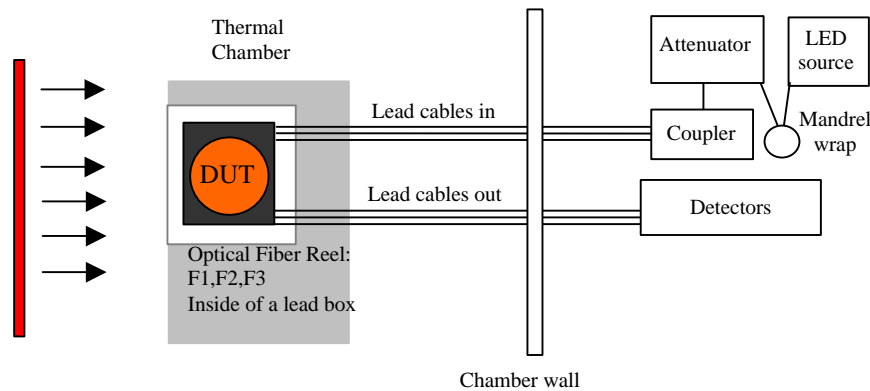


Figure 1: Block diagram of experimental set-up for radiation testing of Lucent SFT optical fiber F1, F2, and F3.

Test Discussion

Two tests were conducted for the purpose of data extrapolation to 42 rads/min for two hours and .5 rads/min for a total of six days (including the two hours) at a constant temperature of -121°C . The thermal chamber was positioned in front of the radiation source shutter to achieve the maximum radiation dose rate at the location of the fiber spool. The largest dose rate achieved was 28.3 rads/min. Therefore, the second dose rate was scaled proportionally from the actual lower dose rate to .34 rads/min. The first test involved exposing the fiber, while at -121°C , to 28.3 rads/min for three hours, which was approximately a total dose of 5.1 Krads. Following the high dose rate exposure, a low dose rate exposure of .34 rads/min was used for the rest of the six-day duration. The dose rate for Test 2 was scaled by a factor of two and therefore a dose rate of 14.2 rads/min was used for the initial 5.1 Krads (six hours). This was followed by a six-day exposure of .17 rads/min at -121°C after which the exposure continued at room temperature, 25°C for two additional days.

In order to maintain a constant temperature of -121°C for six days, several 230 ml nitrogen tanks needed to be on hand for changing of the tank every 21 hours. Several times the tanks were changed prior to reaching 21 hours between tanks to maintain a schedule that allowed this to occur during normal working hours. Whenever a tank substitution occurred, the shutter had to be brought down, but the duration lasted no more than five minutes. It is also the case that for 10 minutes during the change of dose rates from the higher dose rate to the lower dose rate of each test, that the shutter had to be lowered.

There were several "false starts" while trying to conduct testing due to equipment malfunction. The total number of tests conducted was actually four. The last two tests provided the only useful data since the prescribed conditions were met throughout testing.

During Test 1, the EXFO source with internal attenuator was used and found after completion of the test to have large high frequency noise content. It is surmised that during the attenuation calibration the internal modulation was turned on in error. To avoid this error during the calibration for Test 2, the RIFOCS 752L dual wavelength source (certified to +/- .03 dB stability) was substituted with the JDS variable attenuator. There were not enough detector channels to monitor the source power during testing. The sources with the input cables were examined for the launch conditions of the light entering the fiber DUTs. The RIFOCS 752L sets up a standard overfill condition in the 100/140 optical fiber and used with a mandrel wrap ensures that launch conditions are adequate for not over or under estimating the results of the environmental effects on the optical performance of the fiber.[2] Therefore the 752L with mandrel wrap and cables was used as the "model" launch condition. Using the RIFOCS launch condition analyzer, Figure 2 shows the results of analyzing the conditions for 1) the 752L with mandrel wrap after 25 m of cable, 2) 752L with JDS attenuator, mandrel wrap and 25 m of cable, 3) the EXFO, mandrel wrap and 25 meters of cable. This test was used just to verify that the source/attenuator/lead-in cables combination had similar launch conditions to the 752L with mandrel wrap.

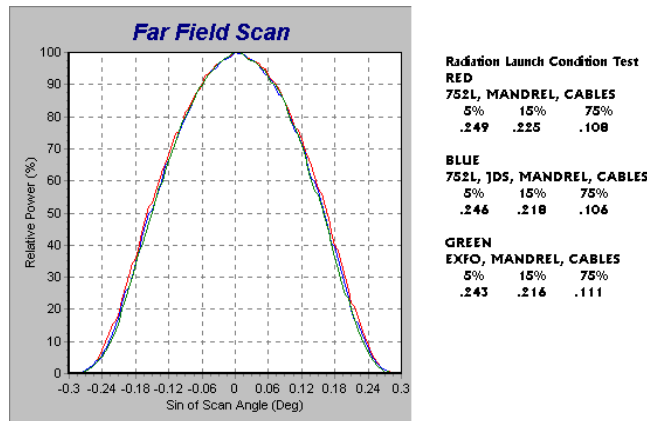


Figure 2: Launch condition analysis of the RIFOCS 752L/JDS HA9 attenuator and the EXFO FLS-2100.

The attenuators on both test set-ups were used to limit the input power to the DUTs to either 1 microwatt or less. This was done as a precaution to avoid most of the photobleaching effects of the source on the radiation performance of the optical fiber. Typically, the higher the optical power is, the more a fiber is capable of annealing due to this effect known as photobleaching, although germanium doped DUTs show little dependence on the amount of optical power injected.[3] Regardless, the optical power was limited to between .5 and 1 microwatt.

Throughout testing the temperature of the thermal chamber was monitored and logged into a text file.

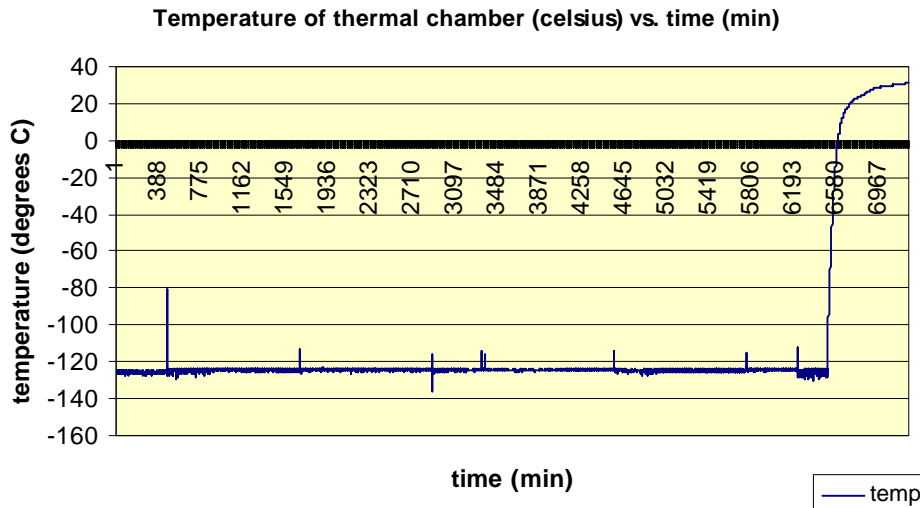


Figure 3: Temperature monitoring of thermal chamber during radiation testing, Test 2.

Figure 3 shows the thermal chamber temperature monitored during Test 2. The "spikes" are events where the nitrogen tanks were substituted. The thermal monitoring detector indicated that the temperature was averaging -125 °C which was a little colder than necessary. For testing of optical fiber, the worst case is usually a colder temperature so the difference will by no means make the data appear optimistic and the deviation is not large enough to simulate over testing.

Table 2: Radiation Test Conditions

Test	High dose rate condition (5.1 Krads)	Low dose rate condition (~6.3 Krads)
1	28.3 rads/min, 3 hours	.34 rads/min, 141 hours
2	14.2 rads/min, 6 hours	.17 rads/min, 138 hours

The radiation exposure test conditions for total dose and dose rates of each test are represented in table 2.

Data and Results

For the data set of Test 1 for all fibers tested, the high frequency modulation content of the EXFO had to be filtered out using a mathematical filter in MATLAB, such that the signal could be analyzed and used for extrapolation. The data was low pass filtered under the assumption that the "darkening" of the optical fiber would be a low frequency change and not a high frequency shift. Data from Test 2 did not contain high frequency modulation and did not require filtering.

Optical Fiber F1

The radiation induced attenuation data from the high dose rate segment of Test 1 & 2 of F1 is shown in Figure 4A. For this segment of the testing the conditions of Test 1 were 28.3 rads/min and for Test 2 were 14.2 rads/min. The plot in blue is from Test 1, and the plot in red is data from Test 2. Although the sampling rate for Test 2 was actually one data point per minute, the data here is represented as one point per every two minutes. This was so that the Test 2 data could be compared to the data from Test 1 which differs in dose rate by a factor of two from the dose rate of Test 2. The data set from Test 1 for all fibers F1, F2 and F3 was normalized to match an exact length of 100 m since the length of the DUTs for Test 1 were actually 96 meters long.

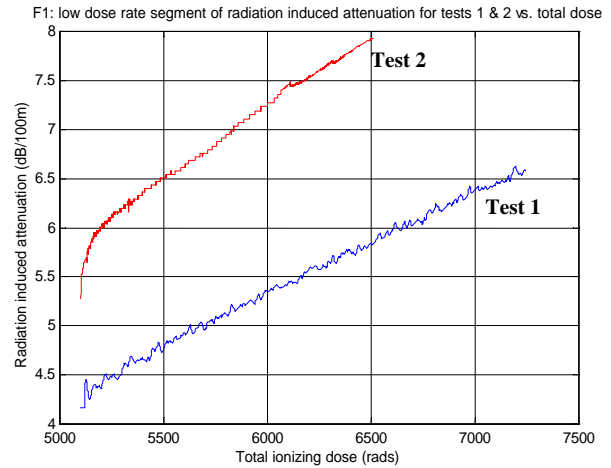
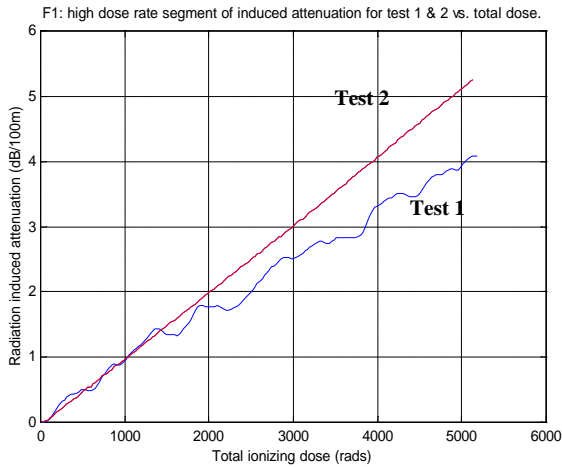


Figure 4: Data of optical fiber F1, A) High dose rate segment of radiation induced attenuation for Test 1 (blue) and 2 (red) at -125 °C with a total dose of 5.1 Krads. B) Low dose rate segment of radiation induced attenuation for Test 1 (blue) and 2 (red) at -125 °C to a total dose of 6.5 Krads for Test 2 and 7.25 Krads for Test 1.

Test 1 actually ended prematurely due to a power outage, but enough data was gathered to conclude what does happen at increasing dose using the higher dose rates of 28.3 rads/min and .34 rads/min. What is missing from the Test 1 data is the radiation induced attenuation values during exposure but after the return to a temperature of ~25 °C. For Test 2 the data set included the effects of a return to room temperature during exposure but is not included in Figure 4B. Figure 5 shows the complete data set of radiation induced attenuation for F1 during test conditions of Test 2.

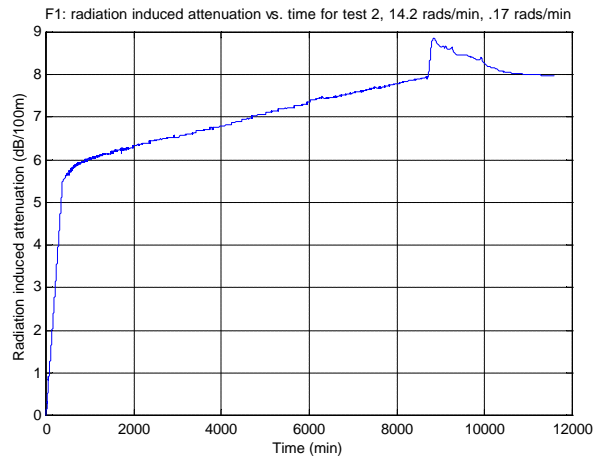


Figure 5: Optical fiber F1, Test 2, complete data set for radiation induced attenuation.

In Figure 5, the data shows that as the thermal chamber returned to 25 °C, the radiation induced attenuation became even larger (at ~8640 min). This was the opposite of the way a typical radiation hardened optical fiber performs. [4] Typically radiation hardened fiber will attenuate more with decreasing temperature and higher dose rate, but in the case of F1, which no doubt is due to the phosphorous dopants used for manufacturing, the attenuation is larger for decreased dose rates at low temperature.[5]

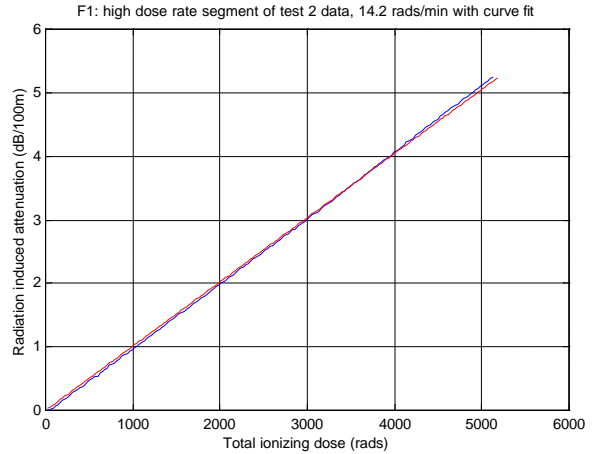
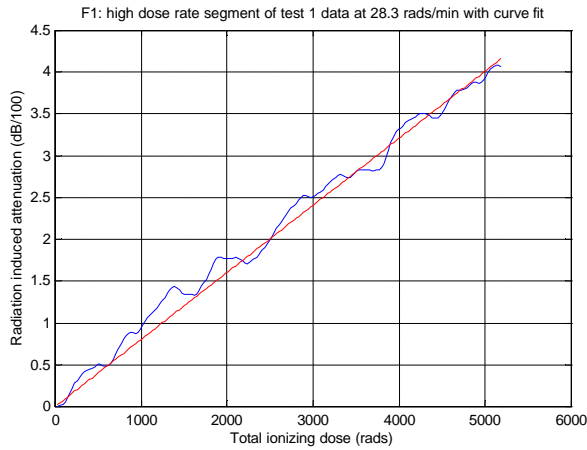


Figure 6: Optical fiber F1, A) Data (blue) with curve fit (red) for high dose rate segment of Test 1, B) Data (blue) with curve fit (red) for high dose rate segment of Test 2.

Using the extrapolation method described in Reference 6, the equation for radiation induced attenuation in optical fiber takes the form $A=CD^f$, where A is the radiation induced attenuation, C is a constant dependent on the radiation dose rate and f is a constant less than one. For Figure 6A, Test 1 with a dose rate of 28.3 rads/min the equation of the curve fit is $A=8.1 \cdot 10^{-4} D^{.999}$ (dB/100m) and for Figure 6B, Test 2 at 14.2 rads/min, the equation is $A=1.02 \cdot 10^{-3} D^{.999}$ (dB/100m). Using these curves one can use the model to extrapolate to larger dose rates and total doses assuming the model is relevant to this type of optical fiber. Figure 7 shows the data curves for 14.2 rads/min, 28.3 rads/min and an extrapolation curve for the dose rate of interest 42 rads/min. Also in Figure 7, there is an extrapolation to a much higher total dose of approximately 16 Krads using the extrapolation curves for all three dose rates and assuming that the temperature would remain constant at -125°C .

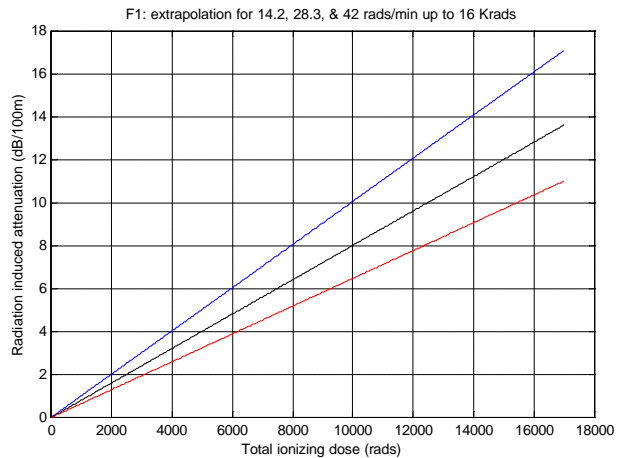
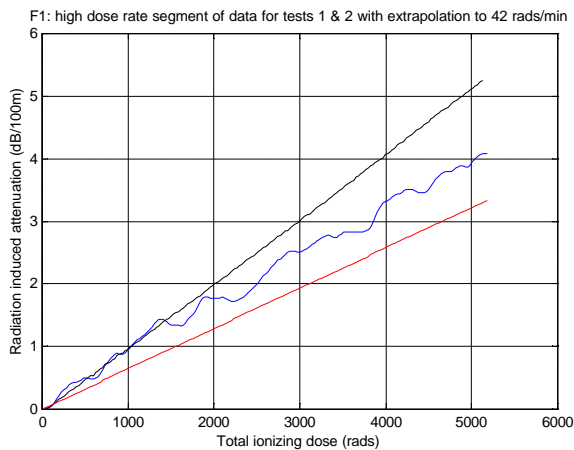


Figure 7: Optical fiber F1, A) High dose rate segments of data from Tests 1 (blue) & 2 (black) with extrapolation curve to 42 rads/min (red), B) Extrapolation curves for 14.2 rads/min (black), 28.3 rads/min (blue) and 42 rads/min (red) to 16 Krads TID.

For extrapolating to 42 rads/min, it was assumed that the larger dose rate, would decrease the radiation induced attenuation based on the test results of Test 1 and 2. The equation that governs the radiation induced attenuation at 42 rads/min at -125°C is $A=6.5 \cdot 10^{-4} D^{.999}$ (dB/100m). The extrapolation curves indicate a nearly linear relationship between total dose and radiation induced attenuation.

Optical Fiber F2

The results of the radiation testing of F2 are in Figure 8. It is evident in Figure 8A that the attenuation curves for Test 1 & 2 differ by very little and that as expected the higher dose rate data curve shows a slightly higher radiation induced attenuation as expected for germanium doped optical fiber. In Figure 8B, the two different tests match exactly showing that at the lower dose rates of .17 rads/min and .34 rads/min, there is no difference in the behavior. It also indicates a saturation behavior of the fiber at the lower dose rates.

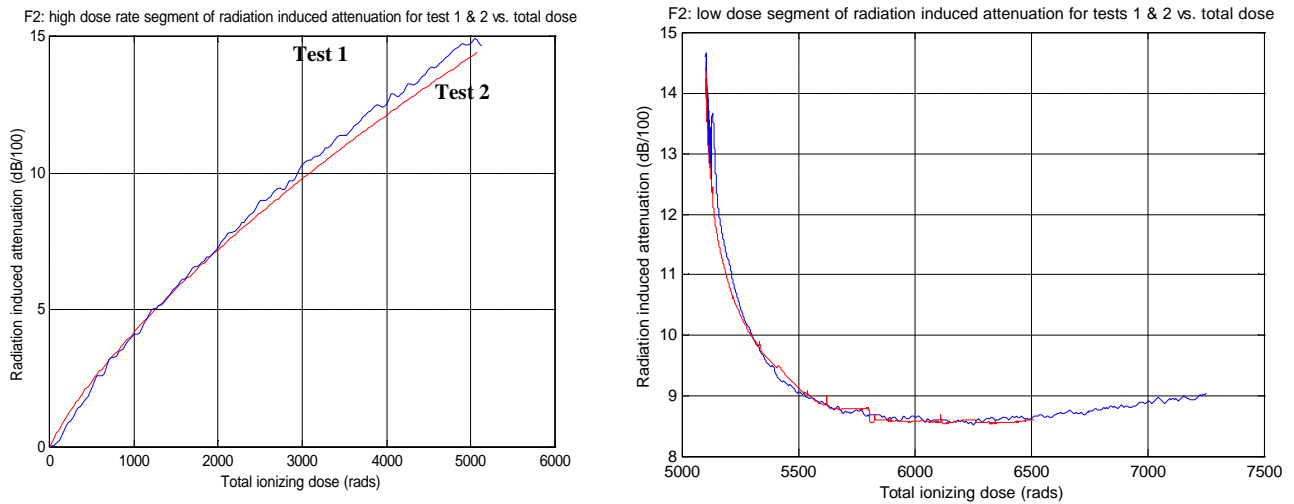


Figure 8: Optical fiber F2 radiation induced attenuation data plots, A) High dose rate segment of Tests 1 (blue) and 2 (red), B) low dose rate segment of Tests 1 (blue) & 2 (red).

Figure 9 shows the entire data set for radiation induced attenuation for Test 2.

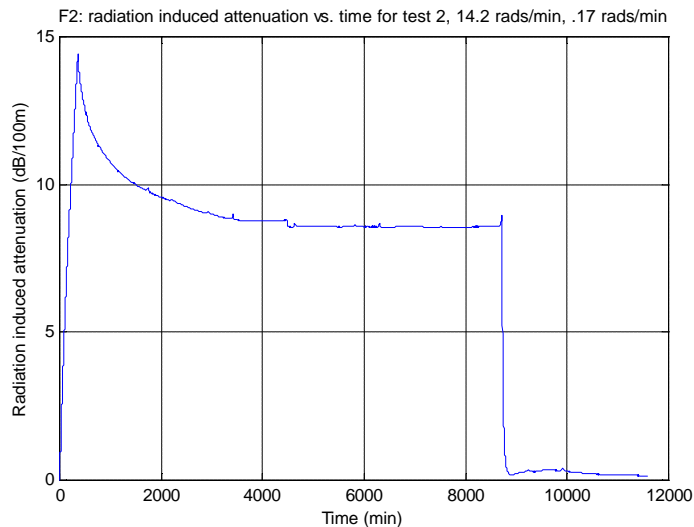


Figure 9: Optical fiber F2, Test 2, complete data set for radiation induced attenuation.

Here in Figure 9, the data shows the expected behavior of a germanium-doped optical fiber. The sharp increase in attenuation for the first six hours (360 minutes) is consistent with a high dose rate of 14.2 rads/min. The curve that appears as though the fiber is "recovering" continues and begins to saturate by the time the six days (~8640 min) at -125°C is completed. The attenuation then appears to be nearly nonexistent while the fiber continues being exposed to .17 rads/min at room temperature for another two days. This represents typical performance for a germanium doped optical fiber. Figure 10 shows the extrapolation curves for the high dose rate segment of both tests for F2 at -125°C.

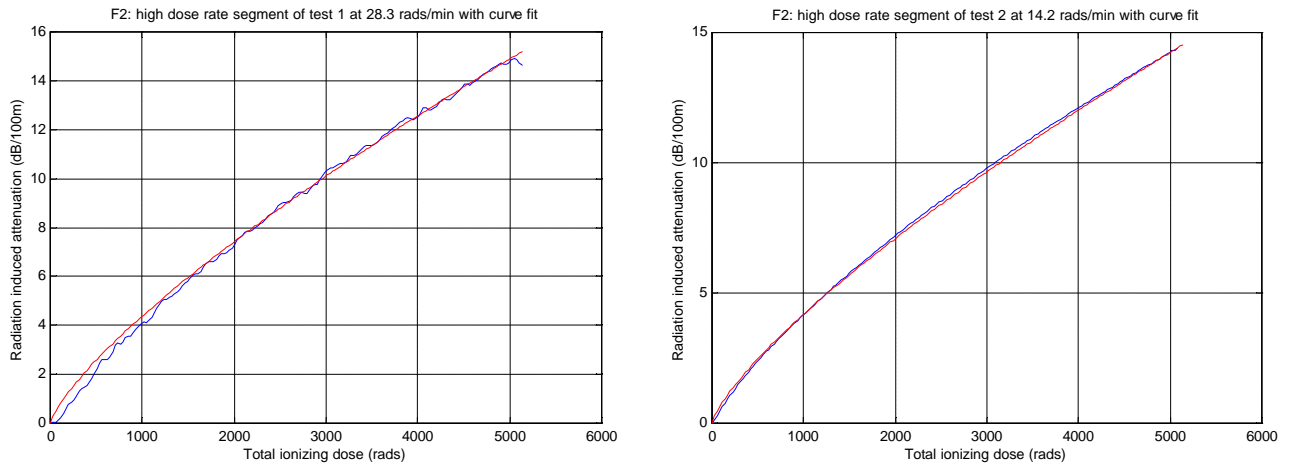


Figure 10: Optical Fiber F2, high dose rate radiation induced attenuation data from A) Tests 1 at 28.3 rads/min exposure (blue) with curve fit in red and B) Test 2 at 14.2 rads/min exposure (blue) with curve fit in red.

In Figure 10A the extrapolation curve is represented by $A=23 \cdot 10^{-3} D^{.76}$ (dB/100m) and this curve fits the data for Test 1 at 28.3 rads/min. For the data represented in Figure 10B, the equation that governs the fitted curve is represented as $A=22 \cdot 10^{-3} D^{.76}$ dB/100m for the data of Test 2 at 14.2 rads/min. The extrapolation curve that represents a model for radiation induced attenuation at 42 rads/min is shown in Figure 11.

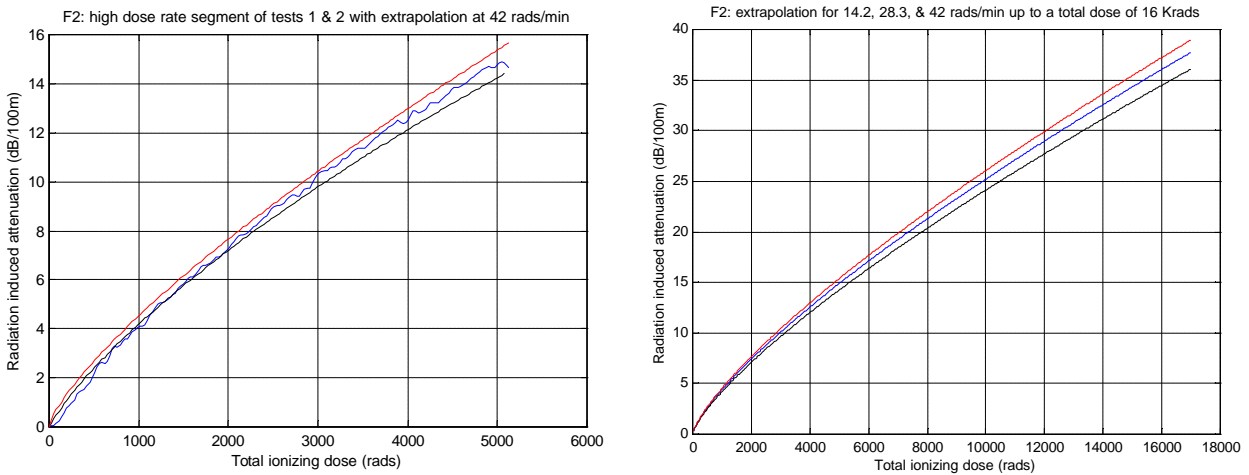


Figure 11: Optical fiber F2, A) radiation induced attenuation data plotted for Test 1 (blue) at 28.3 rads/min and 2 (black) 14.2 rads/min with the extrapolation curve for 42 rads/min (red); B) Extrapolation curves for 14.2 (black), 28.3 (blue) and 42 (red) rads/min to a total dose of 16 Krads at -125 C.

Optical fiber F2 performs predictably and has an extrapolation curve for 42 rads/min that meets expectations of having a greater induced attenuation for a larger dose rate at the same total dose as the lower radiation dose rate data. The equation that governs the extrapolated data for 42 rads/min is $A=23.75 \cdot 10^{-3} D^{.76}$ dB/100m. Figure 11B represents the radiation induced attenuation (in dB/100m) for all the extrapolation curves up to a total dose of 16 Krads assuming a constant temperature of -125 °C.

Optical Fiber F3

The results of both segments (high and low dose rate) of the radiation testing for fiber F3 is shown in Figure 12A and 12B.

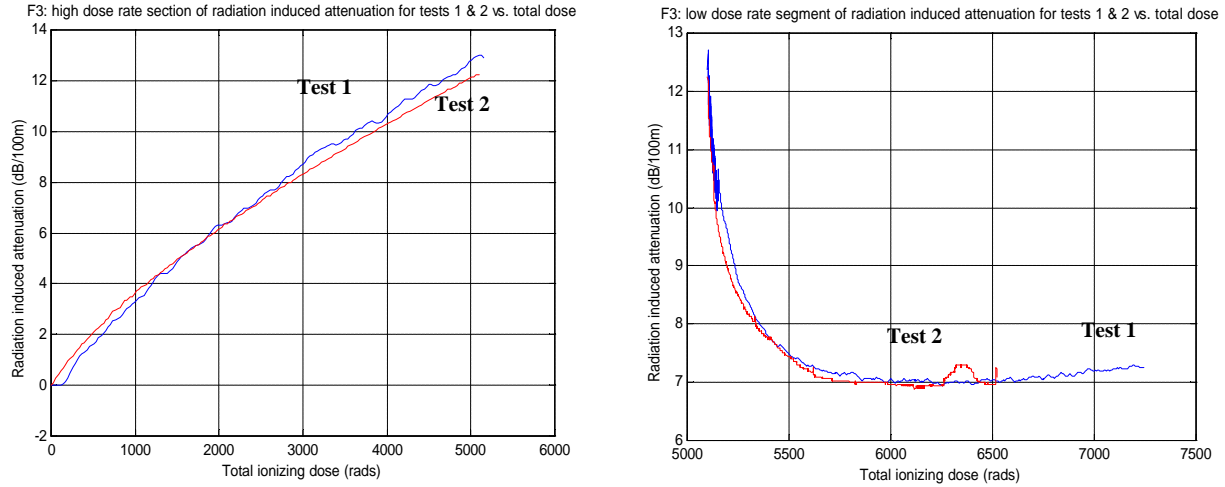


Figure 12: Optical fiber F3 A) high dose rate segment of the radiation induced attenuation data for Test 1 (blue) at 28.3 rads/min and Test 2 (red) at 14.2 rads/min; B) low dose rate segment of the radiation induced attenuation data for Test 1 (blue) .34 rads/min and Test 2 (red) at .17 rads/min to total dose of 5.1 Krads at -125 C.

Again as with fiber F2, the radiation susceptibility of F3 at two different dose rates that differ by a factor of two, appears only slightly different for a total dose of 5.1 Krads. This is seen in Figure 12A at the higher dose rates, but at the lower dose rates illustrated in Figure 12B the performance at both .17 rads/min, and .34 rads/min is nearly identical. There is a slight "dip" in the data for Test 2 on the plot of Figure 12B. It is not likely that this increase in attenuation is due to optical fiber performance and is more likely due to power transients from the equipment or a disturbance of the lead in or lead out test cables.

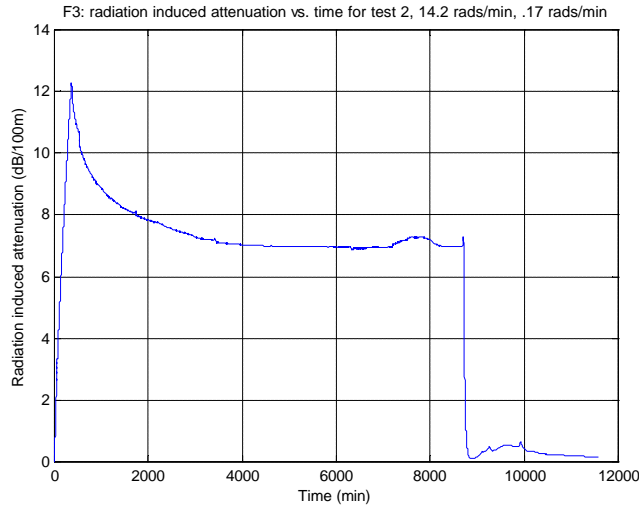


Figure 13: Optical fiber F3, entire data set for Test 2, radiation induced attenuation for dose rate of 14.2 rads/min to a total dose of 5.1 Krads and then a dose rate of .17 rads/min at -125°C to a total dose of 8.64 Krads.

Figure 13 shows the entire data set of radiation induced attenuation for fiber F3 at 14.2 rads/min for the first 360 min and then at .17 rads/min for the remainder of the test. The temperature remains at -125°C up until a time of 8640 min and then the temperature returns to 25°C while still being exposed to the .17 rads/min dose rate. This fiber behaves similar to the fiber F2, with the radiation induced losses of F2 only slightly larger.

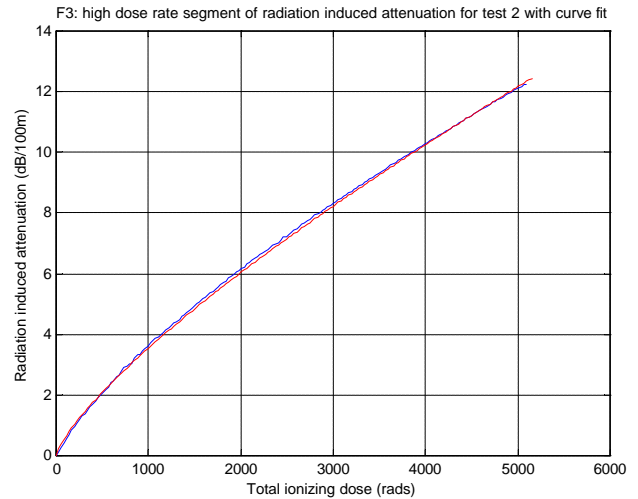
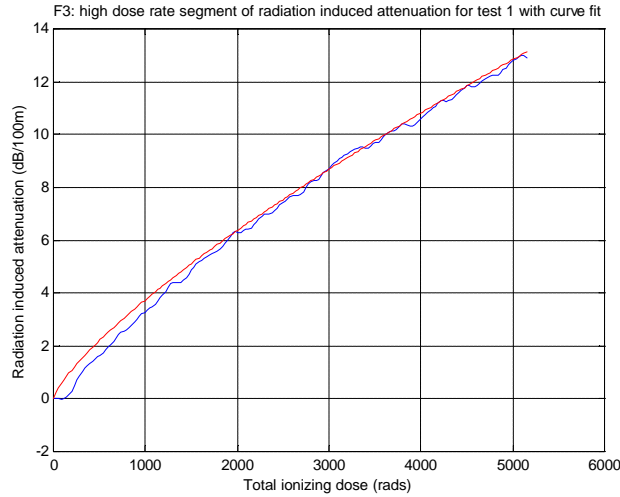


Figure 14: Optical Fiber F3, high dose rate radiation induced attenuation data from A) Tests 1 at 28.3 rads/min exposure (blue) with curve fit in red and B) Test 2 at 14.2 rads/min exposure (blue) with curve fit in red.

In Figure 14A the extrapolation curve is represented by $A=19 \cdot 10^{-3} D^{.765}$ (dB/100m) and this curve fits the data for Test 1 at 28.3 rads/min for optical fiber F3. For the data represented in Figure 14B, the equation that governs the fitted curve is represented as $A=18 \cdot 10^{-3} D^{.765}$ (dB/100m) for the data of Test 2 at 14.2 rads/min. The extrapolation curve that represents a model for radiation induced attenuation at 42 rads/min is shown in Figure 15 for optical fiber F3.

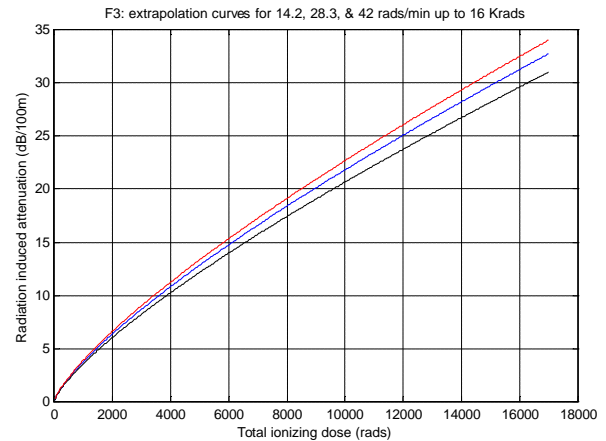
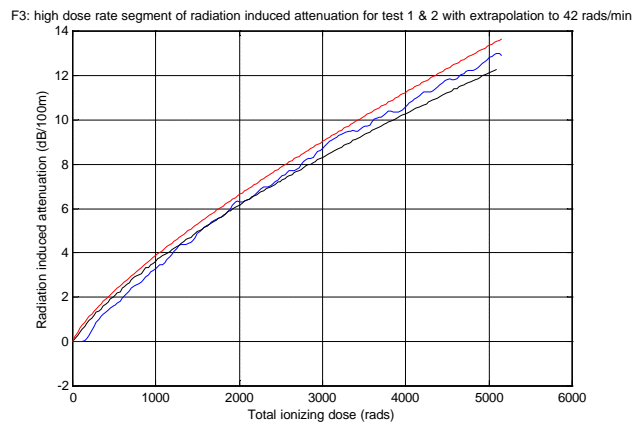


Figure 15: Optical fiber F3, A) high dose rate segment of radiation induced attenuation data for 14.2 rads/min (black), 28.3 rads/min (blue) with extrapolation at 42 rads/min (red) to a total dose of 5.1 Krads; B) High dose rate extrapolation to 16 Krads for dose rates 14.2 rads/min (black), 28.3 rads/min (blue) and 42 rads/min (red).

Optical fiber F3 performs predictably and has an extrapolation curve for 42 rads/min that meets expectations of having a greater induced attenuation for a larger dose rate at the same total dose as the lower radiation dose rate data (Figure 15A). The equation that governs the extrapolated data for 42 rads/min is $A=19.75 \cdot 10^{-3} D^{.765}$ (dB/100m). Figure 15B represents the calculated radiation induced attenuation (in dB/100 m) for all three dose rates (14.2, 28.3, and 42 rads/min) extrapolated up to a total dose of 16 Krads assuming a constant temperature of -125 °C.

Summary and Discussion

The results in terms of radiation induced attenuation are summarized in Table 3.

Table 3: Summary of radiation induced attenuation data from Test 1 and 2.

Test Condition During Exposure	Radiation Induced Attenuation Optical Fiber F1	Radiation Induced Attenuation Optical Fiber F2	Radiation Induced Attenuation Optical Fiber F3
28.3 rads/min 5.1 Krads, -125°C	4.1 dB/100m	14.9 dB/100m	12.9 dB/100m
14.2 rads/min 5.1 Krads, -125°C	5.3 dB/100m	14.4 dB/100m	12.3 dB/100m
.34 rads/min (Test 1) 6.5 Krads -125°C	5.8 dB/100m	8.6 dB/100m	7.0 dB/100m
.17 rads/min (Test 2) 6.5 Krads -125°C	7.9 dB/100m	8.6 dB/100m	7.0 dB/100m
After 6.5 Krads 25°C, Test 2 (.17 rads/min)	8.0 dB/100m	0.15 dB/100m	0.15 dB/100m

Table 3 is based on available data only and not extrapolated or calculated numbers. Examining the results presented in Table 3, it is evident that fiber F1 performs quite differently from the behavior of both F2 and F3 which behave similarly. Radiation induced attenuation for fiber F1, as was evident in the previous results analysis, actually increased as the fiber was tested at a lower dose rate. This is contrary to how F2 and F3 perform. In both tests for the fibers F2 and F3 as the dose rate decreased, so did the amount of radiation induced attenuation. For F1 at 28.3 rads/min to a total dose of 5.1 Krads at -125 °C, the total attenuation at the completion of this segment of the test was 4.1 dB/100m. To clarify, this implies that at a dose of 5.1 Krads and a dose rate 28.3 rads/min, the signal at the output of the optical fiber was down by 4.1 dB from the pre-irradiated measured optical transmission. Under the same conditions but with a lower dose rate of 14.2 rads/min, this attenuation increased to 5.3 dB/100m. So by decreasing the dose rate by a factor of 2, the attenuation increased by 1.2 dB/100m from the previous attenuation at the higher dose rate. This result was unexpected.

The radiation induced attenuation of optical fiber F2 decreased with decreasing dose rate. At the dose rate 28.3 rads/min to a total dose of 5.1 Krads, the induced attenuation was 14.9 dB/100m. By reducing the dose rate by a factor of two to 14.2 rads/min (to a TID of 5.1 Krads), the induced attenuation decreases by .5 dB/100m; from 14.9 dB/100m to 14.4 dB/100m. The same is true for F3 where after reducing the dose rate by a factor of two the radiation induced losses decrease by .6 dB/100m. These fibers perform as expected for typical germanium doped silica. Fibers F2 and F3 perform similarly and only differ by 2 dB in performance under exposure. Where F2 is only slightly more sensitive than F3 to radiation effects.

Both fibers F2 and F3 saturate after a long exposure to both lower dose rates. They saturate at attenuation values that differ by almost 2dB as noticed in the high dose rate data. The lower dose rates used in the second segment of this testing, differ by a factor of two (.34 rads/min for Test 1 and .17 rads/min for Test 2) but have no difference in effect on fibers F2 and F3. For F2, both low dose rate data sets show that the fiber saturates at 8.6 dB/100m and for F3 the saturation point for both low dose rate tests is at 7.0 dB/100m. In contrast, the attenuation continues to increase on fiber F1 showing no effects related to lowering the dose rate. It is also interesting that even when the temperature returns to 25°C after six days prior at -125°C, where the transmission for most optical fibers would return to a nearly nonexistent attenuation, F1 continues to attenuate as if the conditions of temperature had not

changed. It is possibly the case that after a few days F1 would begin to recover such that it would be evident it would eventually reach a much lower attenuation value but that was not yet evident from the 48 hours that it was monitored at room temperature. When F2 and F3 return to 25°C the losses decrease to less than 0.2 dB/100m and would probably decrease even further over a long period of time at this exposure. From viewing the data more closely during the last two days it does in fact appear that fibers F2 and F3 would have continued the downward trend even while being exposed to .17 rads/min.

Overall, the losses for F1 for the high dose rate segment of the testing are much less than that of both F2 and F3. The losses for F1, after the first 5.1 Krads, is more than 10 dB less than the induced attenuation for F2. After the low dose rate testing, even then, F1 is still registering lower losses than F2 and F3 in the case of the higher low dose rate exposure. At the .17 rads/min dose rate exposure F1 is rating between the performance of F2 and F3. This in itself would be promising for the usage of this non rad hard fiber in a space environment. The only unknown is what the fiber F1 will do after constant exposure of .17 rads/min at room temperature. Would it continue to attenuate until it reached values for radiation induced attenuation much larger than those of the high dose rate segment of F2 and F3 or would it eventually saturate and then recover to a much smaller attenuation value? Because this fiber behaves so differently than typical germanium doped optical fiber it is impossible to make any conclusions without conducting more testing. Additional testing would answer the question of whether there is a predictable pattern to the radiation induced attenuation, and whether the fiber would eventually have recovered or continued to attenuate over prolonged low dose radiation exposure.

Table 4 is a summary of the extrapolated data as a result of the analysis discussed previously. The extrapolated data contains the answer to the question "how will this fiber perform in the ISS environment?". In Table 4 the results of extrapolation are shown where the extrapolation high dose rate is 42 rads/min with a low dose rate value of .5 rads/min for all fibers. The largest radiation induced attenuation is seen from fiber F2 at 15.7 dB/100m, and the lowest for F1 at 6.1 dB/100m assuming that the fiber F1 has lower losses for a greater dose rate. The data for F1 indicated this was so under the same -125 °C thermal conditions.

The data was extrapolated to assume that instead of stopping at 5.1 Krads, the exposure would continue until all fibers experienced a total dose of 16 Krads. The data for the 2nd through 4th rows of Table 4 is graphed in Figures 7B, 11B and 15B. It is just interesting to note what the trend would become over a longer total dose. This extrapolation to a larger total dose of 16 Krads is not part of the ISS requirement.

It is safe to assume that both F2 and F3 will perform similarly at a low dose rate of .5 rads/min (ISS environmental requirement) to the way they performed during this testing. Therefore, a conclusion can be made based on this available data that the values for attenuation after this low dose rate exposure of .5 rads/min are the same for both the fibers as shown in Table 3. More data would need to be available to make conclusions on how F1 would perform under the .5 rads/min dose rate following a high dose rate exposure of 42 rads/min. The only assumption that can be made based on available data is that the radiation induced attenuation would linearly increase regardless of the decrease in radiation dose rate.

Table 4: Extrapolated values for radiation induced attenuation

Test Condition During Exposure	Radiation Induced Attenuation Extrapolation Optical Fiber F1	Radiation Induced Attenuation Extrapolation Optical Fiber F2	Radiation Induced Attenuation Extrapolation Optical Fiber F3
42 rads/min 5.1 Krads, -125°C	6.1 dB/100m	15.7 dB/100m	13.4 dB/100m
42 rads/min 16 Krads, -125°C	10.4 dB/100m	37.2 dB/100m	32.5 dB/100m
28.3 rads/min 16 Krads, -125°C	12.8 dB/100m	36.0 dB/100m	31.2 dB/100m
14.2 rads/min 16 Krads, -125°C	16.1 dB/100m	34.5 dB/100m	29.6 dB/100m
.5 rads/min 6.5 Krads -125°C	ND	8.6 dB/100m	7.0 dB/100m
After 6 Days at -125°C .5 rads/min (while at 25 °C)	ND	~ 0.2 dB/100m ↑	~0.2 dB/100m ↑

ND: not enough data to make conclusion.

Conclusions

Three types of Lucent SFT optical fiber were tested for radiation effects using two different sets of conditions towards the goal of extrapolating to the ISS radiation requirements. For both Test 1 and Test 2 the temperature remained at -125°C for a total of six days and at 25°C for two days following. The two dose rate combinations used were chosen to make the extrapolation to a higher dose rate combination, simpler. In both tests, the first dose rate of exposure was approximately two orders of magnitude higher than the second dose rate, to match the radiation environmental requirement of the ISS specification for space flight cable. The collected data for radiation induced attenuation using two dose rate combinations of 28.3 rads/min and .34 rads/min for Test 1, and 14.2 rads/min and .17 rads/min for Test 2, was used to extrapolate to a dose rate combination of 42 rads/min and .5 rads/min. Under the conditions of 42 rads/min to a total dose of 5.1 Krads at -125°C, the fiber F1 would reach an attenuation of 6.1 dB/100m, F2 would reach an attenuation of 15.7 dB/100m, and F3 would experience radiation induced losses of 13.4 dB/100m. After a total dose exposure of 5.1 Krads at 42 rads/min, it was concluded based on available data that the induced loss for F1 could not be predicted but the losses for F2 and F3 would be 8.6 dB/100m, and 7.0 dB/100m respectively. After completion of the six days at -125°C, it is expected that both F2 and F3 would return to less than 0.2 dB/100m during low dose rate exposure of .5 rads/min over a prolonged amount of time. The ISS requirement states that the total dose should be 50.4 Krads at the lower dose exposure and requires a low dose rate of .24 rads/min. It is expected that even up to a total dose of 50.4 Krads that the losses for F2 and F3 would still be less than 0.2 dB/100m. The low dose extrapolation was performed for a dose rate of .5 rads/min but by available data the results show that the effects are the same regardless of a factor of 2 decrease in dose rate (Table 4). This conclusion was made based on the low dose rate data for both F2 and F3. It was not apparent that a recovery would occur for F1 and for now it can only be assumed that the radiation induced attenuation for F1 would only continue to increase even at a low dose rate of .5 rads/min while at 25°C.

References:

1. SSQ 21657 Revision N/C International Space Station Specification for Fiber Optic Cable, Single Fiber, Multimode, Space Quality. Custodian: The Boeing Company, Space and Communications Division.
2. FOTP-50 Light Launch Conditions for Long Length Graded Index Optical Fiber Spectral Attenuation Measurements, EIA/TIA publication 1998.
3. H. Henschel, O. Kohn, H.U. Schmidt, "Radiation Induced Loss Measurements of Optical Fibres with Optical Time Domain Reflectometers (OTDR) at High and Low Dose Rates," IEEE 1992
4. Melanie N. Ott, "Fiber Optic Cable Assemblies for Space Flight II: Thermal and Radiation Effects," Photonics For Space Environments VI, Proceedings of SPIE Vol. 3440, 1998.
5. E. J. Friebele, "Survivability of Photonic Systems in Space" DoD Fiber Optics Conference, McLean VA, March 24-27, 1992.
6. E. J. Friebele, M.E. Gingerich, D. L. Griscom, "Extrapolating Radiation-Induced Loss Measurements in Optical Fibers from the Laboratory to Real World Environments", 4th Biennial Department of Defense Fiber Optics and Photonics Conference, March 22-24, 1994.
7. FOTP-49, Procedure for Measuring Gamma Irradiation Effects in Optical Fiber and Optical Cables, EIA/TIA publication, 1989.

Acknowledgements:

Special acknowledgement is rendered to the following people who made this testing possible and successful:

Claude Smith, QSS/ NASA GSFC
John Slonaker, QSS/ NASA GSFC
Patricia Friedberg, NASA GSFC
Steve Brown, NASA GSFC
Harry Shaw, NASA GSFC
Michelle Manuel, NASA GSFC
Shawn Macmurphy, Sigma Research and Engineering/ NASA GSFC
Jesse Frank, Swales Aerospace/ NASA GSFC
Matt Bettencourt, Sigma Research and Engineering/ NASA GSFC
Bruno Munoz, Unisys/ NASA GSFC
Scott Kniffin, Orbital / NASA GSFC

EVALUATION OF ESD EFFECTS DURING REMOVAL OF CONFORMAL COATINGS USING MICRO ABRASIVE BLASTING

Harry Shaw
NASA/GSFC, Greenbelt, MD
Nitin Parekh, Carroll Clatterbuck
Unisys/NASA, Lanham, MD
Felix Frades
HEI/NASA, Lanham, MD

Abstract

This report details the results and conclusions of an experimental evaluation of a micro abrasive blasting technique to remove urethane and parylene conformal coatings from printed wiring assemblies. This technique is being evaluated as a replacement for solvent based systems. The SWAM BLASTER coating removal system from Crystal Mark, Inc. was used. Four blast medias were evaluated using a total of 20 printed wiring assemblies.

The effectiveness of the microblasting technique was evaluated to determine the electrostatic potential generated at the surface and any visible board damage. The microblaster effectively removed the conformal coatings from all printed wiring assemblies evaluated. However, the concerns of electrostatic potential generation and the effects of a number of variables which were not addressed in this study, needs further research prior to being acceptable for space flight applications.

Background

Conformal coatings are required on printed wiring assemblies (PWAs) used for space flight applications to provide protection and to extend the life of the assemblies in harsh environments.

There are four major types of coating materials, each developed to suit specific applications. These are: acrylics, urethanes, silicones and parylenes. Depending upon the type of coating material and product requirements, conformal coating may be applied by dipping, brushing, spraying, dispensing or chemical vapor deposition.

In order to rework or repair parts on PWAs, the conformal coating must be removed, either entirely or in specific areas. The most commonly used methods for removal involve thermal, chemical, mechanical and micro abrasive processes. Recent environmental regulations such as the Montreal Protocol and Clean Air Act have had a significant impact on solvent based conformal coating removal processes, particularly with regard to control of volatile organic compounds (VOCs) and ozone depleting chemicals (ODCs). Equipment suppliers for coating removal systems have responded by developing environmentally acceptable methods.

The micro abrasive blasting technique offers a fast, cost-effective, easy to control and environmentally friendly non-solvent based method to remove conformal coatings. The

system can remove conformal coatings from a single test node, an axial leaded component, a through-hole integrated circuit (IC), a surface mount component (SMC) or an entire printed circuit board (PCB).

In the micro abrasive blasting process, a precise mixture of dry air or an inert gas and an abrasive media is propelled through a tiny nozzle attached to a stylus which is either hand held or mounted on an automated system. This allows the mixture to be pinpointed at the target area of the conformal coating to be removed. A vacuum system continuously removes the used materials and channels them through a filtration system for disposal. The process is conducted within an enclosed anti-static chamber and features grounding devices to dissipate electrostatic potential.

Micro abrasive systems inherently generate static electricity as the high velocity particles impinge on the surfaces. The voltage generated at the area of impact can cause electrostatic discharge (ESD) damage to the parts and electrical circuits on a PWA.

The current trend in the electronics industry towards higher speed, greater packaging density and lower power consumption has increased static sensitivity so that new techniques emerging in the field of coating technology need more stringent attention than ever before. An ideal blast media in a coating removal process would be the one which will not generate voltage greater than the ESD susceptibility of a particular device on a PWA or damage the board assembly, and is environmentally acceptable.

Conformal Coating Removal

Methodology

The objective of this study is to determine the effectiveness of the micro abrasive blasting technique to remove the conformal coatings from printed circuit boards and assemblies. This evaluation includes determination of the level of electrostatic voltage by measuring the surface voltage generated at the point of contact. It also includes assessing any physical damage caused by the technique. The experimental characterization includes the effects of variables such as type of conformal coating, cutting media, and system parameters on the conformal coating removal process.

Two types of conformal coatings were evaluated. These included urethane and parylene (parylene type C) conformal coatings with 4 mil and 1 mil nominal thicknesses respectively. The PWAs were non-functional. A total of four blast medias were selected. These included: wheat starch, sodium bicarbonate, plastic beads and glass beads.

A SWAM BLASTER Model MV-1 made by Crystal Mark, Inc., Glendale, California was used throughout this study. A Monroe Electronics Model 244 Isoprobe Electrostatic Voltmeter was used to monitor ESD voltages generated at the surfaces. This electrostatic voltmeter used an end-viewing miniature probe (Model 1017) with inert gas purging capability. Clean inert gas is purged through the sensing aperture preventing contamination by the blast medias in the vicinity of the electrode for greater stability of measurement. The probe measures the surface voltage with high accuracy (0.1%) and a test response speed < 3mS throughout a range of ± 3 kilovolts.

The evaluation was performed at the Materials Engineering Laboratory, NASA/GSFC in Greenbelt, Maryland.

Experimental Plan

A total of 20 non-functional PWAs were selected for this evaluation. All PWAs were double sided, 75mm x 125 mm (3" x 5") FR4 laminate. These PWAs have been designed for the use by the NASA Training Center for training in hand soldering, surface mount attachment, cleaning and conformal coating applications. This configuration provided a variety of pad geometries and traces adjacent to the blast sites and in close proximity to through-hole parts, flat packs, and other discrete devices (see figure 2 and 3).

A total of five blast sites were selected for monitoring ESD voltage (see figure 2 and 3). These included:

- Site 1: Pad Area (14-pin flat pack -U6)
- Site 2: Trace Area (near bifurcated turret-E11)
- Site 3: Solder Joint (capacitor-C7)
- Site 4: Pad Area (backside, turret terminal-E14)
- Site 5: Pad Area (14-pin flat pack - U6)

Experimental Matrix

A total of 20 PWAs were coated with urethane and parylene conformal coatings; ten each. All four blast medias were procured from Crystal Mark, Inc. The specifications of these are listed below:

- Wheat Starch: Average particle size - 120 micron, Vendor Specification Number-25A
- Sodium Bicarbonate: Average particle size - 75 micron, Vendor Specification Number - 34
- Plastic Bead: Average particle size - 120 micron, Vendor Specification Number - 45
- Glass Bead: Average particle size - 44 micron, Vendor Specification Number - 39

The sample size matrix is presented in Table 1.

Table 1. Sample Size Matrix

PWAs	Conformal Coating		Cutting Media			
	Type	Nominal Thickness (mil)	Wheat Starch	Sodium Bicarbonate	Plastic Bead	Glass Bead
NASA Training Center Board Assembly	Urethane	4	4	2	2	2
NASA Training Center Board Assembly	Parylene	1	4	2	2	2

Sample Preparation

All test PWAs were fabricated in accordance with NASA handbooks NHB5300.4 (3A-2) on soldering and NAS 5300.4 (3M) covering surface mount technology. All soldering operations and cleaning were performed at the NASA Training Center located at Unisys facility in Lanham, Maryland.

Cleaning

All PWAs were spray cleaned using 1:1 parts by volume of ethyl alcohol/heptane. The cleaning was performed in accordance with the Materials Processing Document - "Conformal Coating and Staking of Printed Wiring Boards Using a Room Temperature Curing Urethane Resin" (MPD S-313-008, Rev. C).

Conformal Coating

A. Urethane - A total of 10 PWAs were coated with urethane conformal coating. The resin formulation included Uralane 5750LV-A, Uralane 5750LV-B and a mixture of toluene and methyl ethyl ketone (MEK) solvents. The urethane conformal coating was applied to the front and back sides of the PWAs using a spray method in accordance with MPD S-313-008, Rev. C. The process parameters were adjusted to achieve a nominal coating thickness of 0.004". After a 7 day cure period at ambient conditions, a visual inspection was performed on all PWAs.

B. Parylene - The parylene conformal coating was applied by a chemical vapor deposition process. The raw material for this process is di-paraxylelene, which is a dimer composition. The system used for parylene conformal coating deposition was a Vapor Deposition Coater from Paratronix, Inc., Attleboro, Massachusetts.

A total of 10 PWAs were loaded into the deposition chamber. The dimer was placed in a glass tube at the opposite end of the deposition chamber. As the dimer vaporizes from a solid to a vapor state it moves into the pyrolysis zone which is maintained at 680°C with a 40 micron vacuum. With these conditions, the dimer cleaves into monomers which reform as a long chain polymer and deposit on the surface of the PWA. A cold trap maintained at -90°C is used to prevent parylene from depositing in the vacuum pump and to prevent backstreaming of pump oil into the chamber.

The process parameters were set to achieve a nominal 0.001" parylene conformal coating thickness.

Conformal Coating Removal System

The system used for the conformal coating removal study was a SWAM BLASTER Model MV-1 micro blasting machine from Crystal Mark, Inc. The model MV-1 is a manual system. The primary components of the system include a microblast unit, a work chamber, a gas dryer, an ESD point ionizer, a dust collector and a source of dry compressed air or an inert gas. The system design allows easy access and flexibility for pressure regulation, media flow control, nozzle replacements and orifice plate changes.

During manual operation, a mixture of micro abrasive media and compressed gas is propelled through a specially designed hand held nozzle. The abrading process is accomplished by introducing a precise amount of finely graded powder (media) into a stream of compressed gas which can be controlled by a foot switch.

The SWAM BLASTER system features a statically controlled work chamber for the protection of ESD sensitive parts. The system has a point ionizer which generates a balanced flow of positive and negative ions. It has a specially designed nozzle which couples the ions directly into the abrasive stream. By combining ESD neutralization directly into the abrasive pathway, the potential for ESD damage is minimized. Without the point ionizer, ESD voltages in excess of 3000 volts are realized.

The work chamber is constructed of conductive laminate. All elements of the system including inside chamber surfaces, point ionizer, media, PWAs and the operator are connected to a common ground to ensure that they are at the same potential.

The general specifications for the system are the following:

- Compressed gas requirements: 40-140 psi
- Operating pressure: 5-140 psi
- Flow rate: 3 cfm @ 80 psi
- Work Chamber Dimensions: 13" x 11" x 13"
- Media Chamber Capacity: 2 lbs. of media
- Weight: 43 lbs.

Figure 1 shows the Microblaster System.

Electrostatic Discharge Voltage Measurement

Electrostatic Voltmeter

In order to measure ESD voltage generated during micro blasting, a high accuracy, non-contacting electrostatic voltmeter (EVM) manufactured by Monroe Electronics was used. The Monroe Electronics Model 244 Isoprobe EVM measures a surface potential with 99.9% or better accuracy regardless of probe-to-surface spacing on sites as small as 0.1" (2.5mm) diameter. The EVM functions by means of a high voltage amplifier which automatically drives the probe to the same potential as that of the surface under measurement. By monitoring the output of the amplifier, an accurate indication of an unknown ESD potential can be achieved.

With the 244 EVM, a high frequency probe (Model 1017) was used to measure surface voltage. The probe had an end-viewing configuration and superior response speed (<3mS) throughout its ± 3 kV range. During all measurements the probe was held stationary 3 mm distance from the blast sites using a spacer attachment. The probe was also equipped with a gas purging option which improved its performance by preventing the entrance of contaminants and by maintaining a clean atmosphere in the vicinity of the electrode.

Electrostatic Fieldmeter

A Model 709 static sensor from 3M Corporation was used to monitor the electrostatic field within the work chamber. This portable sensor did not have high accuracy and was used to get a general indication of the electrostatic field present. The sensor was placed within the work chamber approximately 10" from the probe.

Process Description

The conformal coating removal experiments were conducted for two types of coatings and four blast medias. The following are the key variables involved in the conformal coating removal process:

- Type of Media
- Media Flow Rate
- Gas Pressure
- Nozzle Parameters

Since the type of blast media is the most important variable, the microblaster parameters such as media flow rate, gas pressure and coating removal time were optimized for each media and type of conformal coating. The nozzle parameters including the size, shape of orifice, distance from the PWA and angle of impingement were kept constant throughout the study.

The microblaster was effective in removing both types of coatings within 30 seconds in most cases. It was observed during the trial runs that as the media blasted through the coating, the surface ESD voltage increased. The ESD voltage peaked when the media hits pad or PWB surface. The primary goal of this study was to monitor the level of surface ESD generated during the coating removal process. Therefore, all measurements were taken instantaneously (within a few seconds) at the end of the coating removal. No attempt was made to monitor the rate of ESD voltage decay after the removal of the coating.

Table 2 shows the optimized system parameters used for the removal of urethane and parylene conformal coatings.

Table 2. Microblaster Parameters

Coating Type	Blast Media		Gas Pressure (PSI)	Nozzle Diameter (inch)
	Type	Flow Rate (1-10)		
Urethane	Wheat Starch	5	100	0.032
	Sodium Bicarbonate	4.5	95	0.032
	Plastic Bead	4	60	0.032
	Glass Bead	2	60	0.032
Parylene	Wheat Starch	4	50	0.032
	Sodium Bicarbonate	5	80	0.032
	Plastic Bead	4	60	0.032
	Glass Bead	2	60	0.032

Coating Removal Procedure

At the beginning of each run, all ESD precautions were in effect including grounding the equipment, operator and all elements of the work chamber to a common ground. The point ionization device was used throughout the process except when purposely taking measurements without it. The microblaster reservoir was filled completely with the appropriate media. The blast media was predried at 100°C for 24 hours before use. The microblaster parameters were set to the optimized values as described in Table 2.

The EVM probe was mounted on a stationary fixture with a spacer assembly so that the PWA could be positioned in front of the probe without surface contact. This ensured that all measurements could be taken at 3mm from the blast site irrespective of the location.

The media flow was activated by a foot switch. In order to achieve high cutting speed and uniform removal of the conformal coating, the tip of the nozzle had to be positioned approximately an inch from the blast site and at an angle between 45 and 90 degrees from the PWB surface.

At each site a 20 - 50 square mm area (5-8 mm diameter) was blasted until the conformal coating was completely removed. The total removal time ranged from 10 - 30 seconds for the pad and trace areas and 30 - 60 seconds for the solder joint areas. At the completion of the conformal coating removal the surface voltage measurements were taken within a few seconds. This method allowed a quick and repeatable measurement of surface voltages before the electrostatic charge could dissipate. All PWAs were microscopically inspected (10-40X) for any surface damage.

Results and Discussion

The experimental results of the study are presented in Tables 3 through 8.

Tables 3 and 4 present the ESD surface voltage measurement data for the removal of urethane and parylene conformal coatings respectively for wheat starch media. The ESD surface voltages are reported as minimum, maximum and average measurement values. The data for site 5 shows the surface voltages measured without the use of a point ionizer for ESD control.

The last column reports the electrostatic field within the work chamber measured by the static sensor.

Tables 5 through 7 present the ESD surface voltage measurement data for sodium bicarbonate, plastic bead and glass bead medias respectively.

Table 8 is a summary of ESD surface voltage measurements for all four medias evaluated showing the average surface voltages for sites 1 through 4.

In evaluating the effectiveness of the micro blasting technique to remove the conformal coatings, it became evident that the removability is a strong function of several variables including the type of the coating, it's thickness and the characteristics of a blast media. The results showed that the urethane conformal coating was more difficult to remove than the parylene for all four medias. The urethane conformal coating had tendency to peel off while the parylene conformal coatings eroded.

The cutting performance of the various blast medias showed mixed results. The microblaster parameters were optimized for media flow rate and gas pressure, however the effect of other factors such as nozzle parameters (orifice size and shape) and particle size variation for each media were not considered in this study. The main area of focus of this experimental study was ESD voltage generation during microblasting. The following observations describe the characteristics of the various medias evaluated.

Wheat Starch

Crystal Mark's wheat starch (carbo-blast) media is specially developed for conformal coating removal in ESD sensitive applications. This media is water soluble, biodegradable and considered environmentally friendly. It had an average particle size of 120 micron and showed good flow without any nozzle clogging problems.

Both types of coatings could be easily removed relatively quickly without any visible damage or penetration into the PWB surface. The total time of removal at each site was less than 20 seconds for urethane and less than 10 seconds for parylene. In general, the removal was quicker and more uniform in the pad/trace areas compared to the solder joint areas. This media generated an average ESD surface voltage ranging from 16-66 volts for urethane and less than 30 volts for the removal of parylene.

The data from the voltage measurements when ESD control was not used showed interesting results proving the advantage of using a point ionizer. These measurements were taken at the surface mount device (SMD) pad area (site 5). The ESD surface voltage spiked to an average of 1529 volts for urethane and -445 volts for parylene conformal coating.

Sodium Bicarbonate

The sodium bicarbonate media from Crystal Mark with 75 micron average particle size was used for this study. This media is water soluble, non-toxic and environmentally acceptable.

The cutting characteristics of sodium bicarbonate were good for both types of the conformal coatings. The media flowed well through the microblaster without any nozzle clogging problems. Overall, the coating removal rate was somewhat slower for both types of coatings (approximately 30 seconds) as compared to wheat starch media. The removal time was higher for the solder joint areas (site 3) on urethane attributable to higher coating thickness in those areas.

Sodium bicarbonate was effective in removing both conformal coatings, however, it generated higher levels of surface voltages compared to wheat starch. The average surface voltage ranged from -100 to -150 volts for urethane and spiked to -600 volts for parylene conformal coating. Without the use of a point ionizer, ESD surface voltages spiked to an average of 1400 volts for urethane and 3300 volts for parylene removal.

Plastic Bead

The plastic bead (plastic-blast) media from Crystal Mark had an average particle size of 120 micron. It is commercially used for deflashing plastic electronic component leadframes. This media is not biodegradable.

Overall, this media performed well in removing both types of conformal coatings without any nozzle clogging problems or PWB surface damage. The conformal coating removal times were comparable to those for wheat starch and sodium bicarbonate.

The plastic bead media also generated higher surface voltages during parylene removal compared to urethane. The average ESD surface voltage ranged from -20 to -200 volts for urethane and 25 to -560 volts for the removal of parylene. These values peaked to 3000 volts when the ESD control device was not used.

Glass Bead

The glass bead media with 44 micron average particle size from Crystal Mark was used. This media is considered environmentally safe.

The glass bead media from Crystal Mark did not exhibit acceptable cutting characteristics. The urethane conformal coating on trace areas (Site 2) could not be completely removed after an extended period of blasting. However, for parylene, there were signs of solder joint erosion and board surface damage in some areas.

In addition, this media generated unacceptable levels of surface voltages in both types of conformal coatings. This was observed at low media flow rate and pressure conditions. The average ESD surface voltages spiked to 682 volts and -878 volts for urethane and parylene respectively.

Summary and Conclusions

An experimental evaluation was performed to determine the effectiveness of a micro abrasive blasting technique for the removal of the conformal coatings. The two main areas of concern were ESD voltage generation at the surface and physical damage to the PWAs. Test PWAs used in this evaluation were conformally coated with urethane and parylene. The SWAM BLASTER coating removal system was used with four blast medias including wheat starch, sodium bicarbonate, plastic beads and glass beads.

The conclusions from this evaluation are summarized below:

- The SWAM BLASTER coating removal system was effective in removing both coatings. Overall, urethane coatings had a slower removal rate than parylene.
- Wheat starch demonstrated the best overall cutting characteristics for urethane and parylene coatings indicating that micro abrasive blasting technique may be acceptable for space applications.
- Glass beads showed the worst results for coating removal, high ESD surface voltage generation, and board damage. Sodium bicarbonate and plastic media showed mixed results.
- The ESD surface voltages generated using wheat starch were less than 100 volts and were the lowest levels among all four medias. Sodium bicarbonate, plastic beads, and glass beads generated ESD surface voltage between 100 and 1000 volts.
- The Crystal Mark point ionizer was very effective in reducing the surface voltages generated. The ESD surface voltage measured in excess of 3000 volts without the use of a point ionizer.

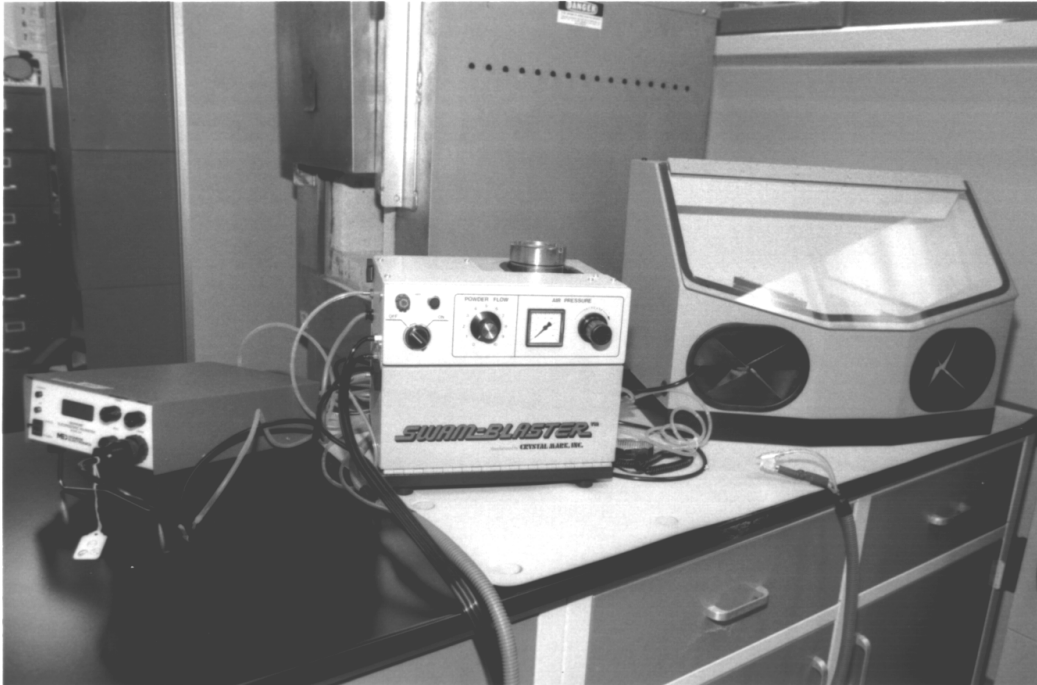


Figure 1. Microblaster System

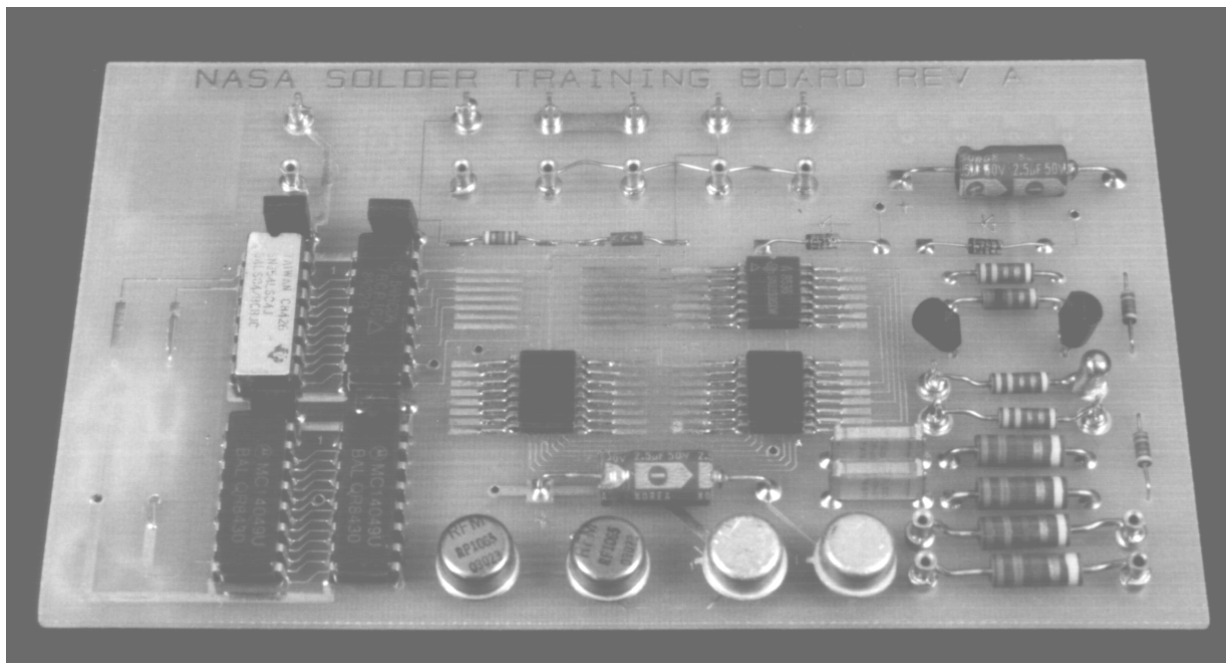


Figure 2. Test Printed Wiring Assembly

Table 3. ESD Voltage Measurement Data for Wheat Starch Media

Conformal Coating Type	Sample ID	Microblaster Parameters				ESD Surface Voltage (Volts)						Electrostatic Field (Volts/Inch)
		Temp. (°C)	Relative Humidity (%)	Media Flow Rate (1-10)	Gas Pressure (PSI)		Site 1	Site 2	Site 3	Site 4	Site 5 (w/o ESD control)	
Urethane	U1	23	50	5	100	Min. Max. Avg.	6 14 10	-6 -24 -15	5 13 9	17 52 34	1880 1862 1871	-115 -290 —
Urethane	U2	23	49	5	100	Min. Max. Avg.	15 28 21	12 36 24	6 6 6	44 48 46	882 900 891	-314 -680 —
Urethane	U3	23	49	5	100	Min. Max. Avg.	24 30 27	38 49 43	32 41 36	60 88 74	1460 1510 1485	-13 -53 —
Urethane	U4	23	49	5	100	Min. Max. Avg.	34 50 42	-19 * -19	10 15 14	95 126 110	1820 1908 1864	-15 -44 —

(* Measurement error due to accidental probe contact)

Table 4. ESD Voltage Measurement Data for Wheat Starch Media

Conformal Coating Type	Sample ID	Microblaster Parameters				ESD Surface Voltage (Volts)						Electrostatic Field (Volts/Inch)
		Temp. (°C)	Relative Humidity (%)	Media Flow Rate (1-10)	Gas Pressure (PSI)		Site 1	Site 2	Site 3	Site 4	Site 5 (w/o ESD control)	
Parylene	P1	23	49	4	50	Min. Max. Avg.	-18 -24 -21	-27 -36 -31	6 10 8	-4 -5 4	566 620 596	-6 -30 —
Parylene	P2	23	49	4	50	Min. Max. Avg.	-27 -30 -28	-18 -23 -20	-33 -25 -29	33 44 38	-220 -263 -241	-3 -12 —
Parylene	P3	23	49	4	50	Min. Max. Avg.	-6 -8 -7	-30 -32 -31	-22 -28 -25	22 16 19	-818 -780 -799	-1 -8 —
Parylene	P4	23	49	4	50	Min. Max. Avg.	-26 -28 -27	-26 -32 -29	7 18 12	34 46 40	-48 -52 -50	-2 -38 —

Table 5. ESD Voltage Measurement Data for Sodium Bicarbonate Media

Conformal Coating Type	Sample ID	Microblaster Parameters				ESD Surface Voltage (Volts)						Electrostatic Field (Volts/Inch)
		Temp. (°C)	Relative Humidity (%)	Media Flow Rate (1-10)	Gas Pressure (PSI)		Site 1	Site 2	Site 3	Site 4	Site 5 (w/o ESD control)	
Urethane	U5	23	50	4.5	95	Min. Max. Avg.	-120 -140 -130	-25 -32 -28	-160 -155 -157	-160 -146 -153	-1580 -1400 -1490	40 360 —
Urethane	U6	23	49	4.5	95	Min. Max. Avg.	-90 -102 -96	-168 -185 -176	-66 -70 -68	-135 -160 -147	-1466 -1248 -1357	20 398 —
Parylene	P5	23	49	5	80	Min. Max. Avg.	50 76 63	-260 -280 -270	-260 -290 -275	-380 -450 -415	-3466 -3432 -3429	27 119 —
Parylene	P6	23	49	5	80	Min. Max. Avg.	160 180 170	-164 -155 -159	-660 -686 -673	-800 -760 -780	-3086 -3422 -3254	32 77 —

Table 6. ESD Voltage Measurement Data for Plastic Bead Media

Conformal Coating Type	Sample ID	Microblaster Parameters				ESD Surface Voltage (Volts)						Electrostatic Field (Volts/Inch)
		Temp. (°C)	Relative Humidity (%)	Media Flow Rate (1-10)	Gas Pressure (PSI)		Site 1	Site 2	Site 3	Site 4	Site 5 (w/o ESD control)	
Urethane	U7	22	49	4	60	Min.	-31	-20	-178	-52	-3378	10
						Max.	-36	-33	-200	-56	-3416	176
						Avg.	-33	-26	-189	-54	-3397	—
Urethane	U8	22	49	4	60	Min.	-2	-26	-218	-340	-2752	20
						Max.	-12	-32	-220	-358	-2760	288
						Avg.	-7	-29	-219	-349	-2756	—
Parylene	P7	22	49	4	60	Min.	16	-76	-220	-480	-2832	8
						Max.	28	-88	-233	-510	-2899	56
						Avg.	22	-82	-226	-495	-2865	—
Parylene	P8	22	49	4	60	Min.	21	-6	-250	-509	-2800	9
						Max.	35	-11	-260	-540	-3005	56
						Avg.	28	-8	-255	-524	-2902	—

Table 7. ESD Voltage Measurement Data for Glass Bead Media

Conformal Coating Type	Sample ID	Microblaster Parameters				ESD Surface Voltage (Volts)						Electrostatic Field (Volts/Inch)
		Temp. (°C)	Relative Humidity (%)	Media Flow Rate (1-10)	Gas Pressure (PSI)		Site 1	Site 2	Site 3	Site 4	Site 5 (w/o ESD control)	
Urethane	U9	22	49	2	60	Min.	*	-44	278	850	-1763	1800
						Max.	*	-51	288	776	-1888	2000
						Avg.	-	-47	283	813	-1825	—
Urethane	U10	22	49	2	60	Min.	280	⊙	140	545	-1786	213
						Max.	303	⊙	145	558	-1806	1690
						Avg.	291	-	142	551	-1796	—
Parylene	P9	22	49	2	60	Min.	*	-898	-929	-926	-1919	56
						Max.	*	-860	-940	-935	-2097	150
						Avg.	*	-879	-934	-930	-2008	—
Parylene	P10	22	49	2	60	Min.	-100	-706	-510	-823	-1821	5
						Max.	-122	-725	-528	-830	-1827	59
						Avg.	-111	-715	-519	-826	-1823	—

* Measurement error due to accidental probe contact

⊙ Coating could not be removed

Table 8. ESD Voltage Comparison Data for Various Medias

Media Type	Average ESD Surface Voltage (Volts)									
	Coating Type									
	Urethane					Parylene				
	Site 1	Site 2	Site 3	Site 4	Overall Average	Site 1	Site 2	Site 3	Site 4	Overall Average
Wheat Starch	25	25	16	66	33	-21	-28	-18	25	23
Sodium Bicarbonate	-113	-152	-112	-100	-119	122	-214	-474	-597	-352
Plastic Bead	-20	-22	-204	-202	-112	25	-45	-240	-559	-217
Glass Bead	291	-47	212	682	308	-111	-797	-726	-878	-628

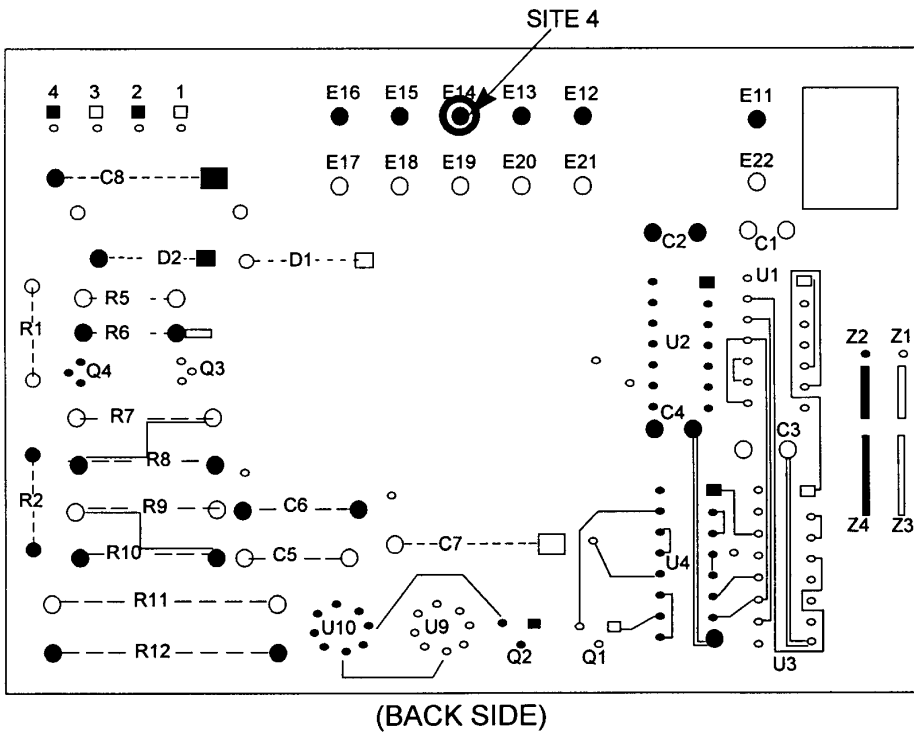
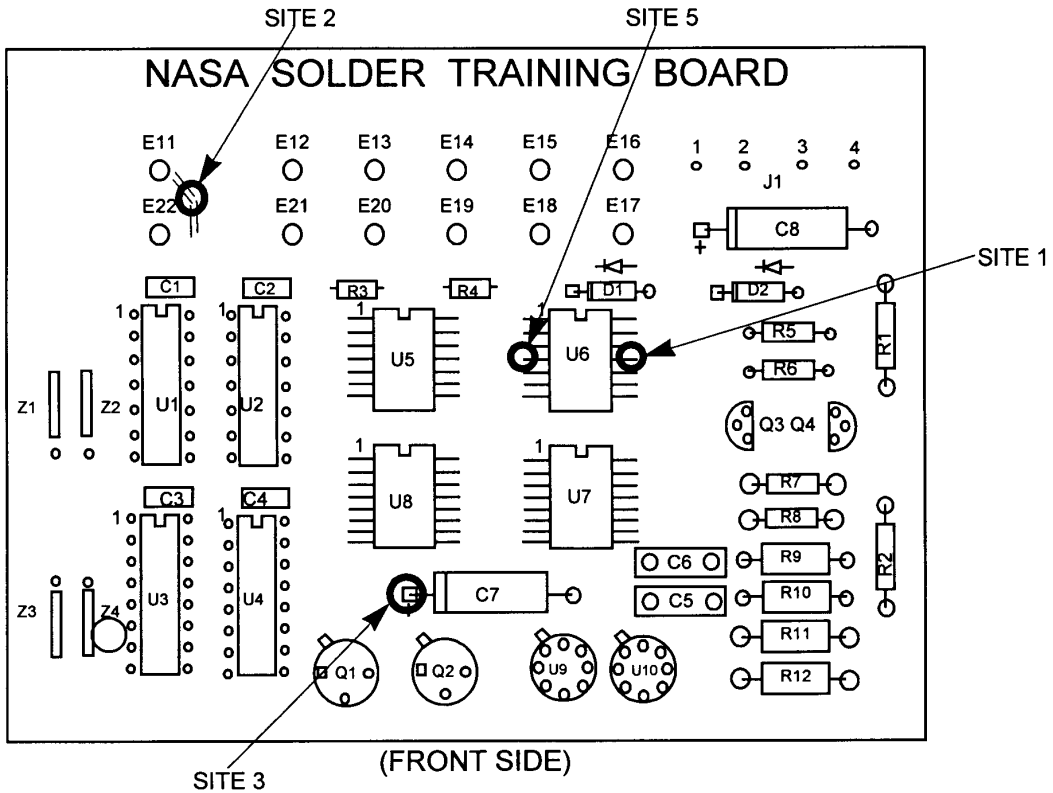


Figure 3. Test Board Configuration

ISS Fiber Optic Failure Investigation

Root Cause Report

This is the Root Cause Report document in PDF format:

[Root_Cause.pdf](#) (4.7 MB)

If you prefer to download the report in smaller files instead of all at once, here is the document broken down into 5 parts:

[Root_Cause_part1.pdf](#) (0.674 MB)

[Root_Cause_part2.pdf](#) (1.256 MB)

[Root_Cause_part3.pdf](#) (0.760 MB)

[Root_Cause_part4.pdf](#) (1.264 MB)

[Root_Cause_part5.pdf](#) (0.880 MB)

To view this document you must have Adobe Acrobat Reader, which is available for free [HERE](#).

For questions please contact [Henning Leidecker](#) or [Jeannette Plante](#).

NASA Website Privacy Statement

This policy establishes how NASA will use information we gather about you from your visit to our website. The privacy of our customers is of utmost importance to NASA.

If you visit a NASA site...

1. To read or download information:

We may collect and store information for statistical purposes. For example, we may count the number of visitors to the different sections of our site to help us make them more useful to visitors. Similar information is gathered for anonymous ftp, remote account login, or for other comparable types of connections.

2. To send us an E-mail:

By sending us an electronic mail message, you may be sending us personal information (e.g., name, address, E-mail address), as in an official FOIA request. We may store the name and address of the requester in order to respond to the request or to otherwise resolve the subject matter of your E-mail.

3. To register:

Some of our sites ask visitors who request specific information to fill out a registration form. For example, vendors looking for marketing opportunities by visiting our NASA Acquisition Internet Service sites may be asked to "register" to obtain email notices of business opportunities. Other information which may be collected at these sites through questionnaires, feedback forms, or other means, enable us to determine a visitor's interests, with the goal of providing better service to our customers.

We want to be very clear: regardless of the information being transmitted to NASA, we will protect all such information consistent with applicable law.

NASA Website Disclaimer Statement

Thank you for visiting this NASA web site. NASA may provide links to web pages which are not part of the NASA web family, or nasa.gov domain. These sites are not under NASA control, and NASA is not responsible for the information or links you may find there. NASA is providing these links only as a convenience. The presence of these links on any NASA website is not intended to imply NASA endorsement of that site, but to provide a convenient link to relevant sites which are managed by other organizations, companies, or individuals.

NASA Website Accessibility Statement

The pages on this website have been reviewed and revised to be accessible to individuals with disabilities in accordance with provisions of Section 508 of the Workforce Investment Act and the Americans with Disabilities Act. If you are having a problem accessing a NASA website please let us know and we will work to ensure accessibility. [If you have any difficulty viewing any page with adaptive technology, click here to let us know.](#)

Use your browser's "BACK" button to return to previous page.

July 17, 2000



October 29, 2001

[Text Only Version](#)[NASA's Vision](#)*(Flash movie)*

"NASA is deeply committed to spreading the unique knowledge that flows from its aeronautics and space research...."

Read NASA Administrator Daniel S. Goldin's [welcome letter](#), [bio](#) and [speeches](#).

[Welcome to NASA Web](#)

Search NASA's Web

Enter search words:

[Search Options](#)[Need help?](#)[Navigating NASA's Strategic Enterprises](#)[Aerospace Technology](#)[Biological and Physical Research](#)[Earth Science](#)[Human Exploration and Development of Space](#)[Space Science](#)

NASA



Bulldozer Rovers Could Get Scoop on Mars



Tiny bulldozer rovers may some day dish up the dirt and pack it in on Mars. The scoop-and-dump design of a prototype bulldozer rover being developed

by NASA engineers mimics that of a bulldozer and dump truck. Unlike a life-size bulldozer and dump truck, these rovers are lightweight, intelligent and can work without an operator at the wheel. Unlike a life-size bulldozer and dump truck, which can weigh several thousand pounds, these rovers are lightweight, intelligent and can work without an operator at the wheel. Yet they have the same capabilities, relative to their size, as their heavy-duty counterparts. Robotics engineers think the basic research on these bulldozing rovers may support future missions to look for life or to sustain a human presence. ([Full Story](#))

(10/29/2001)

today@nasa.gov

[NASA Home Page Survey](#)[Top Search Terms](#)[NASA TV Schedule](#)[See the Space Station](#)

Interested in the latest information NASA has to offer? Then take a look at [today@nasa.gov](#). This on-line newsletter, updated daily, contains the latest news about NASA science and technology.

- [Bulldozer Rovers Could Get Scoop on Mars](#)
- [International Space Station Receives Prestigious Award](#)
- [Space Station: A Year's Worth of Humans](#)

Cool NASA Websites



International Space Station



NASA Webcasts



Mars Odyssey



Space in My Life

[Other Cool NASA Websites](#)

[NASA for Kids](#)

More About NASA:

[Doing Business with NASA](#)

[Educational Resources](#)

[Freedom of Information Act](#)

[History](#)

[Jobs and Internships](#)

[NASA Technology Portal](#)

[News and Information](#)

[Organization and Subject Index](#)

[Project Home Pages](#)

[Research](#)

[Opportunities](#)

[Scientific and Technical Information](#)

[See a Launch](#)

[Launch Schedule](#)

[Speakers Bureau](#)

[Spinoffs and Commercial Technology](#)

[Visiting NASA](#)

[Dreamtime](#)

Do you dream of exploring space or working for NASA? If so, avoid black holes and drugs. [You decide.](#)

[\[Frequently Asked Questions\]](#) [\[Hot Topics\]](#) [\[Multimedia Gallery\]](#) [\[NASA Television\]](#)
[\[Text Only Version\]](#)

[\[NASA Privacy Statement, Disclaimer, and Accessibility Certification\]](#) [\[Site Maps\]](#)



Author: Elvia Thompson
Responsible NASA Official: Brian Dunbar
Site Maintainer: K F Chow
[Comments and Questions](#)

Last Updated: October 29, 2001